UNIVERSITEIT VAN PRETORIA
UNIVERSITY OF PRETORIA
YUNIBESITHI YA PRETORIA

MAXIMUM HEAT TRANSFER RATE DENSITY FROM A ROTATING MULTISCALE ARRAY OF CYLINDERS

by

Oluseun Ifeanyi Ogunronbi

Submitted in partial fulfilment of the requirements for the degree of Master in Engineering

in the

DEPARTMENT OF MECHANICAL AND AERONAUTICAL ENGINEERING

FACULTY OF ENGINEERING, THE BUILT ENVIRONMENT AND INFORMATION TECHNOLOGY

UNIVERSITY OF PRETORIA

Supervisors: Dr. T. Bello-Ochende and Prof. J.P. Meyer

June 2010

Acknowledgements

I would like to thank Dr. Tunde Bello-Ochende for his guidance and support in the course of this work. I would also like to thank Prof. J.P. Meyer, who, as my co-supervisor, provided considerable input and constructive arguments to this work. Special thanks go to all my fellow graduate students for lending their ears during crucial moments: Bode, Lanre, Darshik, Antoine, thank you.

Finally, I would like to thank my guardian, brother and friend Sunday Ogunronbi, without whom this study would have been impossible. Appreciation and gratitude is also due to my parents for their indefatigable support in the course of my education.

This work was supported by the Advanced Engineering Centre of Excellence, NRF, TESP, EEDSM Hub and the CSIR.

Abstract

This work investigated a numerical approach to the search of a maximum heat transfer rate density (the overall heat transfer dissipated per unit of volume) from a two-dimensional laminar multiscale array of cylinders in cross-flow under an applied fixed pressure drop and subject to the constraint of fixed volume. It was furthermore assumed that the flow field was steady state and incompressible. The configuration had two degrees of freedom in the stationary state, that is, the spacing between the cylinders and the diameter of the smaller cylinders. The angular velocity of the cylinders was in the range $0 \leq \widetilde{\omega} \leq 0.1$. Two cylinders of different diameters were used, in the first case, the cylinders were aligned along a plane which lay on their centrelines. In the second case, the cylinder leading edge was aligned along the plane that received the incoming fluid at the same time. The diameter of the smaller cylinder was fixed at the optimal diameter obtained when the cylinders were stationary. Tests were conducted for co-rotating and counter-rotating cylinders. The results were also compared with results obtained in the open literature and the trend was found to be the same. Results showed that the heat transfer from a rotating array of cylinders was enhanced in certain cases and this was observed for both directions of rotation from an array which was aligned on the centreline. For rotating cylinders with the same leading edge, there is heat transfer suppression and hence the effect of rotation on the maximum heat transfer rate density is insignificant. This research is important in further understanding of heat transfer from rotating

cylinders, which can be applied to applications ranging from contact cylinder dryers in the chemical processes industry and rotating cylinder electrodes to devices used for roller hearth furnaces.

Keywords: centreline, co-rotating, counter-rotating, dimensionless, heat transfer rate density, leading edge, multiscale, pressure drop number

Contents

List of Figures

List of Tables

Nomenclature

Be	Bejan number
c_p	heat capacity, $J.kg^{-1}.K^{-1}$
C	constant in power law relationship
$\tilde{d}$	dimensionless smaller cylinder diameter
d	small cylinder diameter, m
D	big cylinder diameter, m
Frossling	$Nu/\sqrt{Re}$
k	thermal conductivity, $W.m^{-1}K^{-1}$
L	length
Nu	Nusselt number
P	pressure, Pa
Pr	Prandtl number
q'	heat transfer rate per unit length, $W.m^{-1}$
q''	heat flux, $W.m^{-2}$
q'''	heat transfer rate density, $W.m^{-3}$
$\tilde{q}$	dimensionless heat transfer rate density
Ra	Rayleigh number
Re	Reynolds number
S	tip-to-tip distance between two consecutive cylinders, m

T	temperature, K
u,v	velocity components, $m.s^{-1}$
x,y	Cartesian coordinates, m

Greek symbols

α	thermal diffusivity, m^2s^{-1}
μ	dynamic viscosity, $kg.m^{-1}.s^{-1}$
ν	kinematic viscosity, $m^2.s^{-1}$
θ	angle, rad
ρ	density, $kg.m^{-3}$
ω	angular velocity, $rad.s^{-1}$
Ω	Re_ω/Re_∞

Subscripts/Superscripts

c	cross-flow
CL	cylinders aligned along the centreline
d	downstream
J	air jet
LE	cylinders aligned along the leading edge
max	maximum
m	maximum

m	exponent in power law relationship
n	exponent in power law relationship
o	characteristic length
opt	optimum
R	resultant velocity
u	upstream
w	wall
ω	rotational
∞	inlet
~	dimensionless unit
-	average

Chapter 1 INTRODUCTION

1.1 Literature Review

Due to the need for more effective heat removal from heat transfer generating equipment such as heat sinks, research has been and is still being conducted with the aim of removing more and more heat from a given volume which generates heat. Effective heat removal will help in the design, manufacture and operation of such equipment. Modern electronic systems produce high amounts of heat due to the power-to-volume or -weight ratio employed in such systems. The heat produced, if not removed efficiently, could lead to failure of parts of the system and in some cases, failure of the whole system.

Heat transfer from a rotating solid to a moving fluid is used in different applications, from the cooling of rotating machinery and re-entry space vehicles to the paper industry. Applications can also be found in the laboratory assessment of the effect of fluid velocity on corrosion rates (Gabe, 1974; Silverman, 1988; Gabe et al., 1998), and theoretical solutions that introduce analogy to the mass transfer from the flow around cylinders (Levich, 1962; Silverman, 2003).

Badr and Dennis (1985) considered the problem of laminar forced convective heat transfer from an isothermal cylinder rotating on its own axis and located

in a uniform stream. Their results emphasised the effect of the rotation on the thermal boundary layer and the local Nusselt number distribution. They hypothesised that one of the reasons for the lack of literature on rotating cylinders was the paucity of information about the boundary layers near such bodies. They found that the overall heat transfer coefficient tended to decrease as the speed of rotation increased; they attributed this to the existence of a rotating fluid layer that acted as insulation from the main-stream coolant.

Furthermore, Badr and Dennis (1985) investigated the effect of rotation on the convective heat transfer while assuming the buoyant forces to be negligible in comparison with the inertial forces due to the difference in temperature. Their tests were conducted in the Reynolds number range of 5 – 100 and with speed ratios (the ratio between the cylinder circumferential velocity and the velocity of the free-stream coolant) between the values of 0.1 and 4. Their results showed that the local Nusselt number was highly dependent on the rotational motion of the cylinder. Also, at the different fixed free-stream Reynolds numbers tested, it was seen that the average Nusselt number decreased when the speed ratio was increased. However, at higher Reynolds numbers the value of the average Nusselt number was higher than those obtained at corresponding speed ratios of prior and lesser Reynolds numbers. Their argument was that with the increase in velocity ratio, the heat transfer from the cylinder became dominated by the speed of rotation much more than the main flow velocity.

Badr and Dennis (1985) explained this phenomenon as the effect of the cylinder being surrounded by a certain volume of rotating fluid that does not mix with the free-stream fluid. This flow field is then assumed to restrict the heat transfer from the cylinder and consequently the overall heat transfer rate is decreased.

Ingham (1983) considered the flow generated by a rotating cylinder with the cylindrical angular velocity lower than the velocity of the uniform stream. He additionally considered the effect of the boundary conditions on the wake of the flow far away from the cylinder. The work focused on low Reynolds numbers and highlighted the flow structure when rotation was present. Also, the behaviour of the wake on a cylinder was investigated and considered in the location of more cylinders downstream of the initial array.

Chiou and Lee (1993) investigated the convection from a rotating cylinder cooled by an air jet; their tests were conducted in the Reynolds number range of $10^2 \leq \mathrm{Re} \leq 10^3$ and the rotational Reynolds number was in the range of $0 \leq \mathrm{Re}_\omega / \mathrm{Re}_J \leq 1$ where the subscript J denoted the air jet Reynolds number and the subscript ω denoted the rotational Reynolds number.

At lower rotational Reynolds numbers, Chiou and Lee (1993) found that the overall heat transfer was enhanced, while the converse holds for higher rotational Reynolds numbers. This is due to what they termed “a layer of dead air around the cylinder”.

Chiou and Lee's (1993) work also reveals the existence of two solution modes for the flow. At slow rotation speeds, there are two separation points with one moving in the direction of the rotation without any significant influence from the other. This leads to an overall heat transfer enhancement. In the other case, with the high rotation Reynolds number, there occurs a layer of dead air around the cylinder. In this scenario, the heat transfer rate is more uniform but it is lower than the heat transfer rate from a stationary cylinder.

Jones et al. (1988) studied mixed convection, with the goal of determining the overall heat transfer rate dependence on the free-stream Reynolds number, the rotational Reynolds number and the Rayleigh number. Their work presents the three mechanisms through which convection transports heat, namely forced convection from the free-stream coolant, forced convection due to rotation and natural convection.

Jones et al. (1988) also concluded by stating that the effect of rotation on natural convection was an enhancement in heat transfer, with the limitation that there appeared to be a limit of speed ratio beyond which such enhancement was no longer seen. They stipulated a general correlation for the heat transfer, as represented by the Nusselt number, as

$$Nu = 0.1\left[Re^2 + Re_\omega^2\right]^{0.36} \qquad 0 < Re < 35\,000$$

$$0 < \mathrm{Re}_{\omega} < 5\,000$$

Bejan and Morega (1993) investigated, by analytical means, the optimal spacing of stacked plates which emit heat and were cooled by free-stream flow of the ambient fluid. Their work helps in defining the rationale behind the optimisation of space among heat-generating materials. Optimisation was conducted for a single-scale structure, with the said scale being the distance between the plates. Bejan and Morega further found that the optimal spacing in a turbulent flow increased as the Prandtl number and the width-to-length ratio increased.

Mohanty et al. (1995) compared the flow around a rotating cylinder with the model of transport from the leading edge of a turbine blade. Comparisons were made between the heat transfer coefficient of pure cross-flow across the cylinder and the heat transfer coefficient of pure rotation of the cylinder. Experiments showed that the heat transfer from the stagnation point under pure rotation was lower than that of pure cross-flow. Additionally, the heat transfer coefficient of pure cross-flow was seen to undergo a huge drop, attributable to laminar separation. The drop of the heat transfer coefficient of a rotating cylinder was much less, leading to a higher average heat transfer coefficient for a rotating cylinder than that seen on a stationary cylinder. It was found that the average Nusselt number with respect to the maximum Reynolds number was, $\overline{\mathrm{Nu}} = 0.38\mathrm{Re}_{\mathrm{m}}^{0.58}$.

It was noted by Mohanty et al. (1995) that the heat transfer is higher for rotational convection than for pure cross-flow. Mohanty et al. further combined both regimes. They used the Reynolds number based on the resultant velocity (Re_R) of both regimes to develop the following correlation for the average Nusselt number:

$$\overline{Nu} = 0.393 Re_R^{0.577}$$

The study concluded by noting that the effect of rotation and cross-flow depends on the ratio of the cross-flow Reynolds number (Re_c) to the resultant Reynolds number (Re_R), with the following enhancements:

Re_c/Re_R	Percentage increase in enhancement of heat transfer
0.2	4
1	35
2	91

Stanescu et al. (1996) conducted an experimental and numerical study; they were able to conclude that with an increase in the Reynolds number based on the free-stream velocity, the optimal spacing decreased as the thermal conductance increased. They provided a good basis for the use of a fixed pressure drop as the flow driver, because the velocity parameter does not change with variation in spacing between the cylinders. In terms of the

average Nusselt number, the heat transfer around a cylinder is typically denoted by the power law relationship, $\overline{Nu} = C\,Re^{m}Pr^{n}$, where C, m and n are constants.

Sanitjai and Goldstein (2004) determined the average heat transfer from measured local heat transfer rates and developed an empirical equation thereof. They also confirmed the increase in Nusselt number with increase in Reynolds number. The Nusselt number was the highest at the front stagnation point, with a gradual decrease due to the increase of thermal resistance from the growth of the boundary layer.

Heat transfer variation in this study was grouped into three regions, namely growth of the laminar boundary layer, reattachment of the free-stream shear layer and periodic vortices. In some ranges of the Reynolds number, the average heat transfer increased sharply due to flow transition from laminar to turbulent flow.

Optical techniques in investigating the heat transfer from a rotating cylinder were employed by Gschwendtner (2004). Results noted in this work are the effect of rotation on the boundary layer and the flow patterns of the coolant. This work also supports what was said by Badr and Dennis (1985), with respect to the effect of the velocity ratio on the flow patterns and the heat transfer rate of the cylinder.

It was found that above $\Omega = 2$ (Ω is the ratio of the rotational Reynolds number, Re_{ω} to the free-stream Reynolds number, Re_{∞}), rotation dominated over cross-flow. Gschwendtner (2004) also idealises the fluid flow over a hot rotating body as flow over a heated wall should the cylinder be straightened out.

Results obtained in the work of Badr and Dennis (1985) was also supported by the work of Kays and Bjorklund (1958), who noted that at $\Omega \approx 2$, rotation plays the determining role in heat transfer. This creates a boundary layer that surrounds the cylinder and the heat transfer becomes dependent on the rotational velocity. Gschwendtner's (2004) work confirms the known fact that a hot wall has a destabilising effect on the boundary layer of gases. The conclusive point noted from this work is that there is definitely a more uniform heat transfer from a cylinder when rotation is present.

One of the pioneering works on multiscale cylinders is that of Bello-Ochende and Bejan (2004). This study looked at two different scales, the diameters as well as the spacing between cylinders which were stationary against a coolant in cross-flow. The heat transfer rate density, also termed the overall thermal conductance, was maximised in this study.

In this work, there is evidence of the effect of the increase of the pressure drop number, the Bejan number on the optimal spacing between the cylinders. It

shows a decrease in spacing as the Bejan number is increased. There is also an increase in heat transfer rate density when the Bejan number is increased.

Bello-Ochende and Bejan (2004) further increased the complexity of their structure by including a smaller diameter cylinder, with the research showing that the optimal non-dimensionless diameter size of the smaller diameter being 0.25 regardless of the Bejan number used. In this configuration, it was further shown that the optimal spacing was larger than the spacing between a single-scale cylinder array. The ratio of such spacing was, however, constant for all parameters tested. The study concluded that for different diameter cylinders, the heat transfer rate density of an additional length scale structure was much higher than the heat transfer of the single-scale structure.

An additional cylinder, making a total of three different diameters, was then included in the structure, with the distance between the smaller cylinders being a new parameter for optimisation. Bello-Ochende and Bejan (2004) then noted that the maximised heat transfer rate density was larger than all those previously calculated. This shows the effect of the extra geometrical degree of freedom. The study stopped at the juncture where cost considerations were believed to outweigh any potential benefits.

In further work done by Bello-Ochende and Bejan (2005), the focus this time was on natural convection. It followed the same methodology as used in the work on forced convection, but the smaller cylinders were located in the

entrance region between the bigger cylinders to utilise the coolant, which was unaffected by the bigger cylinder's temperature. The optimal heat transfer was found to be at:

$$\frac{S_{opt}}{D} = 1.32Ra^{0.22}$$

$$\tilde{q}_m = 0.65Ra^{0.30}$$

At the optimal position, it was found that the cylinders were at a distance at which their thermal boundary layers just touched. Scale analysis was further employed to ascertain this.

In the consequent phases, smaller diameter cylinders were placed in between the optimised distances and the process repeated. It was conclusively noted that by increasing the number of smaller cylinders inserted, the optimal spacing increased. The maximised heat transfer rate density also increased with the Rayleigh number

$$\tilde{q}_m = 0.85Ra^{0.3}$$

A different point noted from the work of Bello-Ochende and Bejan (2005) is the ability of multiscale structures to "morph" under different flow conditions. This ability is shown by the ease of such structures to adapt to their arrangements, and the adaption is easier than the redesign of the solid components that generate heat.

Misirlioglu (2006) conducted research into the effect of a rotating cylinder in a square cavity with the primary focus on the natural convection but also focused on forced convection and mixed convection. In the forced convection regime tested, it was shown that it was the Reynolds number which defined the amount of heat transfer and which translated to an increase in Nusselt number.

Joucaviel et al. (2008) conducted work on a rotating array of cylinders. This is a combination of many of the aforementioned works. They suggested that the most heat exchange occurred at the cylinder-side which faced the coolant flow. They further stated that when the cylinders were too closely located, there was more resistance against the fluid moving across and downstream from the cylinders. The other results observed is that the heat transfer per unit volume decreased. Results show that the optimal spacing between the rotating cylinders decreased when the Bejan number was increased, while the heat transfer rate density increased with an increase in Bejan number.

Joucaviel et al. (2008) tested two cases; consecutive cylinders counter-rotating and the case where they were co-rotating. In the counter-rotation regime, with an increase in the rotational velocity, the optimal distance between the cylinders was decreased. Furthermore, as the Bejan number increased the heat transfer rate density increased, though it can be seen that at Be = 100, the heat transfer rate density at a non-dimensionalised angular velocity, $\tilde{\omega}$, of 1 was

lower than that seen at $\tilde{\omega} = 0$ and $\tilde{\omega} = 0.1$. They noted that $\tilde{q}_m(\tilde{\omega} \neq 0) > \tilde{q}_m(\tilde{\omega} = 0)$ for some values of Be. Also, it was noted that a greater angular velocity resulted in a greater heat transfer rate density (Joucaviel et al., 2008).

On the numerical simulation of co-rotating cylinders, they concluded that this was not an efficient configuration, with the results contrary to those obtained for counter-rotating cylinders, that is, lower heat transfer rate density and bigger spacing between the cylinders than for a stationary cylinder. Joucaviel et al. (2008) finally conducted tests on asymmetrical spacing between the counter-rotating cylinders. It was concluded that in the case where the coolant direction was enhanced by the rotational direction, the spacing could be further reduced with the opposite occurring when the cylinder velocity direction opposed the oncoming coolant.

Cheng et al. (2008) investigated the heat transfer coefficient on a radially rotating cylinder. They used the cylinder as an idealised version of the leading edge of a turbine blade. The Frossling factor was employed as the normalising unit. The rotation of the cylinder was perpendicular to the free-stream flow direction and this led to increased mixing of the flow.

Cheng et al. (2008), however, confirmed that heat transfer enhancement was higher at lower Reynolds numbers than at higher Reynolds numbers. However, their results further show that the heat transfer enhancement at the

stagnation point is greater at a higher rotation number than at a lower rotation number.

Mandhani et al. (2002) also noted an increase in the Nusselt number when the Peclet number is increased, with a local maximum seen at the stagnation point.

Khan et al. (2005) considered the use of boundary layer analysis done with the Von Karman-Pohlhausen method to conduct the hydrodynamic and heat transfer research on a circular cylinder. They considered both isothermal and isoflux wall boundary conditions. It was found that with an increase in the Reynolds number, the Nusselt number also increased. The increase in the uniform wall temperature was, however, less than the increase under uniform flux conditions.

Furthermore, the heat transfer behaviour showed that the local dimensionless average heat transfer coefficient reduced from a maximum at the stagnation point of the cylinder to a minimum at the point of separation.

Paramane and Sharma (2009) numerically solved the forced convection heat transfer across a cylinder. Their work supports the results of Badr and Dennis (1985). With an increase in Reynolds number, there is a commensurate increase in the local Nusselt number for stationary cylinders. In this instance of rotating cylinders, it was first noted that the location of the maximum local Nusselt number changed on the circumference of the cylinder in the direction

of the rotation, but the local Nusselt number decreased with an increase in the rotational velocity and became independent of the free-stream Reynolds number at higher rotation rates.

It was also found that there was a decrease in the average Nusselt number for each incremental Reynolds number. At increasing rotation rates, it was suggested that fluid was entrapped in the enveloping vortex, which restricted heat transfer to pure conduction. Additionally, the size of the entrapment zone increased with an increase in the velocity ratio, which further reduced the conduction heat transfer; this was also seen by the drop in the Nusselt number. At some velocity ratio, the Nusselt number became independent of the Reynolds number and became constant. The advantage gained from Paramane and Sharma's (2009) work is that cylinder rotation can be used to suppress heat transfer quite effectively.

1.2 Objectives and scope of the Study

The primary purpose of this study is to maximise the heat transfer rate density in an array of cylinders, in which two configurations are studied: (i) cylinders with two different diameters rotating in the same direction, and (ii) two consecutive cylinders with different diameters rotating in opposite directions. In order to achieve the main objective, the following steps were taken:

(i.) The cylinders were subjected to laminar two-dimensional forced convection in which the flow was perpendicular to the plane of the cylinders.

(ii.) The spacing between two consecutive cylinders was optimised

(iii.) The diameter of the smaller cylinders were optimised in each case and

(iv.) The effect of rotation on heat transfer rate density was determined.

In attempting to find solutions to the objectives stated in the preceding section, the governing equations which are used to solve the problem posed at the beginning of this chapter are identified in the second chapter. Thereafter, a stationary domain grid refinement is conducted. In the third chapter, the smaller cylinder diameters are first optimised, this is followed by optimisation of the arrangement of cylinders, which are located in line with their spacing and the maximum heat transfer rate density.

In the fourth chapter, the flow is solved numerically for the array in which the cylinders are located along the leading edge. The steps investigated for inline-located cylinders are also repeated here. At each juncture, an attempt is made to validate the simulations by comparing them with known solutions.

In the fifth chapter, the conclusion of this work is presented and recommendations are made on the direction to be taken to enhance the knowledge gained from this work. In all cases, the results are compared with those obtained for stationary cylinders.

Chapter 2 THEORY

2.1 Mathematical model

This chapter presents the model used in optimising the heat transfer rate density from an array of different scaled cylinders, where the characteristic length is the diameter of the bigger cylinder. The chapter starts off by presenting the governing equations, which are solved for the heat transfer and fluid motion around the array. This is followed by the simplification of the governing equations through dimensional analysis. The boundary conditions of the problem are then stated. Finally, the domains are discretised and a grid independence study is performed on the stationary assembly, to ensure confidence in the results obtained.

The numerical study conducted in this work was done with the finite volume method, and a commercial computational fluid dynamics (CFD) code, Fluent^{TM}(1998), was used. CFD is a numerical solving technique, which solves the Navier-Stokes and energy equations on a discretised domain given the relevant flow boundary conditions.

In the first case of this work, the cylinders are aligned on the same centreline and in the second case, the array of cylinders is aligned along the leading edge. The research proceeds by optimising the diameter of the smaller cylinder

under different pressure drop numbers; while the cylinders are kept stationary. Thereafter, simulations are conducted on the array with the optimum smaller cylinder for different rotational velocities and also under different Bejan numbers.

Figure 2.1 depicts the model which represents a multiscale array of cylinders set along the centreline, while Figure 2.2 shows a stack of cylinders aligned on the leading edge. Conditions of periodicity then reduce the numerical area of the study to that of two cylinders, as shown in Figure 2.3 and Figure 2.4 consecutively.

The domain of interest in this study is two-dimensional and the cylinders are considered to be of unit depth in the direction of the paper (z-direction). The flow is driven by fixed pressure drop between the inlet boundary and the outlet boundary of the domain.

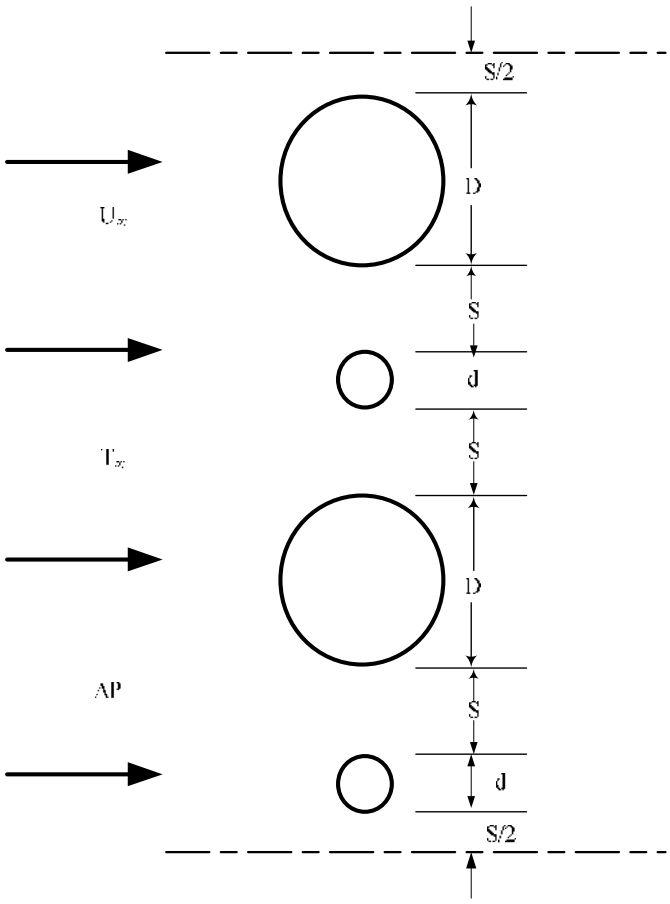

Figure 2.1 Stack of cylinders aligned along the centreline

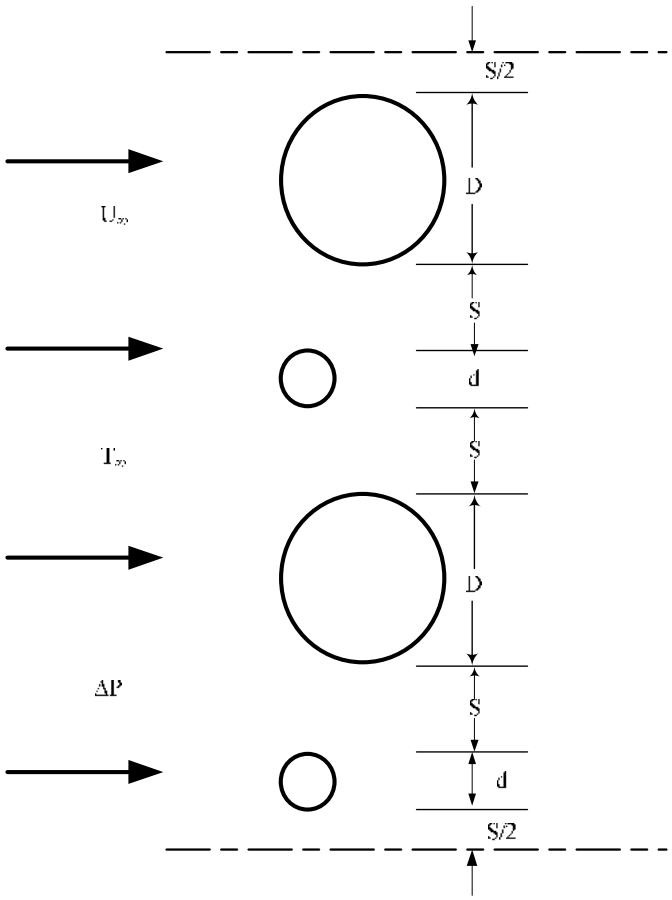

Figure 2.2 Stack of cylinders aligned on the leading edge

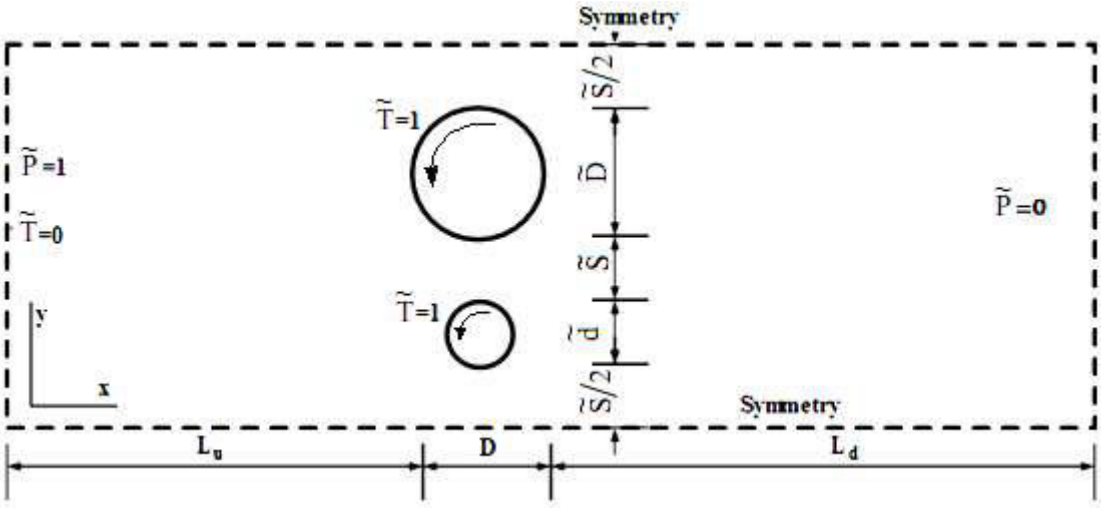

Figure 2.3 The numerical domain of centreline-placed cylinders

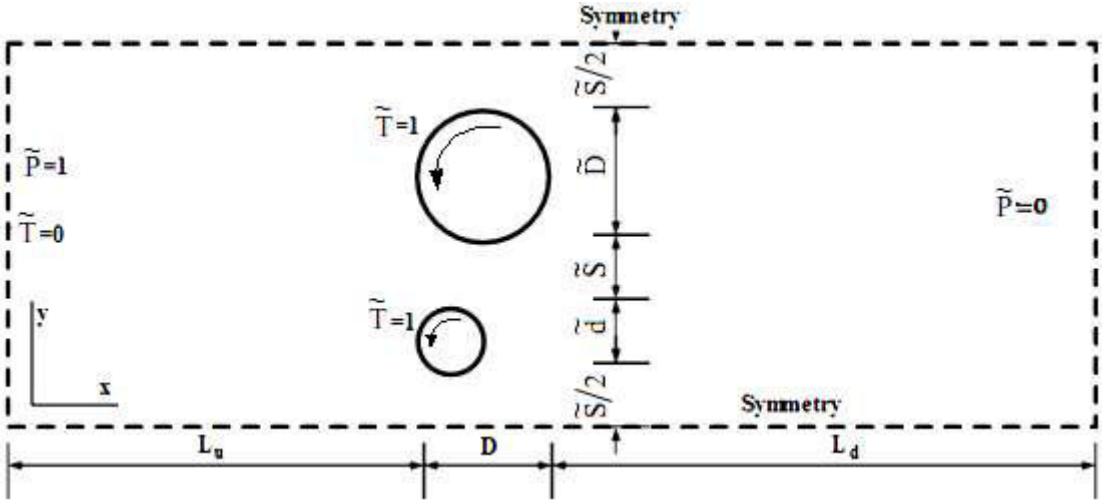

Figure 2.4 The numerical domain of cylinders aligned on the leading edge

Figures 2.3 and 2.4 indicate that two means of rotation are applied, co-rotation and counter-rotation, by means of the sign which dictates the directions of the rotational velocity. The above diagrams show the cylinders co-rotating with each other. In the case where the cylinders are co-rotating, the rotational velocities of both cylinders have the same sign; and in the case where the cylinders are counter-rotating, they have opposite signs.

2.2 Numerical method

The governing systems of equations that describe the flow field are a set of non-linear partial differential equations. This set of equations is known as the Navier-Stokes and energy equations; they enforce the principles of mass, momentum and energy conservation. The equations in two dimensions are thus given in the primitive form as:

$$\frac{\partial u}{\partial x} + \frac{\partial v}{\partial y} = 0 \tag{2.1}$$

$$\rho\left(u\frac{\partial u}{\partial x} + v\frac{\partial u}{\partial y}\right) = -\frac{\partial P}{\partial x} + \mu\left(\frac{\partial^2 u}{\partial x^2} + \frac{\partial^2 u}{\partial y^2}\right) \tag{2.2}$$

$$\rho\left(u\frac{\partial v}{\partial x} + v\frac{\partial v}{\partial y}\right) = -\frac{\partial P}{\partial y} + \mu\left(\frac{\partial^2 v}{\partial x^2} + \frac{\partial^2 v}{\partial y^2}\right) \tag{2.3}$$

$$\rho c_p\left(u\frac{\partial T}{\partial x} + v\frac{\partial T}{\partial y}\right) = k\left(\frac{\partial^2 T}{\partial x^2} + \frac{\partial^2 T}{\partial y^2}\right) \tag{2.4}$$

Where u and v represent the velocity components in the Cartesian coordinate directions, x and y. ρ is the density, μ is the viscosity, k is the thermal conductivity, c_p is the heat capacity, P is the pressure, and T is the temperature. The equations have been simplified as laminar, incompressible and two-dimensional in nature. Additional assumptions include constant solid and fluid properties, negligible heat transfer due to radiation and negligible viscous dissipation due to the nature of the flow.

2.2.1 Dimensionless Parameters

The use of dimensionless parameters reduces the amount of variables introduced in the simulation; this also enhances the analysis of the results. The dimensionless variables considered in this work include geometrical, velocity, temperature and pressure groups, which are:

$$\tilde{x} = \frac{x}{D}, \qquad \tilde{y} = \frac{y}{D}$$

$$\tilde{u} = \frac{u}{\Delta PD/\mu}, \qquad \tilde{v} = \frac{v}{\Delta PD/\mu}$$

$$\tilde{T} = \frac{T - T_\infty}{T_w - T_\infty}, \qquad \tilde{P} = \frac{P}{\Delta P}$$

$$\tilde{S} = \frac{S}{D}, \qquad \tilde{d} = \frac{d}{D}$$

Utilising the above dimensionless parameters into the Navier-Stokes equations leads to

$$\frac{\partial \tilde{u}}{\partial \tilde{x}} + \frac{\partial \tilde{v}}{\partial \tilde{y}} = 0 \tag{2.5}$$

$$\frac{Be}{Pr}\left(\tilde{u}\frac{\partial \tilde{u}}{\partial \tilde{x}} + \tilde{v}\frac{\partial \tilde{u}}{\partial \tilde{y}}\right) = -\frac{\partial \tilde{P}}{\partial \tilde{x}} + \frac{\partial^2 \tilde{u}}{\partial \tilde{x}^2} + \frac{\partial^2 \tilde{u}}{\partial \tilde{y}^2} \tag{2.6}$$

$$\frac{Be}{Pr}\left(\tilde{u}\frac{\partial \tilde{v}}{\partial \tilde{x}} + \tilde{v}\frac{\partial \tilde{v}}{\partial \tilde{y}}\right) = -\frac{\partial \tilde{P}}{\partial \tilde{x}} + \frac{\partial^2 \tilde{v}}{\partial \tilde{x}^2} + \frac{\partial^2 \tilde{v}}{\partial \tilde{y}^2} \tag{2.7}$$

$$Be\left(\tilde{u}\frac{\partial \tilde{T}}{\partial \tilde{x}} + \tilde{v}\frac{\partial \tilde{T}}{\partial \tilde{y}}\right) = \frac{\partial^2 \tilde{T}}{\partial \tilde{x}^2} + \frac{\partial^2 \tilde{T}}{\partial \tilde{y}^2} \tag{2.8}$$

In equations 2.6 and 2.7, the Prandtl number, $Pr = \nu/\alpha$, is 0.71 as air is the coolant fluid used in this study, and in equations 2.6 to 2.8, the Bejan number is, $Be = \Delta PD^2/\alpha\mu$ The Bejan number is the dimensionless pressure drop number.

2.2.2 *Boundary Conditions*

The flow boundary conditions are such that there is neither slip nor penetration on the cylindrical surfaces; $\tilde{P} = 1$, $\tilde{T} = 1$, $\partial\tilde{u}/\partial\tilde{x} = \tilde{v} = 0$ at the inlet of the plane; $\tilde{P} = 0$ and $\partial(\tilde{u}, \tilde{v})/\partial\tilde{x} = 0$ at the outlet of the domain; free slip and no penetration on the horizontal surfaces of the upstream and downstream sections of the computational domain. The thermal boundary conditions are: $\tilde{T} = 1$ on the cylindrical surfaces, and $\tilde{T} = 0$ on the inlet plane of the computational domain. The remaining portions of the computational domain are adiabatic.

Angular velocity is used as a boundary condition of the cylinder walls when they are rotating, $\tilde{\omega} = \omega\mu/2\Delta P = \pm 1$, the signs denote the direction of rotation of the cylinders.

2.2.3 *Heat Transfer Rate Density*

The primary objective of this dissertation was to investigate the effect of different length scales on the heat transfer from the cylinders. The term heat transfer rate density, which is the heat transfer rate removed from the cylinder per unit volume is introduced. The heat transfer rate density is obtained by the

integration of heat flux (q''_W) around the surface of the cylinder and assuming a unit length for the cylinders:

$$q' = \frac{D}{2}\int_0^{2\pi} q''_w d\theta + \frac{d}{2}\int_0^{2\pi} q''_w d\theta \tag{2.9}$$

The volume per unit depth occupied by the numerical domain representing the geometries of the cylinders is $D(D + d + 2S)$, consequently the heat transfer rate density is

$$q''' = \frac{q'}{D(D + d + 2S)} \tag{2.10}$$

The above function is made dimensionless in the following form:

$$\tilde{q} = \frac{q'}{D(D + d + 2S)k(T - T_\infty)} \tag{2.11}$$

This is the objective function, which is to be maximised and used to determine the optimal configuration, and the effect of rotation on the heat transfer rate density and the optimal configuration.

2.3 Domain Discretisation

In this section, the numerical model used in solving the proposed problem is constructed. Afterwards, the model is verified by conducting grid independence tests and comparing specific cases against the work of others. With the model, a solver is used to solve the non-dimensionalised Navier-Stokes equations with respect to the problem in question.

Computational fluid dynamics is a numerical modelling technique that solves the Navier-Stokes and energy equations on a discretised domain. To initiate this process, the domain must be modelled after which a grid is created. The grid generation process deals with the division of the domain into smaller control volumes; this is referred to as discretisation.

In basic forms, the numerical algorithm integrates the governing equations into the control volumes. With the aid of discretisation, the integral equations are converted to algebraic equations, which are then solved iteratively (Versteeg and Malalasekera, 2007). It is in these smaller volumes that the Navier-Stokes and energy equations are solved or approximated.

A commercial automated grid generator, GAMBIT (Geometry and Mesh Building Intelligent Toolkit), which is part of Fluent™(1998), was used to generate the grid. It works with a graphical user interface in creating the grid. An important competency of GAMBIT is the ability to parameterise the

source file of the domain. This enables a quasi-automation of the grid generation by the use of journal files. These are text files that contain commands which indicate the steps to be taken in the design of the model of interest. The use of the journal files eliminates the need for the graphical user interface or the repetition involved in its usage.

Figure 2.5 and Figure 2.6 show the numerical domain of the cylinders aligned on the centreline and cylinders aligned on the leading edge in their respective meshed form. In this work and from tests conducted for the different types of meshes (triangular, quadrilateral and hybrid), it was found that the least computational expensive is the quadrilateral meshes.

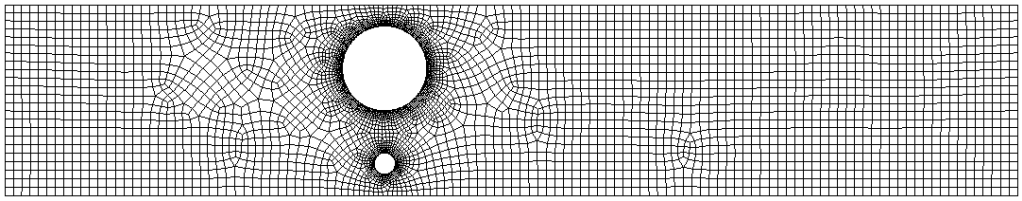

Figure 2.5 The meshed domain of centreline-aligned cylinders

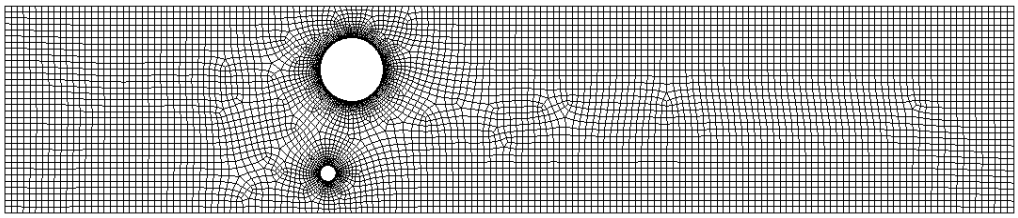

Figure 2.6 The meshed domain of leading-edge-aligned cylinders

The flow and heat transfer across the above domain were solved by using the finite volume code, FLUENT. The convection-diffusion equations were solved by means of the second-order upwind differencing scheme. The scheme was based on the backward differencing formula and used consistent forms to calculate the fluxes through the cell faces and this reduced the possibility of numerical diffusion errors (Versteeg and Malalasekera, 2007). The SIMPLE algorithm (Patankar, 1980) was employed in the solution of the pressure-velocity coupling. Convergence of the simulated runs was obtained when the normalised residuals for the mass and momentum became less than 10^{-3} and that of the energy equation less than 10^{-6}.

2.3.1 Grid Independence Study

To enable validation of the numerical model, grid independence checks were conducted. This helped in eliminating errors due to the coarseness of the grid. In terms of grid independence, the number of cells were sequentially reduced in the meshed domain until a chosen important result did not change. The key result chosen was the dimensionless heat transfer rate density and how it changed from one iteration ($\tilde{q}_i$) to the previous iteration ($\tilde{q}_{i-1}$).

2.3.1.1 Cylinders aligned on the centreline

Table 2.1: Domain independence study with $L_u = 4$, Be = 10^3 and S = 1

L_d	$\tilde{q}$	$\left\|\frac{\tilde{q}_i - \tilde{q}_{i-1}}{\tilde{q}_i}\right\|$

5	19.93	-
7	19.90	0.0015
10	19.84	0.003

Table 2.2: Domain independence study with $L_d = 7$, Be = 10^3 and S = 1

L_u	$\tilde{q}$	$\left\|\frac{\tilde{q}_i - \tilde{q}_{i-1}}{\tilde{q}_i}\right\|$
3	19.93	-
4	19.90	0.0015
5	19.83	0.0035
7	19.91	0.004

Table 2.3: Grid independence study with $L_u = 4$, $L_d = 7$, Be = 10^3 and S = 1

Nodes	Cells	$\tilde{q}$	$\left\|\frac{\tilde{q}_i - \tilde{q}_{i-1}}{\tilde{q}_i}\right\|$
4013	3864	19.90	-
6960	6692	19.64	0.013
9665	9309	19.74	0.005

From Tables 2.1 and 2.2, it follows that the upstream and downstream lengths which satisfy the criteria are at L_d and L_u equal to 7 and 4 respectively. Under these conditions the change in heat transfer rate density is less than 2%.

Table 2.3 shows that the optimal mesh density that implements the solution in the least computational time and within the criteria of satisfaction is with a mesh size of 6 692. At this mesh density, the heat transfer rate density is already less than 2%. In subsequent sections, this chosen numerical domain is used in solving flow fields and heat transfer, which are compared with results found in literature.

2.3.1.2 Cylinders aligned on the leading edge

Tables 2.4 and 2.5 show the domain independence tests used in arriving at the upstream and downstream length used. The upstream length of the domain at which changes in the value of the heat transfer rate density are less than 2% is seen to be at a value of five times the characteristic length of the bigger cylinder; while the downstream distance at which the change in heat transfer rate density of the cylindrical array is less than 2% is obtained at 10 times the characteristic length of the bigger cylinder. These values are therefore assumed sufficient for the boundaries of the numerical domain.

Table 2.4: Domain independence study with L_d = 10, Be = 10^3 and S = 1

L_u	$\tilde{q}$	$\left\lvert \frac{\tilde{q}_i - \tilde{q}_{i-1}}{\tilde{q}_i} \right\rvert$
5	16.25	-
7	16.23	0.0017
9	16.21	0.0057

Table 2.5: Domain independence study with $L_u = 5$, $Be = 10^3$ and $S = 1$

L_d	$\tilde{q}$	$\left\|\frac{\tilde{q}_i - \tilde{q}_{i-1}}{\tilde{q}_i}\right\|$
8	16.26	-
10	16.25	0.0017
12	16.21	0.0057
15	16.17	0.0032

2.4 Summary

Some background to the numerical method used in investigating this work was given, this includes the governing equations necessary for solving the thermodynamic features around the cylindrical array and for obtaining the optimal spacing, which gives the maximum heat transfer rate density.

The main geometric parameters were also identified by means of the grid independence study and although this was performed for stationary cylinders, it is the assumption in this work that the results stay the same in the case where rotation is included.

Chapter 3 CYLINDERS ON THE SAME CENTRELINE

3.1 Procedure for multiscale cylinder on the same centreline

In this chapter, the first configuration of the array of cylinders, c.f Figure 2.1, is investigated with respect to the optimal non-dimensional smaller cylinder diameter ($\tilde{d}_{opt}$). The configuration is such that the cylinders are placed on the same centreline. The motivation for this case is to obtain the maximum heat transfer possible with two degrees of freedom, that is the spacing between the cylinders and the diameter of the smaller cylinder.

The optimal configurations obtained are those that produce the maximum amount of heat that can be dissipated from the array under the constraint of fixed dimensionless pressure drop numbers. Four different diameters are compared under stationary conditions and at different Bejan numbers, in the range of $10 \leq Be \leq 10^4$.

Figure 3.1 to Figure 3.5 graphically show the effect of the different diameters and the spacing on the maximum heat transfer rate density which was obtained from the numerical domain.

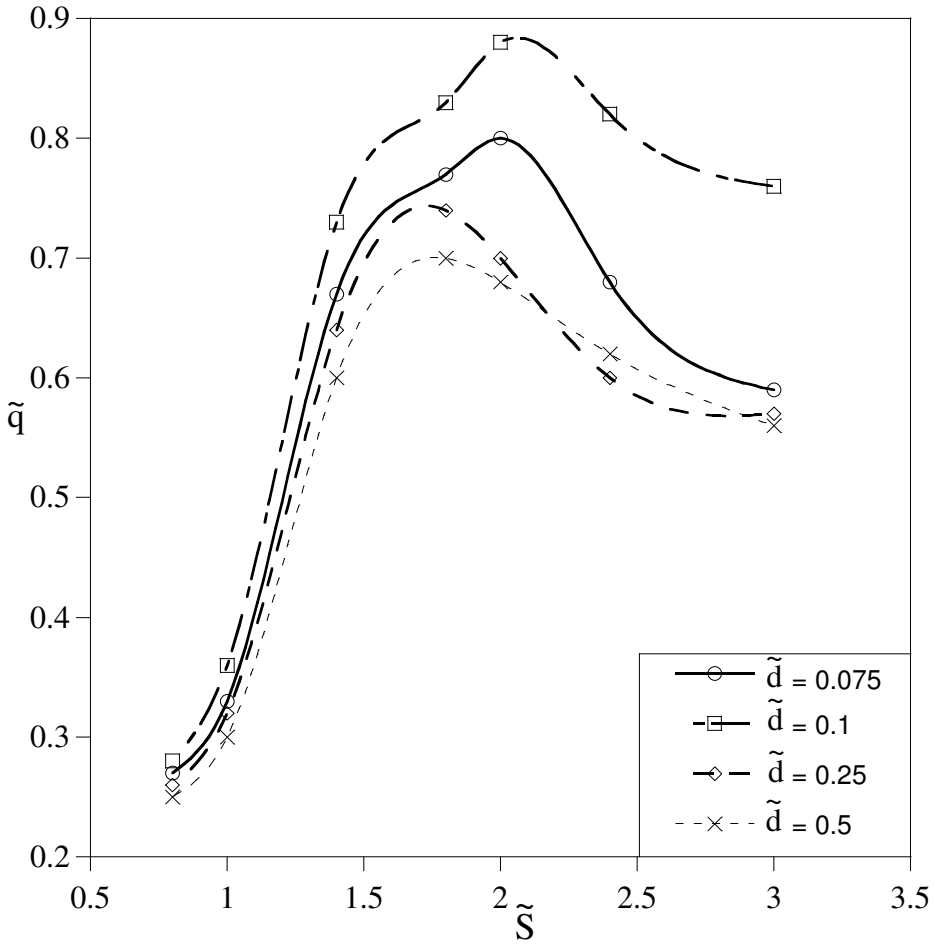

Figure 3.1 Variation of heat transfer rate density at Be = 10

Figure 3.1 shows the result from a simulation run at Be = 10, the optimal diameter of the smaller cylinder and the spacing, which gives the maximum heat transfer rate density from the stationary array as $\tilde{d} = 0.1$ and $\tilde{S} = 2.15$.

Figure 3.2 to Figure 3.5 show the optimal diameter and the corresponding spacing between the cylinders, which gives the highest heat transfer rate density. The optimal diameter is fairly constant for the range of $10^2 \leq \text{Be} \leq 10^4$. The optimal diameter, $\tilde{d}_{opt}$ is equal to 0.5 and the optimum

spacing, $\tilde{S}_{opt}$ varies from 1.2 for a Bejan number of 100 to 0.43 for a Bejan number of 10^4.

The result observed at Be = 10 is different from the overall trend and this can be attributed to the slow flow and consequently thick boundary layer that happens in such flows. Thus the optimal smaller cylinder diameter of 0.5 is used as the test case to determine the effect of rotation on the heat transfer from the heated array of cylinders. This is based on the assumption that the optimal smaller cylinder diameter in the stationary configuration is also the optimal diameter in the case where rotation is applied to the cylinders. It also reduces the parameters of the study to a manageable extent while allowing a clear comparison between the case of stationary cylinders and rotating cylinders to be conducted.

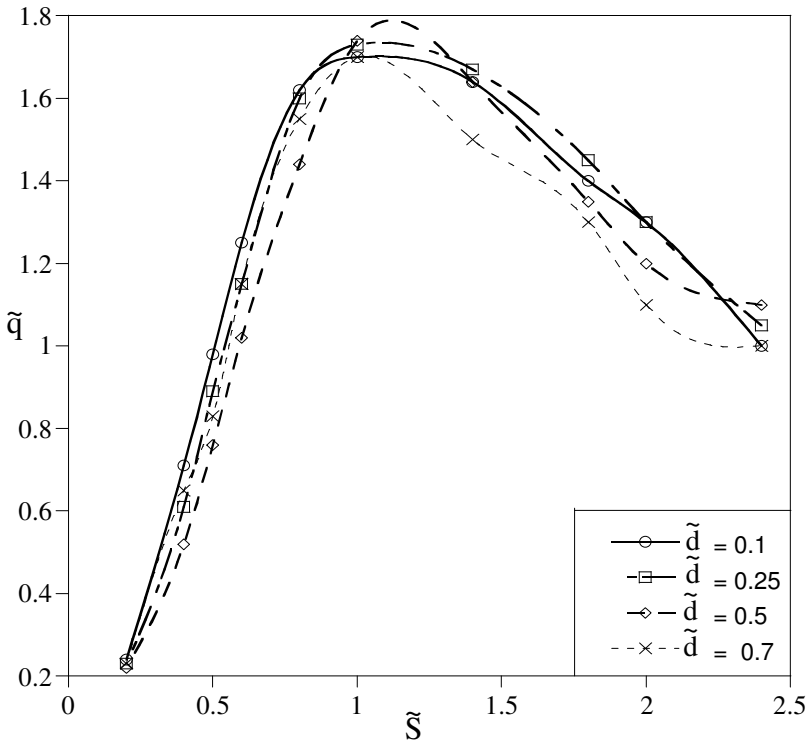

Figure 3.2 Variation of heat transfer rate density at Be = 10^2

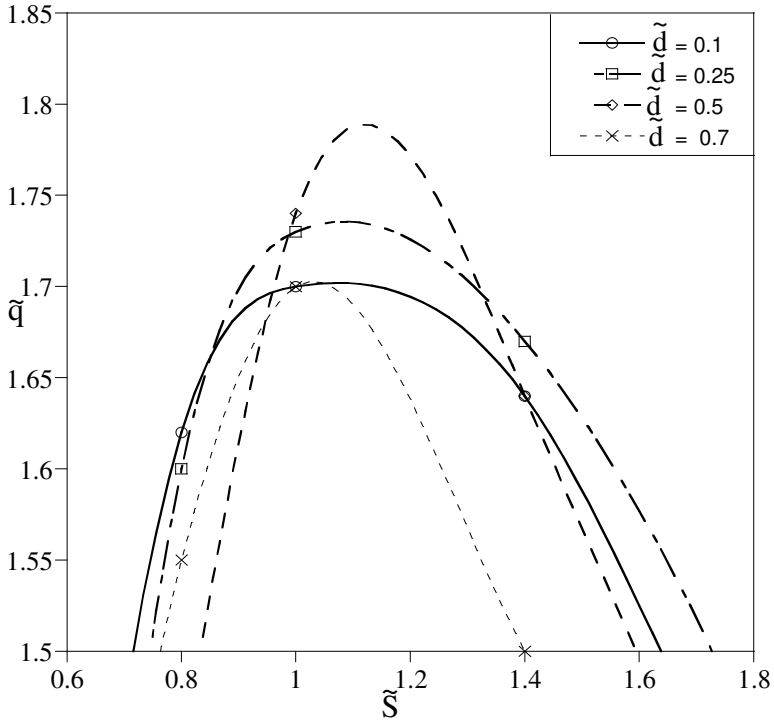

Figure 3.3 Close-up view of Figure 3.2

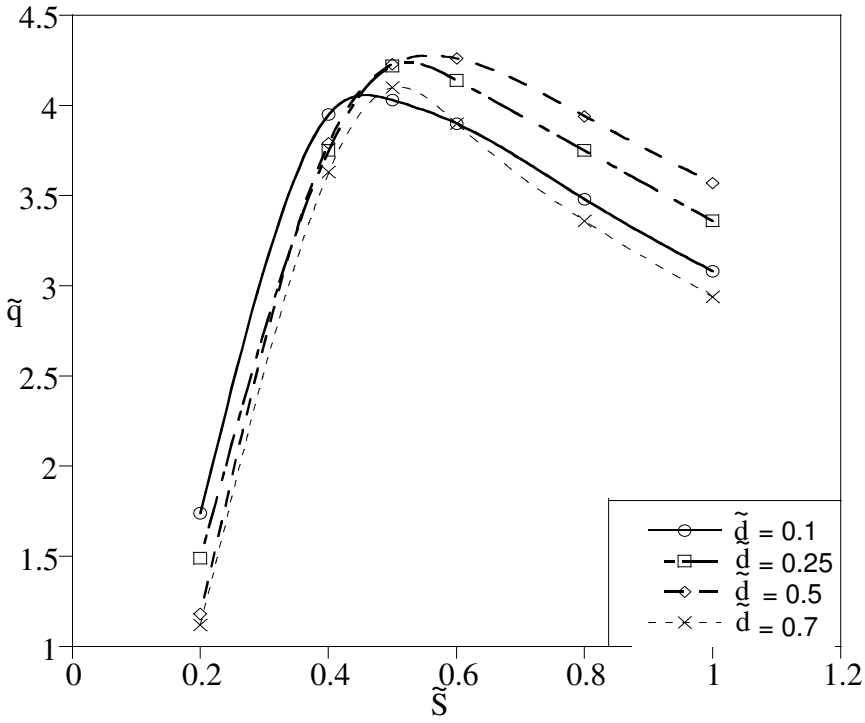

Figure 3.4 Variation of heat transfer rate density at Be = 10^3

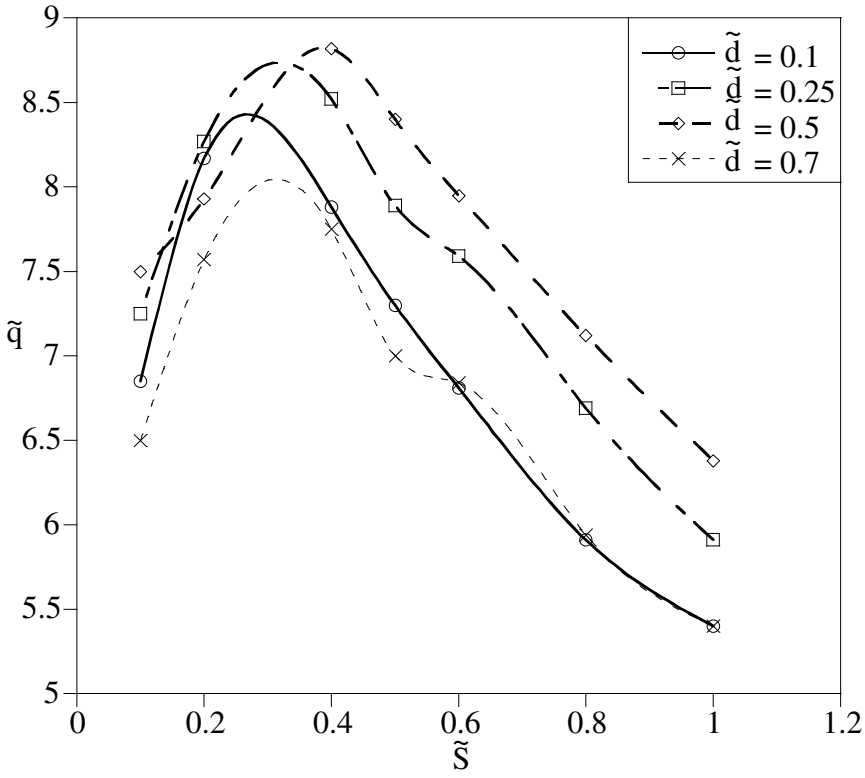

Figure 3.5 Variation of heat transfer rate density at Be = 10^4

3.2 Optimal Configuration for Stationary Cylinders

The results obtained from Section 3.1 and Figures 3.1 to 3.5 are summarised and shown in Figure 3.6. As the Bejan number increases from 10 to 10^4, the optimal spacing, $\tilde{S}$, between the cylinders drops from 2.15 to 0.43. However, with the optimal diameter, $\tilde{d}_{opt}$, although it increases from 0.1 to 0.5 as the Bejan number increases from 10 to 100, the optimal spacing remains constant ($\tilde{d}_{opt} = 0.5$) if the Bejan number is equal or larger than 100. This is in agreement with the results by Bejan and Morega (1993):

"The optimum heat transfer is obtained at the point where the thermal boundary layers of the structure just touch each other."

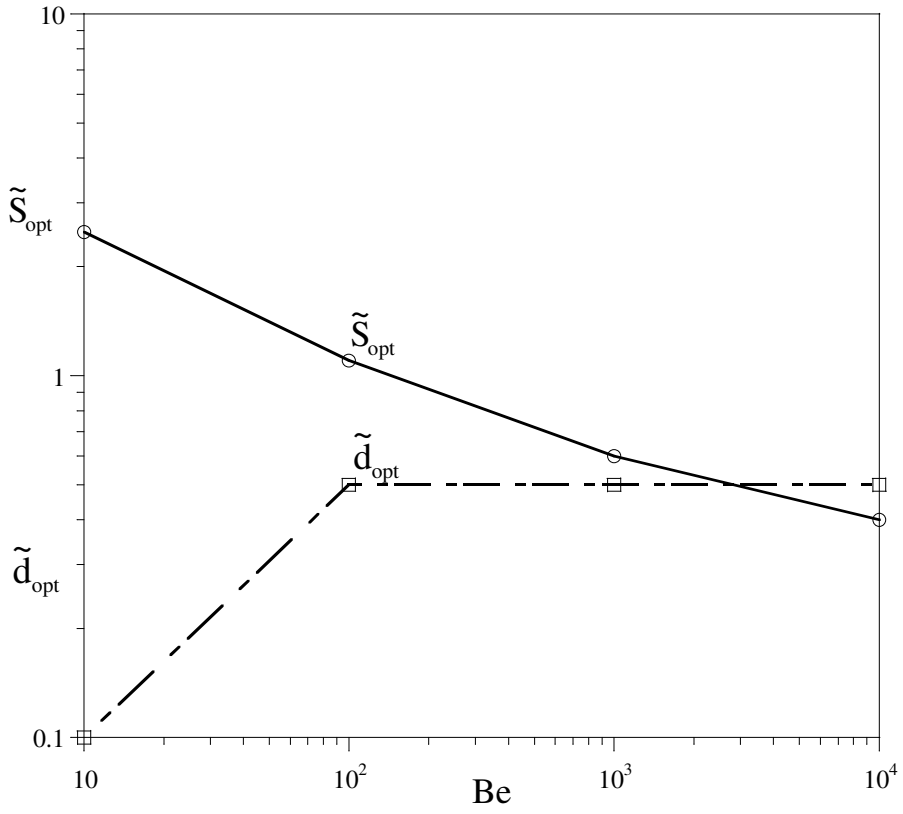

Figure 3.6 Optimal spacing between cylinders with respect to the pressure drop number for $\tilde{d}_{opt} = 0.5$

In the range of $10 \leq Be \leq 10^4$, the optimal spacing can be correlated as:

$$\tilde{S}_{opt} = 2.99Be^{-0.22} \qquad 10 \leq Be \leq 10^4 \tag{3.1}$$

Another trend observed from Figure 3.7, shows the effect of the Bejan number on the maximum heat transfer from the array of cylinders. As the Bejan number increases, there is a commensurate increase in the maximum heat transfer rate density. The relationship between the heat transfer rate density and the Bejan number is correlated as:

$$\tilde{q}_{max} = 0.32Be^{0.37} \qquad 10 \leq Be \leq 10^4 \qquad (3.2)$$

This trend is similar in all cases of the smaller diameter cylinder considered.

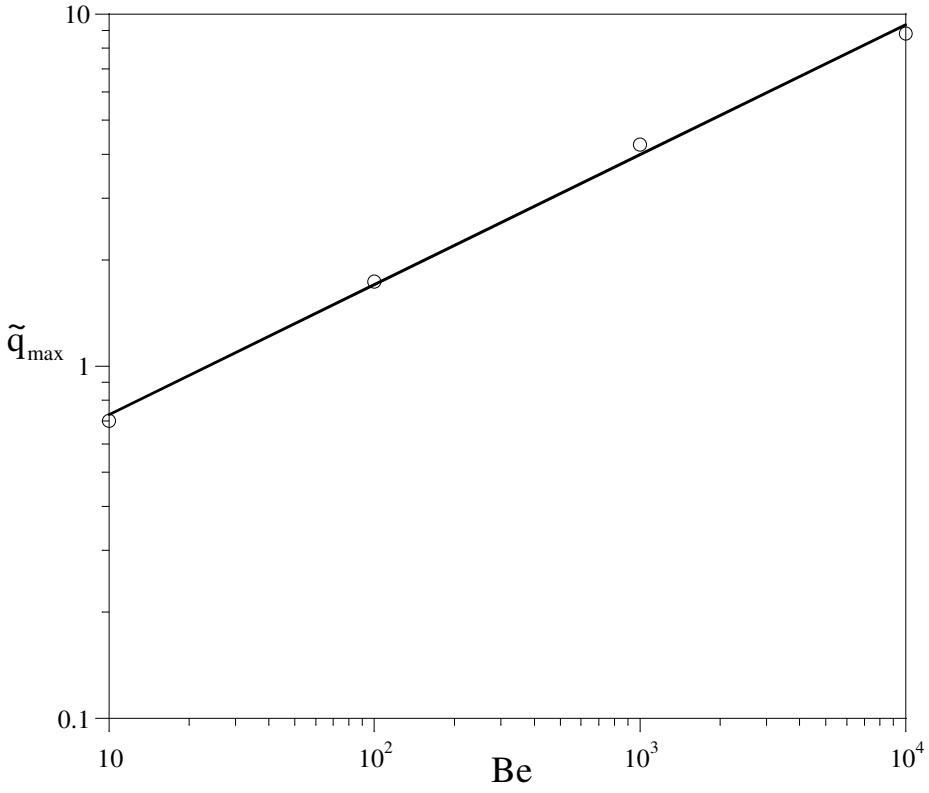

Figure 3.7 Maximum heat transfer rate density from the stationary array for different cases of the pressure drop number

3.3 Effects of Rotation on the Cylinders

In Section 3.2, the optimal diameter of the smaller cylinder was determined from the model shown in Figure 2.1. In order to improve the heat transfer rate density, rotation of the cylinders was introduced into the simulation while keeping the diameter of the smaller cylinder constant at $\tilde{d}_{opt} = 0.5$. In this section, the effects of rotation on the heat transfer rate density are considered.

3.3.1 Co-rotation

Figure 3.8 shows that an optimal spacing exists when the cylinder are co-rotating for the dimensionless pressure drop of Be = 10^3. The figure also shows that in the range of $0 \leq \tilde{\omega} \leq 0.1$, the angular velocity $\tilde{\omega} = 0.01$ gives the highest heat transfer rate density.

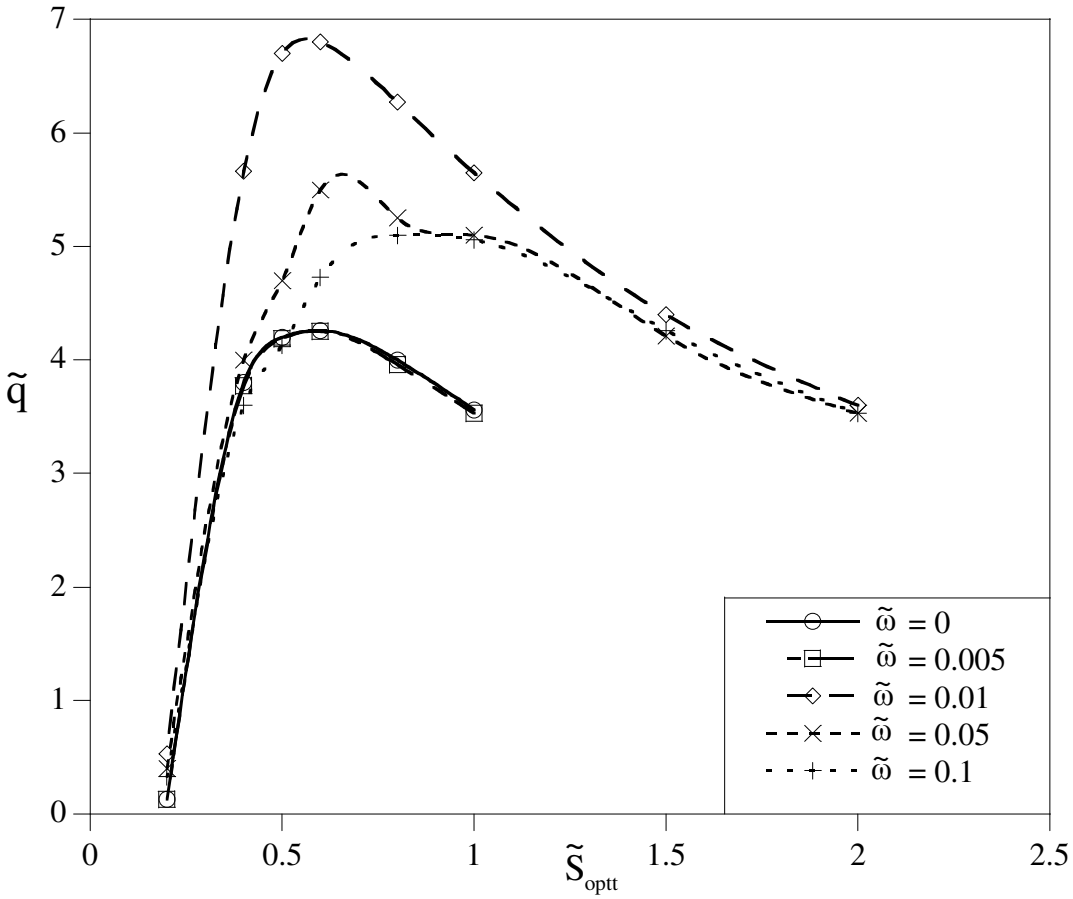

Figure 3.8 Heat transfer rate density and spacing of co-rotating cylinders compared with stationary cylinders at Be = 10^3

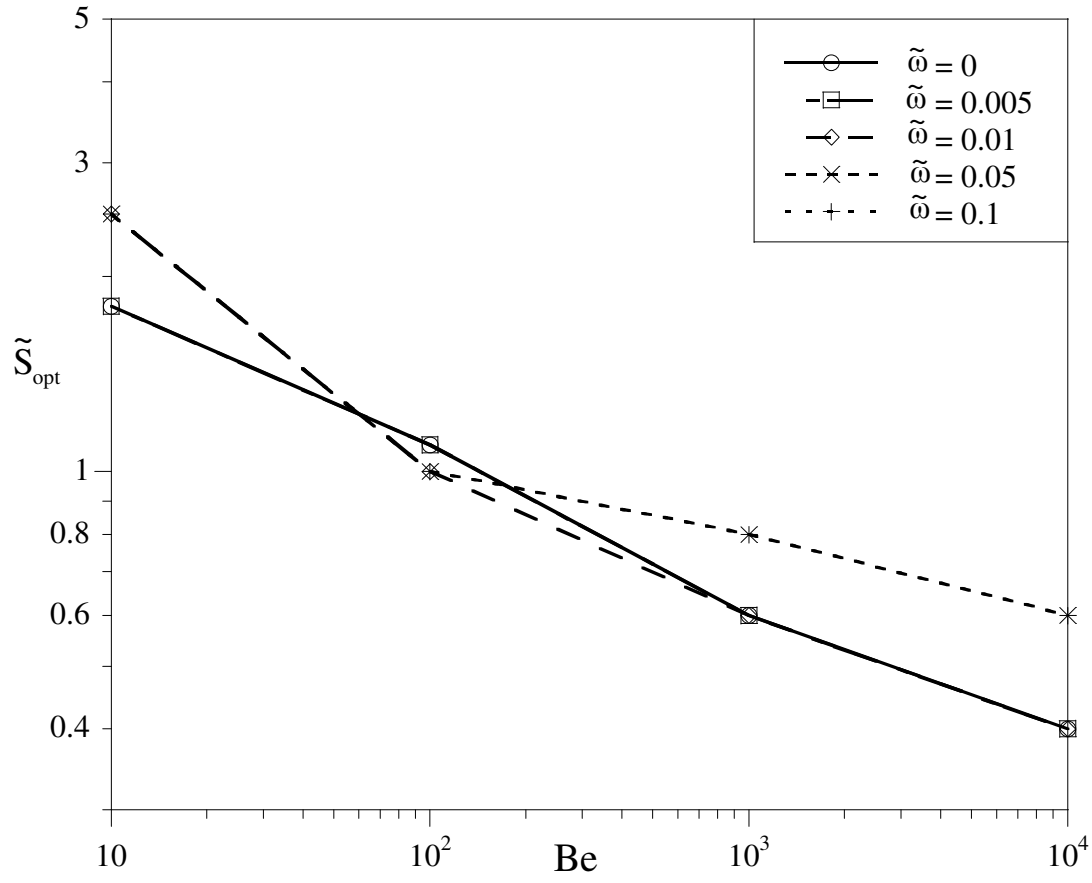

Figure 3.9 Optimal spacing for co-rotating cylinders

Figure 3.9 shows the summary of the results obtained for the optimal spacing between the cylinders in the range of $10 \leq Be \leq 10^4$ and for $\tilde{d}_{opt} = 0.5$. The result shows that as the dimensionless pressure drop number increases, the spacing between the cylinder decreases for rotational velocity in the range of $0 \leq \tilde{\omega} \leq 0.1$.

The trend is the same for all the rotational velocities, and the optimal spacing is of the same order of magnitude.

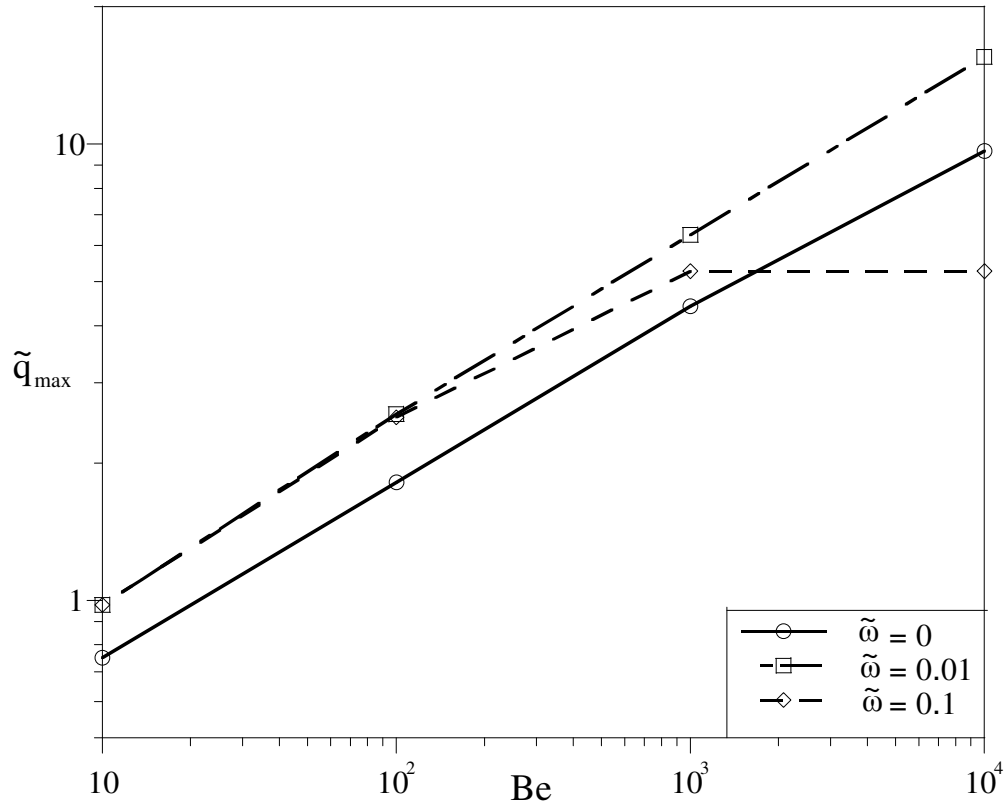

Figure 3.10 Heat transfer rate density of co-rotating cylinders compared with stationary cylinders

Figure 3.10 shows the maximum heat transfer rate density obtained in the range of $10 \leq Be \leq 10^4$. From the figure, two particular cases of angular velocity are considered against the stationary configuration, that is $\tilde{\omega}$ equals 0.01 and 0.1. It shows that as the dimensionless pressure drop number increases, the heat transfer rate density also increases. The trend is the same for all rotational velocities considered. In the region $10 \leq Be \leq 10^3$, the results show that rotating the cylinder in co-rotational mode results in an increase in heat transfer over a stationary cylinder, ($\tilde{\omega} = 0$). In the range of 10^3 to 10^4, rotation of cylinders is only beneficial at $\tilde{\omega} = 0.01$. In this range, there is heat transfer suppression when the rotational velocity, $\tilde{\omega}$, is equal to 0.1 and this

can be attributed to the thermal fluid creating a wall around the cylinder and thus acting as a form of insulation against the possible transfer of heat.

It can therefore be concluded that the optimal rotational velocity for co-rotation is $\tilde{\omega}_{opt} = 0.01$. The optimal spacing between the cylinders from Figure 3.9 for the case where $\tilde{\omega} = 0.01$ is correlated by:

$$\tilde{S}_{opt} = 3.95Be^{-0.26} \qquad 10 \leq Be \leq 10^4 \tag{3.3}$$

And the maximum heat transfer for the case where $\tilde{\omega} = 0.01$, as shown in Figure 3.10, can be correlated as:

$$\tilde{q}_{max} = 0.39Be^{0.4} \qquad 10 \leq Be \leq 10^4 \tag{3.4}$$

3.3.2 Counter-rotation

In this section, the effect of counter-rotating the cylinders on the heat transfer rate density is studied. Figure 3.11 shows that an optimum exists for a case where $Be = 10^3$. The figure shows that counter-rotation does increase the heat transfer rate density. From the figure, it can further be seen that the highest heat transfer rate density is obtained when $\tilde{\omega} = 0.01$. It can be deduced that the optimal rotation is obtained when $\tilde{\omega} = 0.01$ for $\tilde{d}_{opt} = 0.5$.

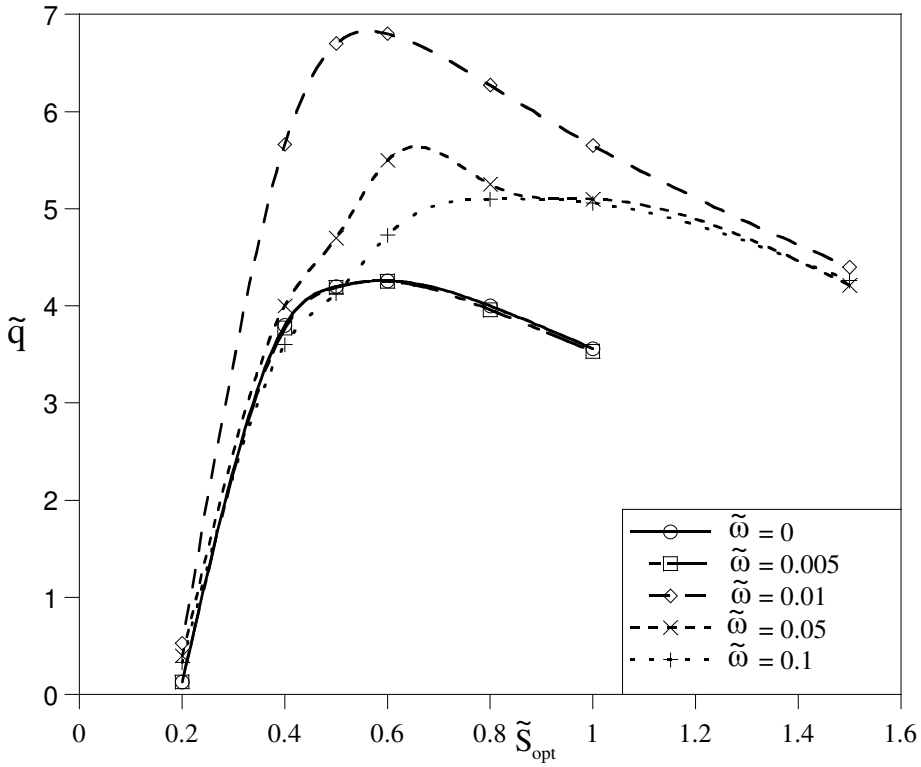

Figure 3.11 Heat transfer rate density and spacing of counter-rotating cylinders compared with stationary cylinders at Be = 10^3

Figure 3.12 shows the optimal spacing between the cylinders in the range of $10 \leq \mathrm{Be} \leq 10^4$, the trend is similar to the case of co-rotating cylinders. It is observed that as the pressure drop number increases, the optimal distance between the cylinders decreases. In the range of $10^3 \leq \mathrm{Be} \leq 10^4$, the graph of optimal spacing at $\tilde{\omega} = 0$ and $\tilde{\omega} = 0.01$ coalesces. This means that at a higher Be, the optimal spacing is not affected by rotation.

Figure 3.13 shows the heat transfer rate density in the range of $10 \leq \mathrm{Be} \leq 10^4$. The behaviour is similar to what is observed for the case of co-rotation where rotating the cylinders produces a better heat transfer and this trend is only

broken in the range of $10^3 \leq Be \leq 10^4$, when the cylinders are rotating at $\tilde{\omega} = 0.1$. At this point, the heat transfer rate remains constant and becomes smaller than the heat transfer of the stationary cylinder array. Similar reasoning as co-rotation could be proposed for the case of counter-rotation in which thermal boundary layer is observed around the rotating cylinder and could be attributed to the insulating effect on the cylinders.

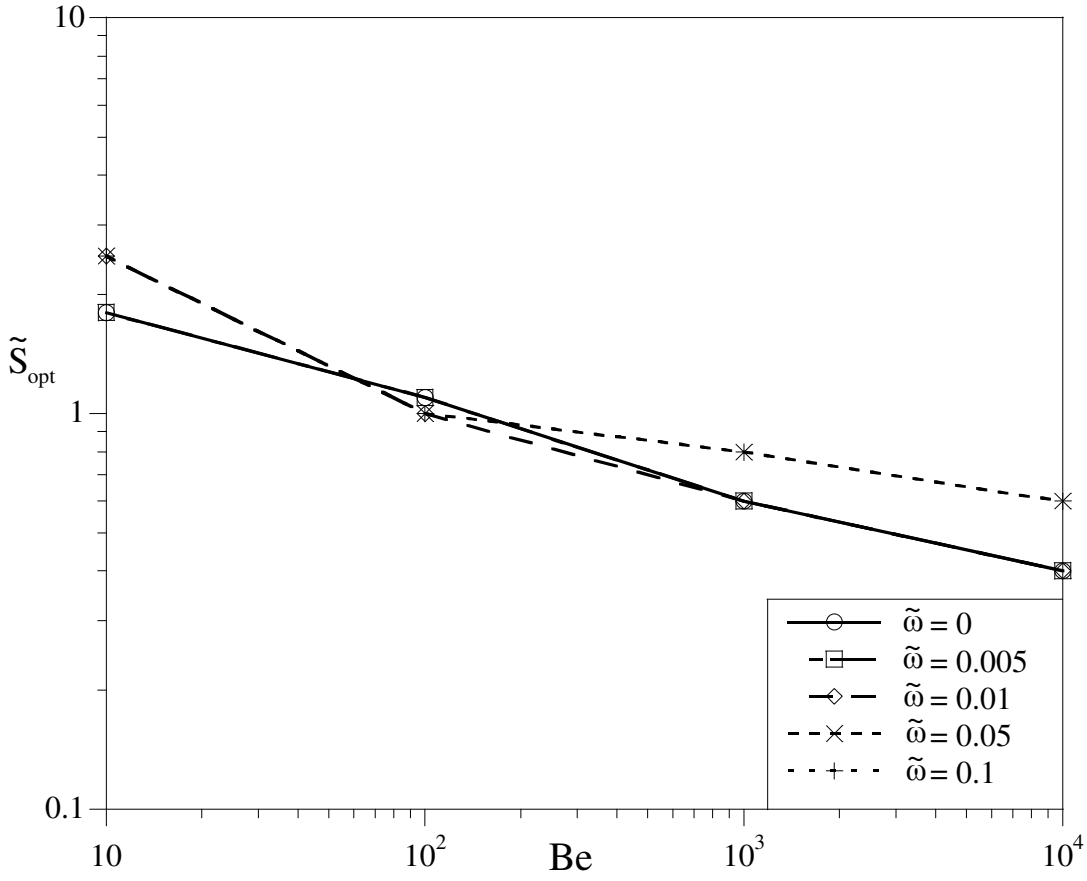

Figure 3.12 Optimal spacing for counter-rotating cylinders

Figures 3.8 to 3.13 lead to the conclusion that angular rotation is at its optimum when it is approximately equal to 0.01 for $\tilde{d}_{opt} = 0.5$, and at this

velocity there is an improvement in the heat transfer rate density but the optimal spacing between the cylinders remains the same.

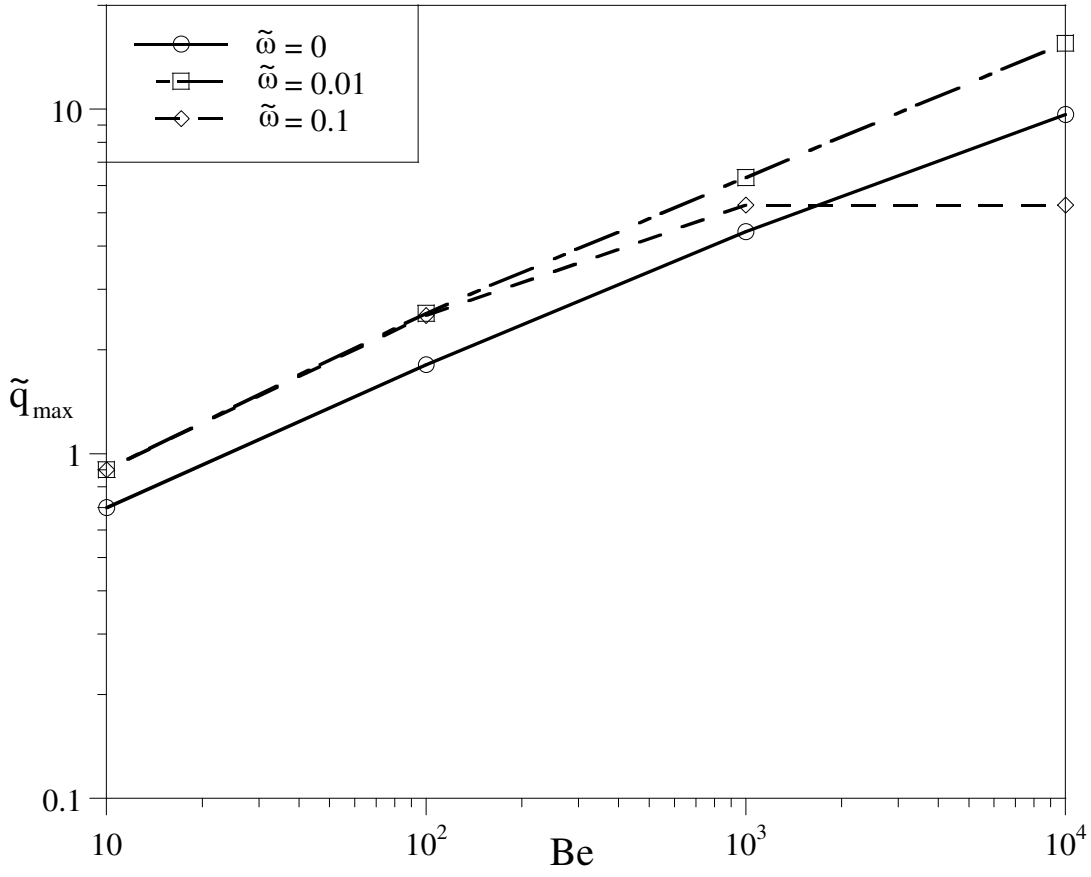

Figure 3.13 Counter-rotation compared with stationary cylinders

The optimal spacing for the case where $\tilde{\omega} = 0.01$ is correlated by:

$$\tilde{S}_{opt} = 3.95Be^{-0.26} \qquad 10 \leq Be \leq 10^4 \tag{3.5}$$

and the maximum heat transfer is correlated by:

$$\tilde{q}_{max} = 0.39Be^{0.4} \qquad 10 \leq Be \leq 10^4 \tag{3.6}$$

The above correlations are the same as those obtained when the cylinders are co-rotating, this means that no major difference is observed between the

different modes of rotation for the case where the cylinders are located on a plane across their centrelines.

This effect is also depicted in the temperature contours, shown in Appendix A, where it is seen that with increased rotation the heated fluid tends to encapsulate the cylinder and forms a boundary insulation which reduces the potential amount of heat that can be carried away from the cylinders.

3.4 Summary

In this chapter, numerical simulations were conducted for cylinders which were aligned on their centreline. The smaller cylinder diameter was first optimised and $\tilde{d} = 0.5$ was found to be the diameter which provided the highest heat transfer rate density in the range of $10^2 \leq Be \leq 10^4$. Results show that the maximum heat transfer rate density of cylinders rotating at $\tilde{\omega} = 0.01$ is higher than that of stationary cylinders in the range of $10 \leq Be \leq 10^4$, while cylinders rotating at $\tilde{\omega} = 0.1$ result in a higher heat transfer rate only in the range of $10 \leq Be \leq 10^3$ after which the heat transfer remains constant. This trend is the same for both co-rotating and counter-rotating cylinders.

Chapter 4 CYLINDERS ON THE SAME LEADING EDGE

4.1 Introduction

This chapter studies the heat transfer from an array of cylinders in which both cylinders are aligned on their leading edge. The smaller cylinder is therefore less affected by the heated fluid of the bigger cylinder as compared with the case where all the cylinders are on the same centreline as was considered in Chapter 3.

Simulations are carried out in the Bejan number range of 10 to 10^4. This is firstly done for stationary cylinders. Numerical experiments are then conducted to determine the effect of rotation on the co-rotating and counter-rotating cylinders, with the optimal diameter of the smaller cylinder chosen from the results obtained for the stationary cylinder.

Figures 4.1 to 4.5 show the optimal spacing, optimal diameter and the corresponding maximum heat transfer density for the dimensionless pressure drop number in the range of $10 \leq Be \leq 10^4$. It can be noted, cf. Figure 4.8, that as the dimensionless pressure drop number, Be, increases the optimum spacing decreases.

Figure 4.1 shows that the maximum heat transfer rate density is 0.84 and this was obtained at an optimal spacing, $\tilde{S}_{opt} = 2.5$.

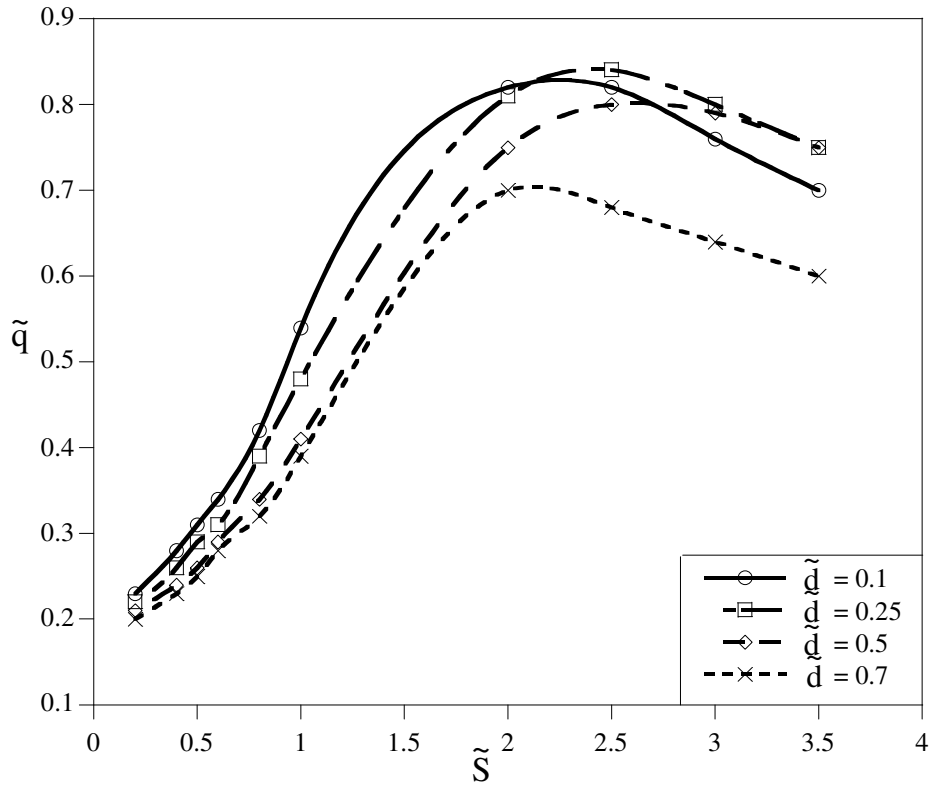

Figure 4.1 Heat transfer rate density from various smaller diameter ratios at Be = 10

Furthermore, when the Bejan number is increased to 10^2 at Figure 4.2, the maximum heat transfer rate density is 2.8 with an optimal cylinder-to-cylinder spacing of 1.4. Figures 4.3 and 4.5 show the maximum heat transfer rate density to be 7.1 and 16.75 respectively and the optimal spacing corresponding to these is 0.44 and 0.25 respectively.

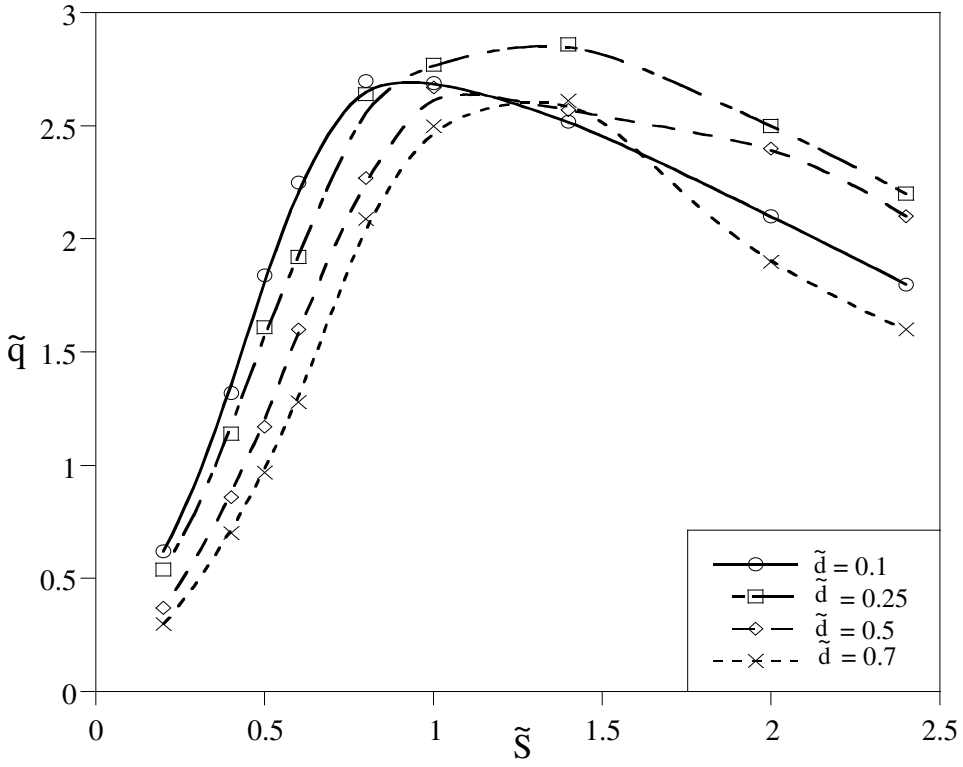

Figure 4.2 Heat transfer rate density at Be = 10^2

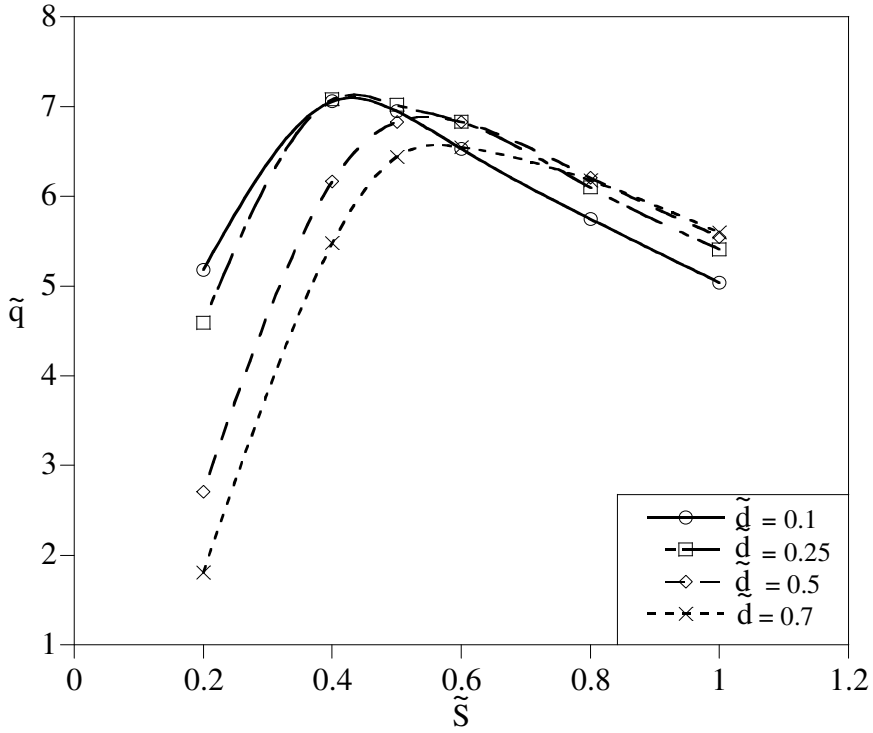

Figure 4.3 Heat transfer rate density at Be = 10^3

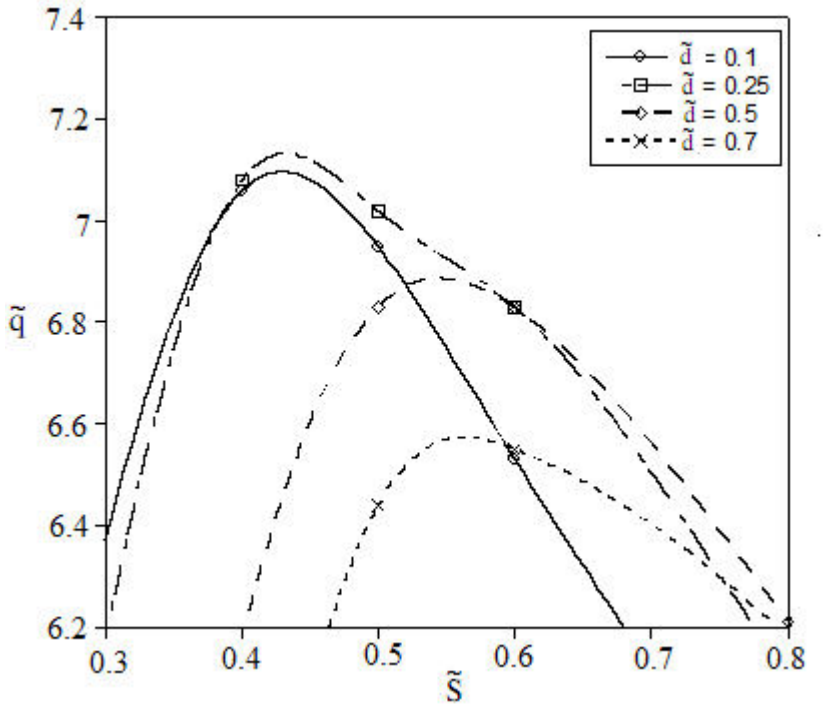

Figure 4.4 Expanded view of Figure 4.3

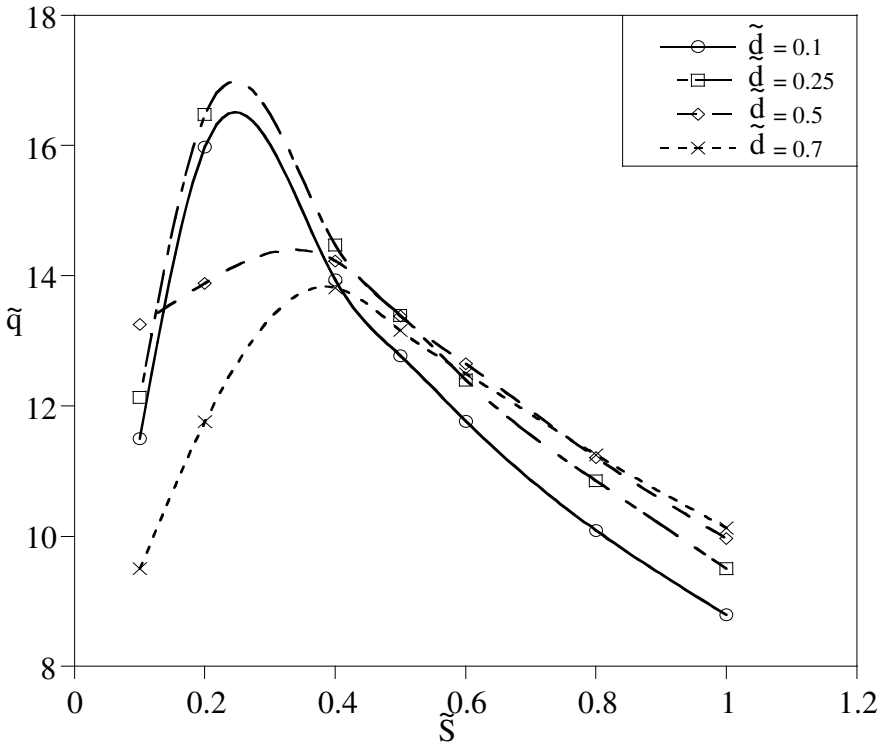

Figure 4.5 Heat transfer rate density from various smaller diameter ratios at Be = 10^4

In the range of figures considered (Figures 4.1 to 4.5) the maximum heat transfer rate density for the range $10 \leq \mathrm{Be} \leq 10^4$ is all obtained from the cylindrical array with an optimal smaller cylinder diameter, $\tilde{d}_{opt}$, of 0.25. This means the effect of Be on the optimal diameter for the smaller cylinder is insignificant and thus the optimal smaller cylinder diameter can be said to be independent of the Bejan number.

4.2 Optimisation Procedure for Stationary Cylinders on the same Leading Edge

This section optimises the diameter of the smaller cylinder, similar to the process carried out for cylinders which are located on the same centreline.

As investigated in Chapter 3, two degrees of freedom are optimised, the smaller cylinder diameter and the spacing between the cylinders, and the heat transfer rate density from the array of cylinders is the objective function, which is maximised.

Figure 4.6 shows the result obtained from the simulation when the cylinders are stationary. For brevity, the results are summarised in the range of $10 \leq \mathrm{Be} \leq 10^4$ and $0.1 \leq \tilde{d} \leq 0.7$. The optimal diameter is fairly constant and robust with respect to the dimensionless pressure drop number, and the

optimal diameter, $\tilde{d}_{opt}$ = 0.25. This result is also in agreement with the result obtained by Bello-Ochende and Bejan (2004).

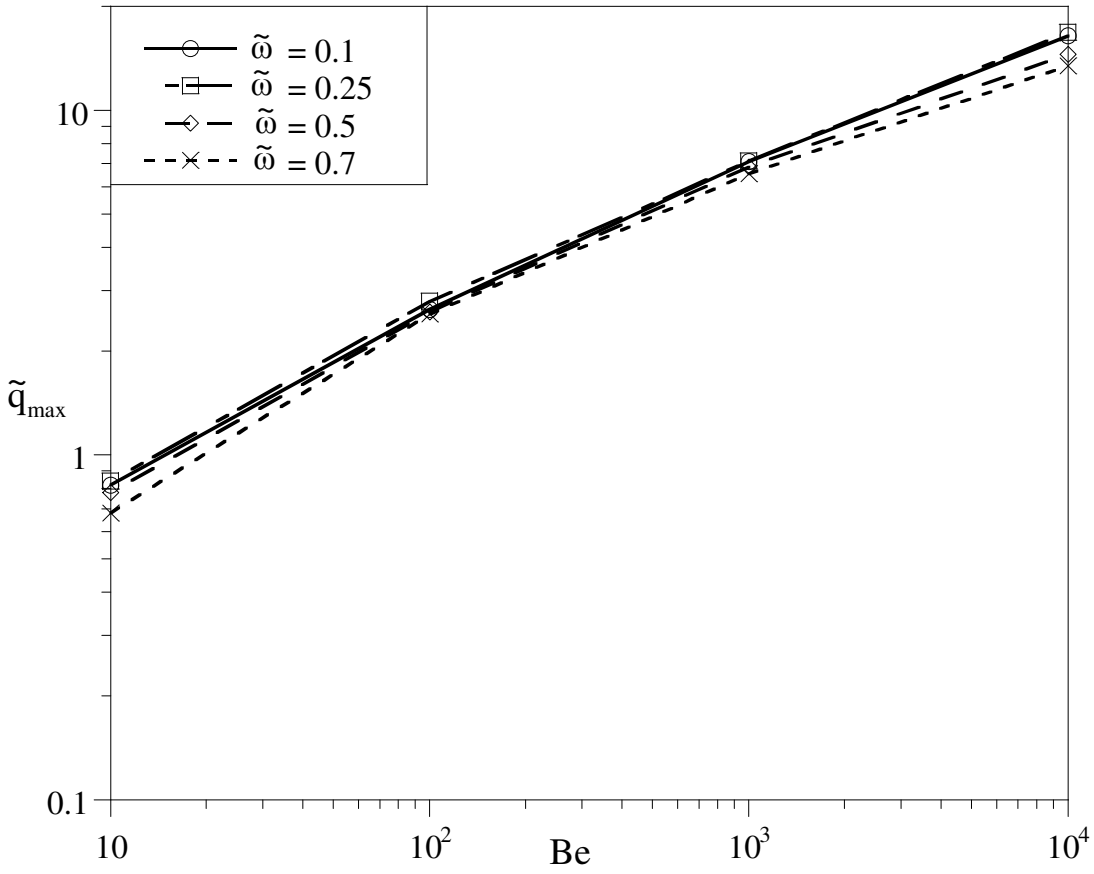

Figure 4.6 Optimal smaller cylinder diameter

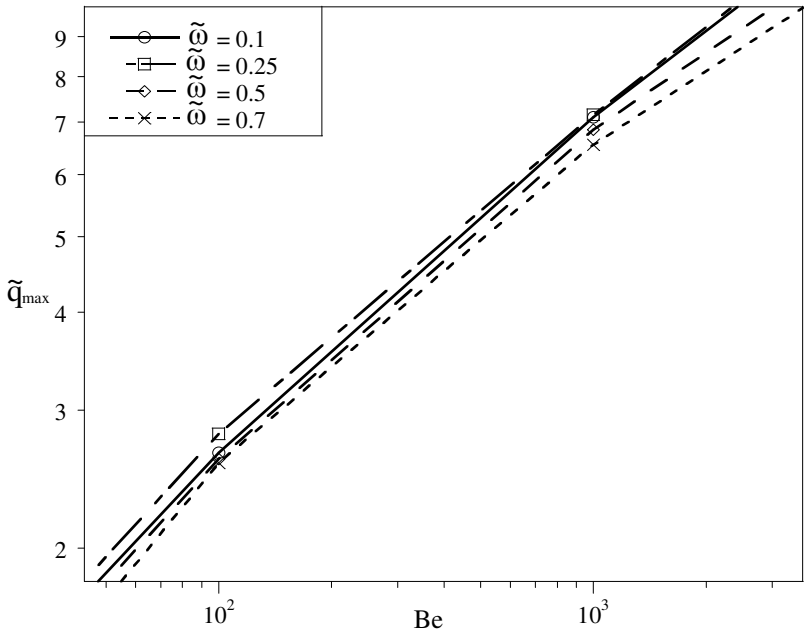

Figure 4.7 Close-up view of Figure 4.6

From the simulations conducted, it is observed that the optimal diameter of the smaller cylinder is 0.25, this consistently provides a higher heat transfer than the other values, in the range of $0.1 \leq \tilde{d} \leq 0.7$ simulated. The optimal diameter of the smaller cylinder, $\tilde{d}_{opt} = 0.25$ is independent of the Bejan number.

4.3 Optimisation of the Stationary Array of Cylinders

The optimisation in this section is done with respect to the optimal diameter, $\tilde{d}_{opt} = 0.25$. This is conducted under stationary conditions and allows comparison with literature. This section summarises the results obtained from Section 4.1 and 4.2, that is, the optimal configuration for stationary cylinders.

Figure 4.8 shows the optimal spacing between the cylinders as well as the optimal diameter of the smaller cylinder as a function of the dimensionless pressure drop number. The trend shows that as Be increases, the optimal spacing decreases and the optimal diameter for the smaller cylinder is invariant with Be. Figure 4.9 indicates that as the dimensionless pressure drop number increases, the maximum heat transfer rate density also increases.

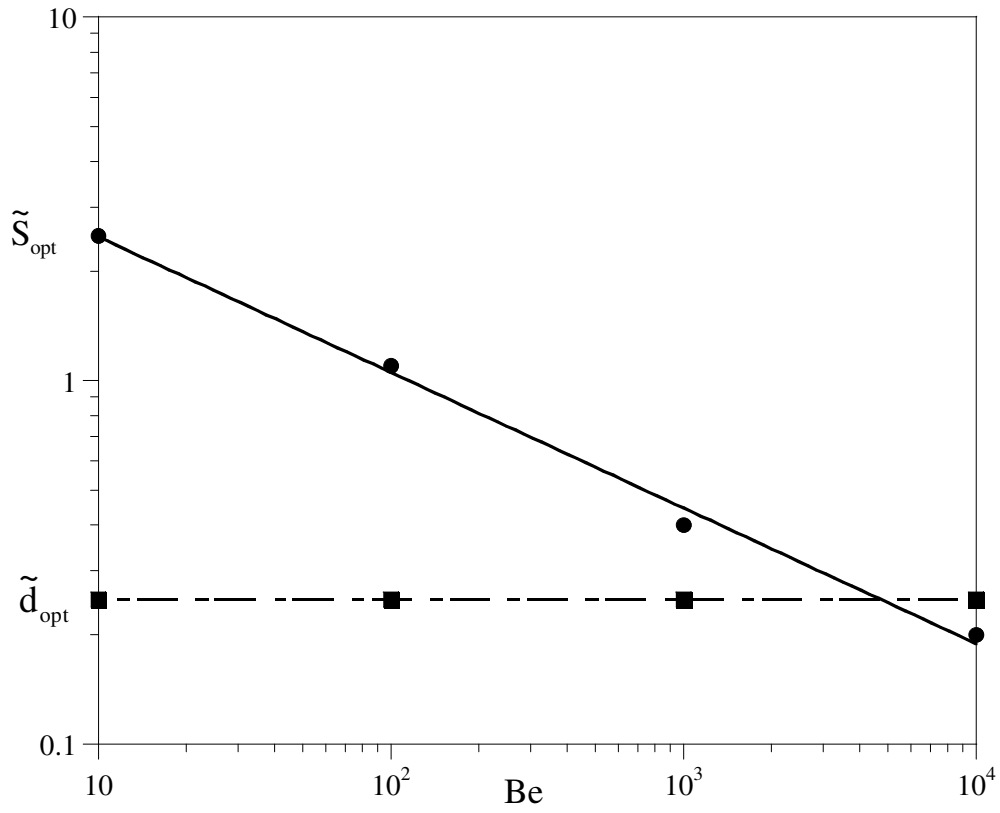

Figure 4.8 Optimal spacing of stationary cylinders with optimal smaller cylinder diameter

From Figure 4.8, the relationship between the optimal cylinder spacing can be correlated by:

$$\tilde{S}_{opt} = 6.85\,Be^{-0.39} \qquad 10 \leq Be \leq 10^4 \tag{4.1}$$

And from Figure 4.9, the maximum heat transfer rate density can be correlated as:

$$\tilde{q}_{max} = 0.34Be^{0.43} \qquad 10 \leq Be \leq 10^4 \tag{4.2}$$

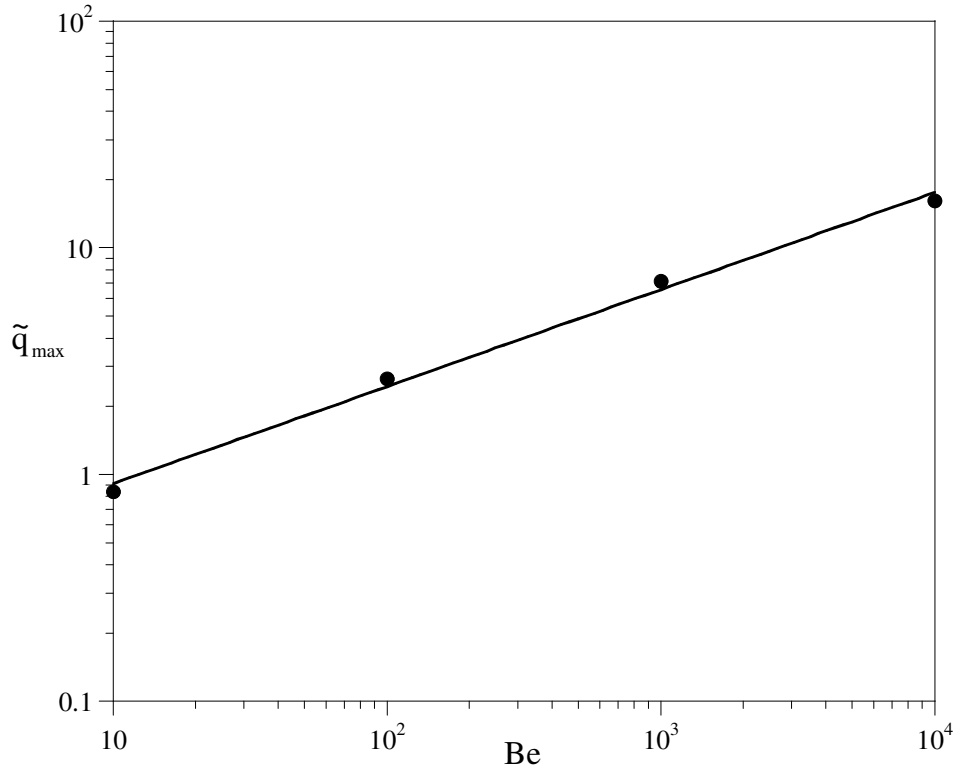

Figure 4.9 Maximum heat transfer rate density for the array of stationary cylinders

The results displayed in Figure 4.9 are similar to what is obtained with cylinders located on the centreline (Figure 3.7). The difference is that the spacing between the cylinders aligned on the leading edge is smaller than the spacing obtained for cylinders on the same centreline. The cylinders located at the leading edge are therefore more compact than the cylinders located on the centreline.

4.4 Effects of Rotation

This section deals with the effect of rotation on cylinders aligned on the leading edge. The previous section dealt with the determination of the optimal diameter of the smaller cylinder in relation to the bigger cylinder whose diameter was used as the characteristic length scale. Based on the choice of the optimal smaller cylinder diameter of $\tilde{d}_{opt}$ as 0.25 obtained from stationary cylinders on the leading edge, this is used to simulate the rotational effect on heat transfer rate density.

4.4.1 Co-Rotation

The cylinders are rotated in the same direction; this is similar to the study conducted in Section 3.3.1 for cylinders which are located on a plane that cuts across their centreline. The configuration of the cylinders in this case enables detailed comparison with results obtained from the stationary configuration of Bello-Ochende and Bejan (2004) and Joucaviel et al. (2008).

Figure 4.10 shows the heat transfer and the optimal spacing obtained at Be = 10^3. Co-rotation provides minimal improvement in heat transfer. This is observed when the angular velocity, $\tilde{\omega}$, is 0.01. And when the angular velocity is 0.1, there is a suppression of heat transfer. This is due to the surrounding thermal boundary layer around the cylinder, which is a result of rotation

(Chiou and Lee, 1993) and is a form of insulation, which limits the heat transfer from such cylinder. Figure 4.10 also shows that co-rotation of the cylinder does not produce a significant enhancement of heat transfer.

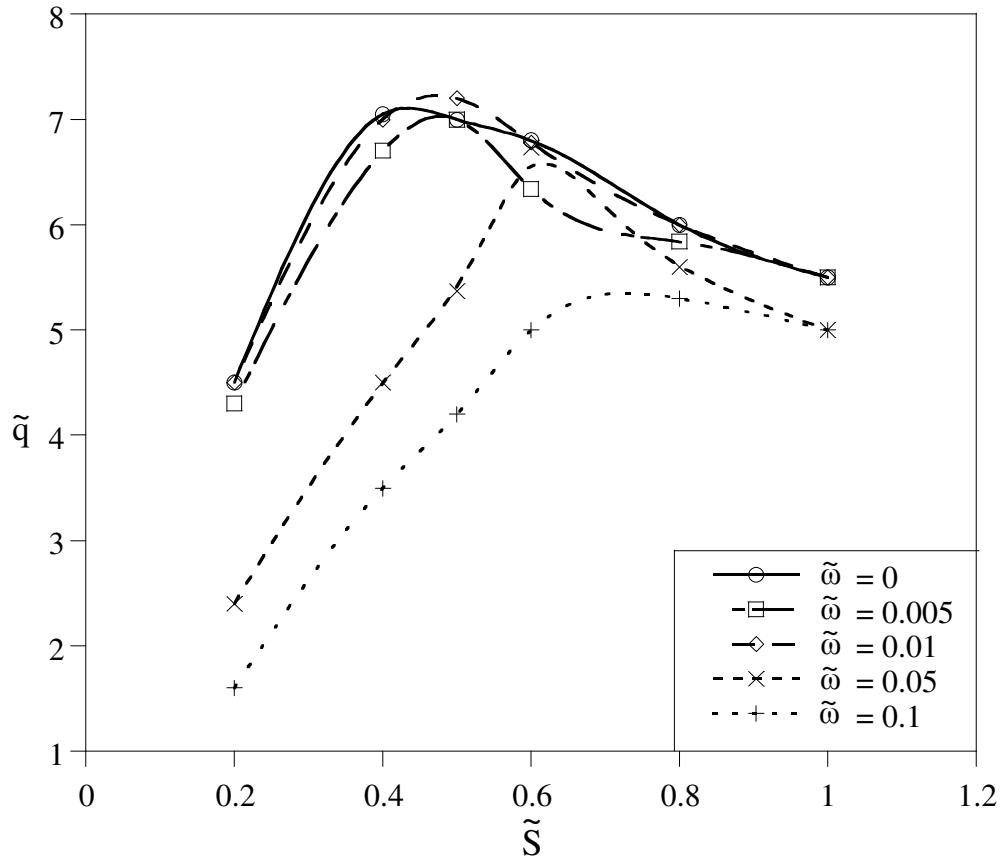

Figure 4.10 Heat transfer rate density of co-rotating cylinders at Be = 10^3

Figure 4.11 shows the optimal spacing of the cylindrical array of different dimensionless pressure drops in the range of $10 \leq Be \leq 10^4$ and for the angular velocity range of $0 \leq \tilde{\omega} \leq 0.1$. With co-rotation, the optimal spacing follows the trend of the optimal spacing observed for stationary cylinders, however, when the angular velocity, $\tilde{\omega}$ is equal to 0.1, the spacing is larger and results are only obtained in the range of $10 \leq Be \leq 10^3$. When the dimensionless

pressure drop number is greater than 10^3, the results become non-physical because the laminar assumption of the flow disintegrates due to the wake and consequent turbulence, which dominates the flow behind the rotating cylinders. It is also seen that in general the stationary cylinder array allows the most compact packing of heated cylinders. However, at Be = 10^4, the optimal spacing for the stationary cylinders coalesces with that of cylinder rotating at $\tilde{\omega} = 0.01$.

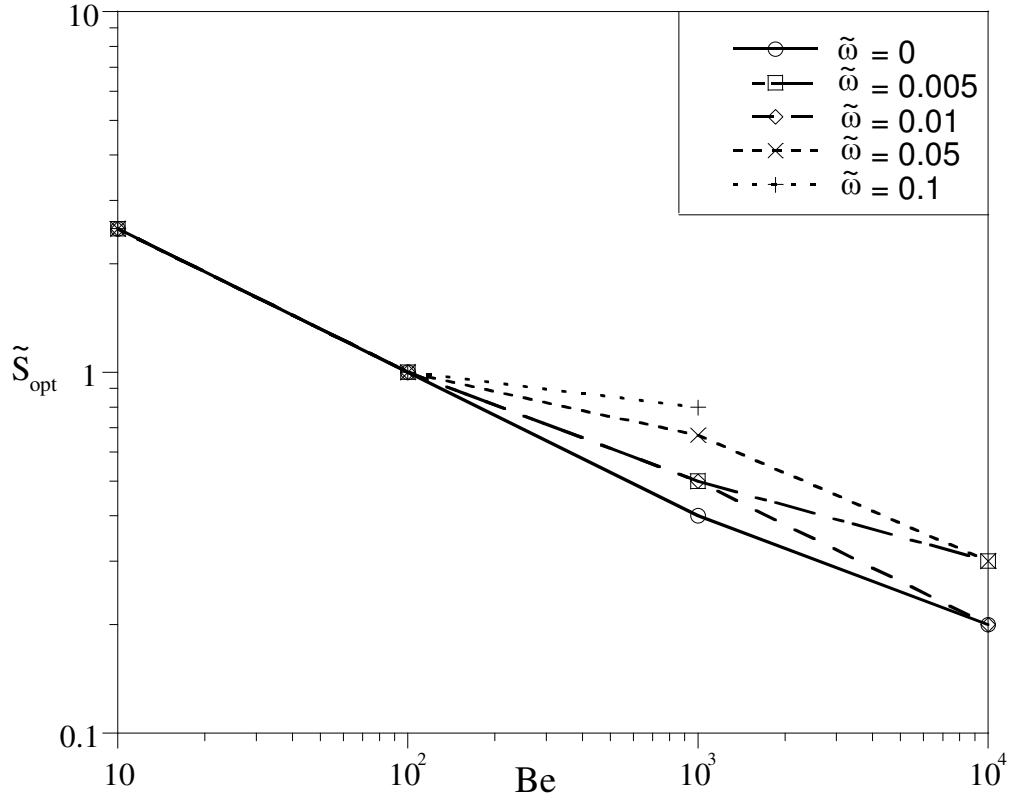

Figure 4.11 Optimal spacing of co-rotating cylinders

Figure 4.12 shows the maximum heat transfer rate density for the cylindrical array when the cylinders are co-rotating. It is observed that with co-rotation there is no significant increase in the heat transfer rate density over the heat transfer obtained from stationary cylinders. When the cylinders are co-rotating

at $\tilde{\omega} = 0.01$, the maximum heat transfer rate density coalesces with the heat transfer rate density of stationary cylinders. At the angular velocities, $\tilde{\omega}$, of 0.005, 0.05 and 0.1 the heat transfer rate density in the range of $10^2 \leq Be \leq 10^4$ is less than that obtained for $\tilde{\omega} = 0$ and $\tilde{\omega} = 0.01$.

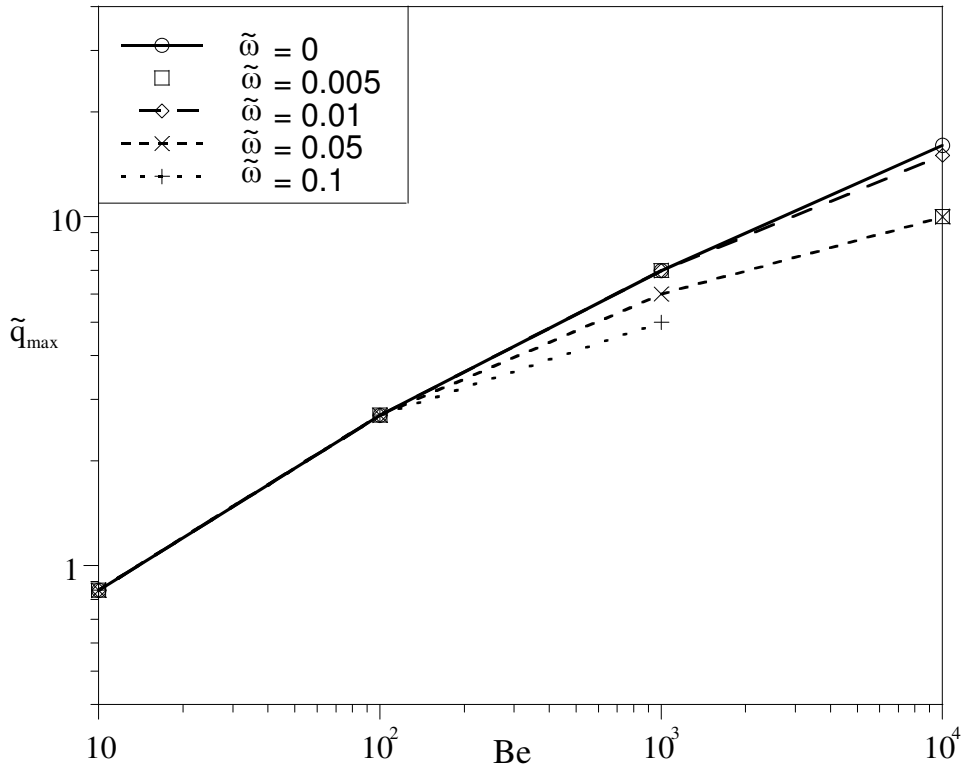

Figure 4.12 Maximum heat transfer rate density of co-rotating cylinders

The effect of co-rotation at $\tilde{\omega} = 0.1$ beyond $Be = 10^3$ could not be investigated due to the reasons adduced in the investigation of rotation on the optimal spacing.

To enable comparisons in the subsequent section, the optimal spacing (cf. Figure 4.11) and the maximum heat transfer rate density of co-rotating cylinders at $\tilde{\omega} = 0.01$ are correlated by:

$$\tilde{S}_{opt} = 5.59\,Be^{-0.36} \qquad 10 \leq Be \leq 10^4 \tag{4.3}$$

And from Figure 4.12, the maximum heat transfer rate density is correlated as:

$$\tilde{q}_{max} = 0.36 Be^{0.42} \qquad 10 \leq Be \leq 10^4 \tag{4.4}$$

4.4.2 Counter-Rotation

As the name suggests, counter-rotating cylinders have opposing rotational velocities imposed at the boundary condition. It is suggested that with counter-interacting flows from the cylinders, the heat transfer would be better than that observed with co-rotating flows. The heat transfer for such an array is further compared with heat transfer from stationary flows.

Figure 4.13 shows the result for the particular case of dimensionless pressure drop number, Be = 10^3. There is no significant difference in the heat transfer rate density between an array of cylinders rotating in the range of $0.005 \leq \tilde{\omega} \leq 0.01$ and stationary cylinders ($\tilde{\omega} = 0$). However, the cylinders at $\tilde{\omega}$ = 0.1 dissipate less heat transfer than both stationary cylinders and those rotating at $\tilde{\omega}$ = 0.01 and the heat transfer from cylinders at $\tilde{\omega}$ = 0.05 lies between the upper and lower values obtained .

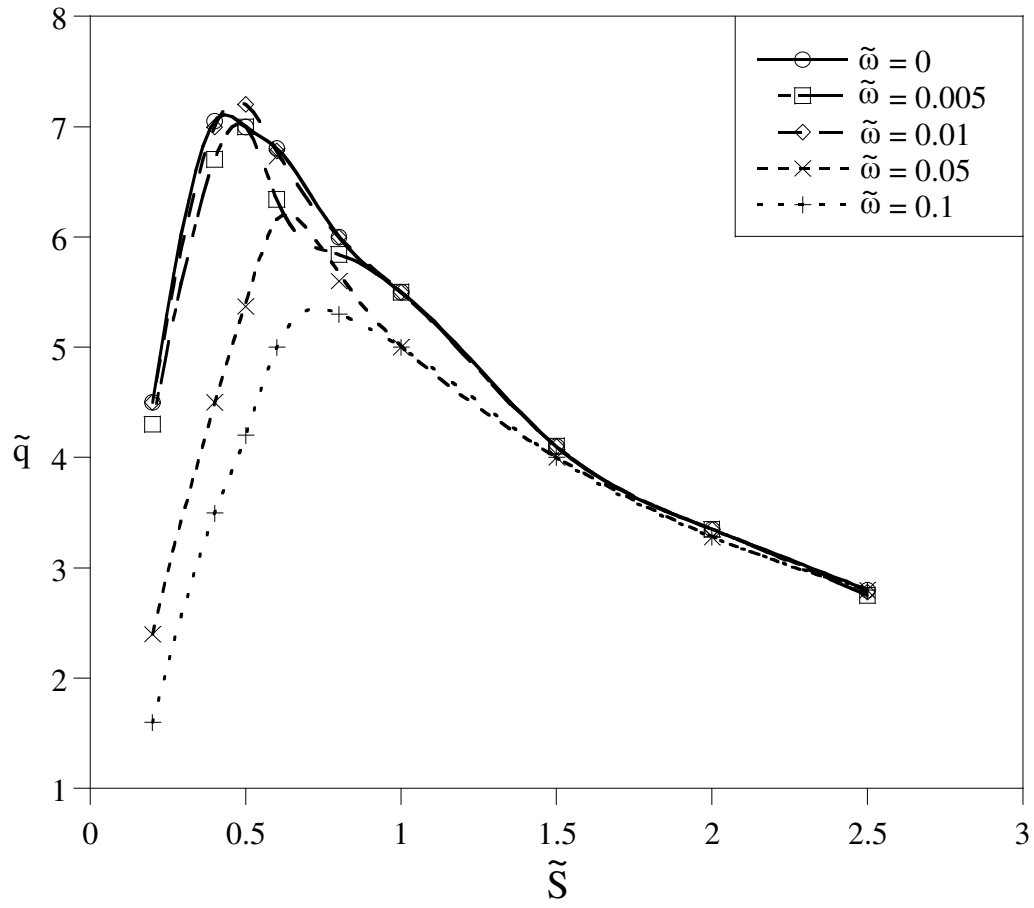

Figure 4.13 Heat transfer rate density of counter-rotating cylinders at Be = 10^3

Figure 4.14 shows the summary of counter-rotation on the array of cylinders in the range of $10 \leq \mathrm{Be} \leq 10^4$. It is observed that there is no improvement in heat transfer when the cylinders are counter-rotating. At $\tilde{\omega} = 0.01$, the heat transfer is in exact agreement with the heat transfer obtained from stationary cylinders.

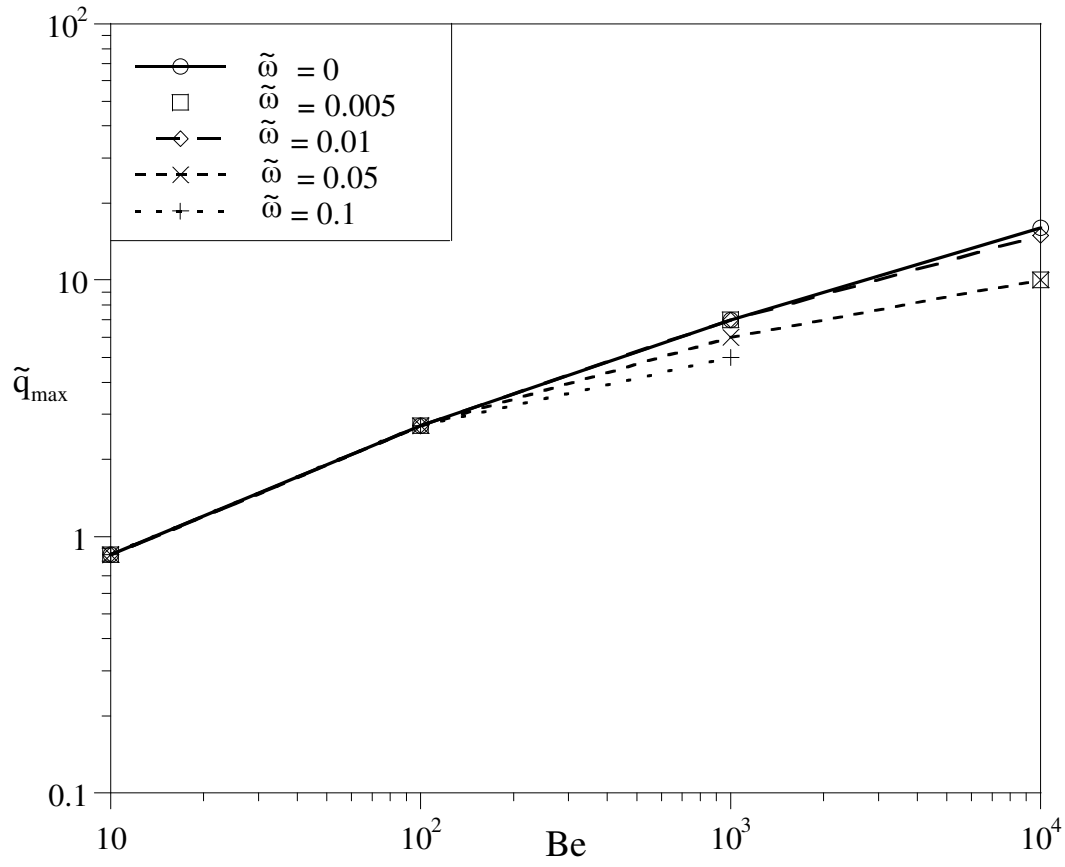

Figure 4.14 Maximum heat transfer rate density for the array of counter-rotating cylinders

The figure further shows that the maximum heat transfer rate density of cylinders rotating at 0.005 and 0.5 is less than the maximum heat transfer arte density of those that are stationary or rotating at 0.01. In the range of $10^2 \leq \text{Be} \leq 10^3$, the heat transfer rate density of cylinders rotating at $\tilde{\omega} = 0.1$ becomes less than that of cylinders rotating in the range $0 \leq \tilde{\omega} \leq 0.01$. However, when the dimensionless pressure drop number is greater than 10^3, the numerical simulation cannot converge due to errors in the assumption of a laminar flow from the wake generated in the domain by the magnitude of rotation of the cylinders.

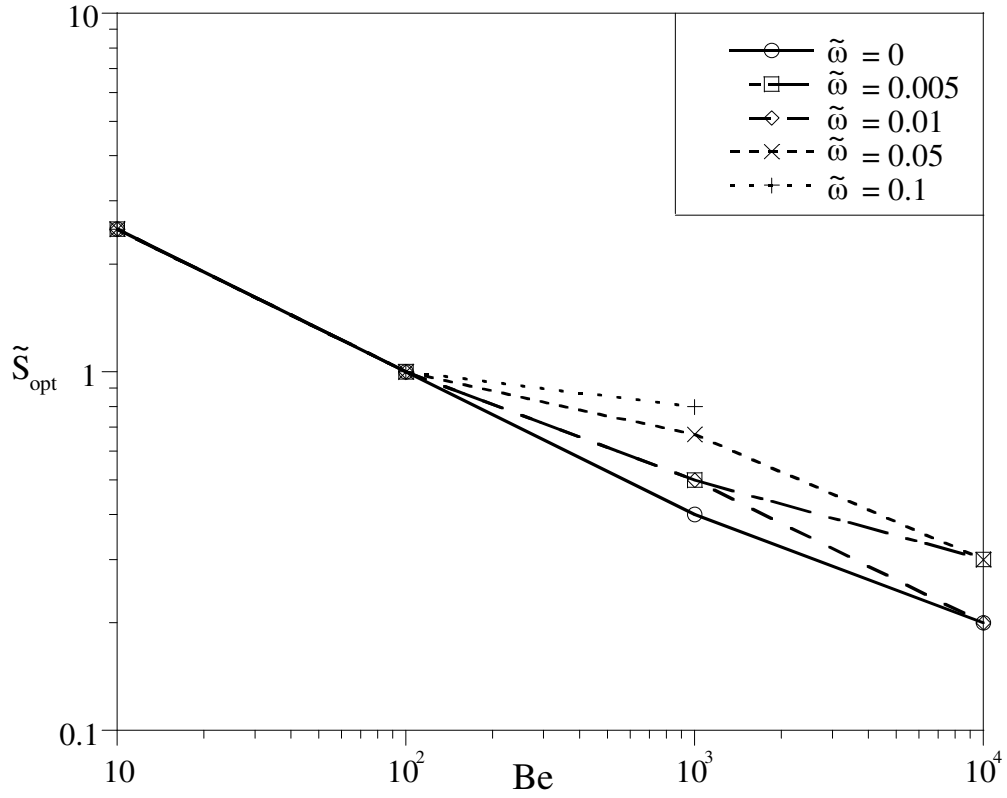

Figure 4.15 Optimal spacing of counter-rotating cylinders

The optimal spacing between the cylinders is shown in Figure 4.15, and it is seen that the trend is similar to that of co-rotating cylinders. In the case where $\tilde{\omega} = 0.01$ and at Be = 10^3, the optimal spacing is marginally higher than the optimal spacing obtained for stationary cylinders. When the cylinders are rotating at 0.005, the optimal spacing is the same as cylinders rotating at 0.01 in the range of $10 \leq \text{Be} \leq 10^3$. However, when the Bejan number is greater than 10^3, the spacing obtained for cylinders rotating at 0.005 becomes equal to cylinders rotating at 0.05. The optimal spacing obtained for both these velocities is consequently larger than the spacing observed for cylinders rotating at 0.01 and stationary cylinders. For cylinders rotating at $\tilde{\omega} = 0.1$, the

optimal spacing is equal to that of stationary cylinders only in the range of $10 \leq Be \leq 10^2$. When $Be > 10^2$, the spacing increases and results cannot be obtained for flows with $Be > 10^3$ due to reasons given in the case of the maximum heat transfer rate density of Figure 4.14.

The optimal spacing for rotating cylinders is thus correlated for $\tilde{\omega} = 0.01$ as:

$$\tilde{S}_{opt} = 5.59\, Be^{-0.36} \qquad 10 \leq Be \leq 10^4 \tag{4.5}$$

And the maximum heat transfer rate density is correlated by:

$$\tilde{q}_{max} = 0.36 Be^{0.42} \qquad 10 \leq Be \leq 10^4 \tag{4.6}$$

It should be noted that the above correlations are virtually the same as those obtained for the co-rotating array of cylinders, which means that in the case where the cylinders are aligned along the leading edge, there is no noticeable advantage of one means of rotation over the other. The above correlations enable the comparisons of the case considered here with results obtained from earlier studies and also with results that exist in available literature.

4.5 Comparison with Known Results

4.5.1 Comparison with Centreline-aligned Cylinders

Comparison is done between the optimal spacing and the maximum heat transfer obtained from both the array of cylinders aligned along the centreline and the array of cylinders aligned along the leading edge. The comparison is done for the stationary case and also for the rotational velocity, which has

been determined to be optimal. In all cases considered, the optimal rotational velocity is $\tilde{\omega} = 0.01$.

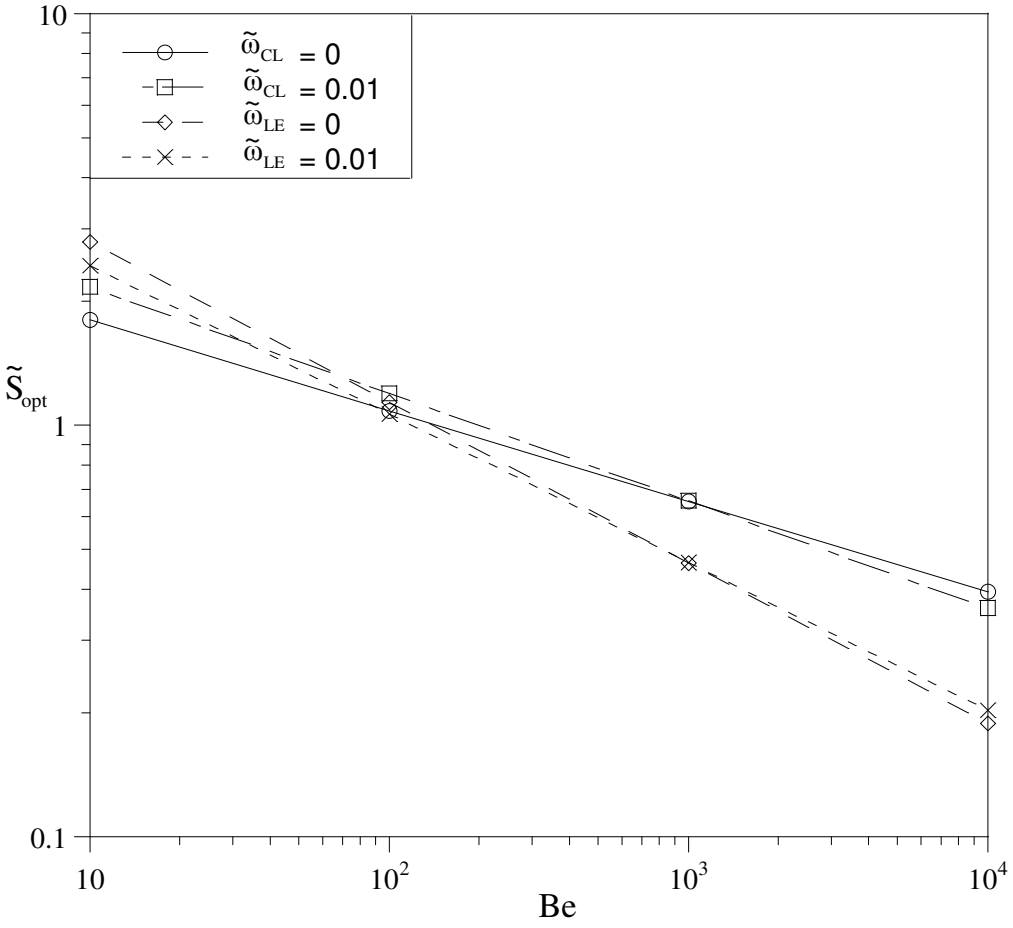

Figure 4.16 Comparison of the optimal spacing of cylinders on the same centreline (CL) and cylinders aligned on the same leading edge (LE)

The figure above shows the optimal spacing of the cylinders, for both stationary and rotating cylinders, aligned along the centreline and compared with cylinders which are aligned along the leading edge. When the dimensionless pressure drop is less than 10^2, the cylinders aligned along the centreline have a more compact spacing, that is, the optimal spacing between such cylinders is smaller than cylinders which are aligned along the leading

edge. However, in the range of $10^2 \leq Be \leq 10^4$, cylinders which are aligned along the leading edge have a more compact spacing corresponding to the maximum heat transfer rate density.

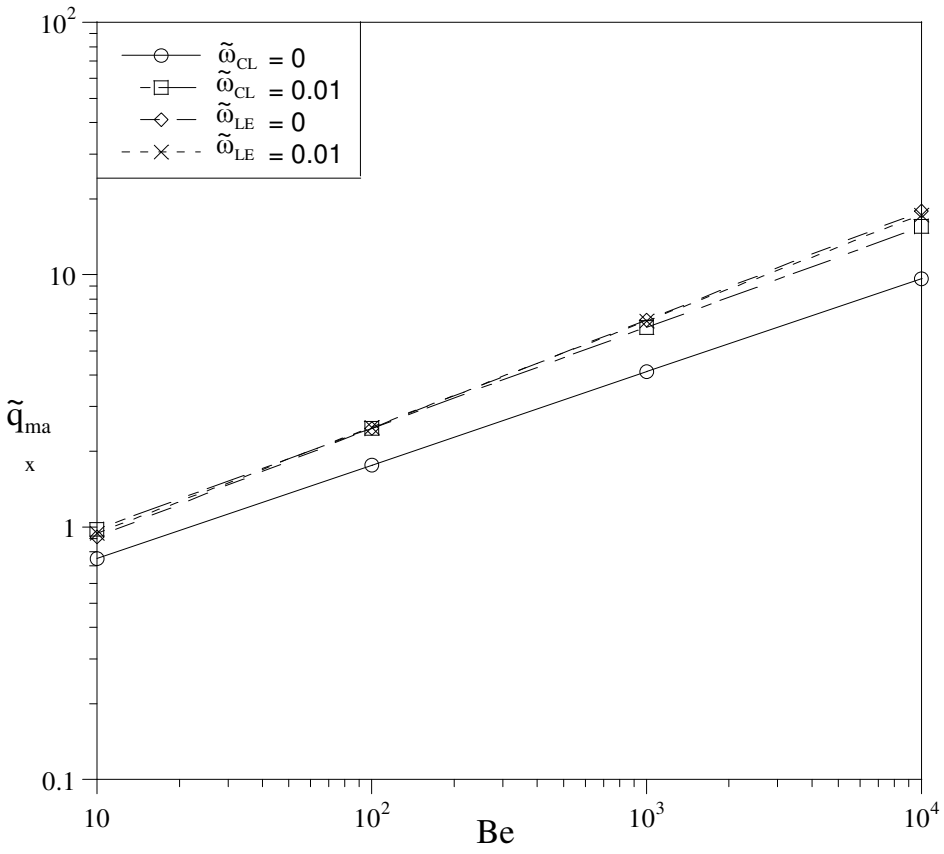

Figure 4.17 Comparison of the maximum heat transfer rate density of cylinders on the same centreline (CL) and cylinders aligned on the same leading edge (LE)

Figure 4.17 shows the maximum heat transfer rate density of both the array of cylinders aligned along the centreline and the array of cylinders aligned along the leading edge. It can be seen that there is little difference in the heat transfer rate density of cylinders which are aligned on the leading edge for cases where they are either stationary or rotating. For cylinders which are aligned along the

centreline, rotation produces an improvement in the heat transfer, which is better than the heat transfer obtained for cylinders which are stationary.

A further explanation which has been put forward in this work is the effect of the thermal boundary layer around the cylinders. This limits the heat that can be transferred from the array, due to a resemblance of insulation from such boundary layer.

4.5.2 *Comparison with Past Experimental/Numerical Cases*

To validate the results obtained in this work, it is compared with similar numerical studies done on heated cylinders.

The results of Bello-Ochende and Bejan (2004) and Joucaviel et al. (2008) are specifically chosen for comparison. Table 4.1 summarises the power law fit of the cases considered in this work and those studied by Bello-Ochende and Bejan (2004) and Joucaviel et al. (2008).

Table 4.1: Comparison between numerical model and references for stationary cylinders

Bello-Ochende and Bejan (2004)	Joucaviel et al. (2008)	Numerical results for inline cylinders	Numerical results for leading-edge-placed cylinders
$\tilde{S}_{opt} = 1.41Be^{-0.23}$ $10^3 \leq Be \leq 10^6$	$\tilde{S}_{opt} = 1.77Be^{-0.25}$ $10^2 \leq Be \leq 10^4$	$\tilde{S}_{opt} = 2.99Be^{-0.22}$ $10 \leq Be \leq 10^4$	$\tilde{S}_{opt} = 6.85Be^{-0.22}$ $10 \leq Be \leq 10^4$
$\tilde{q}_{max} = 1.1Be^{0.26}$ $10^3 \leq Be \leq 10^6$	$\tilde{q}_{max} = 1.15Be^{0.26}$ $10^2 \leq Be \leq 10^4$	$\tilde{q}_{max} = 0.32Be^{0.37}$ $10 \leq Be \leq 10^4$	$\tilde{q}_{max} = 0.34Be^{0.43}$ $10 \leq Be \leq 10^4$

In Figure 4.18, the relationship between the optimal spacing of the cylinders, $\tilde{S}_{opt}$, is compared with that of Bello-Ochende and Bejan (2004) and Joucaviel et al. (2008). In the region of $10^3 \leq Be \leq 10^4$, this work overlaps with the previous work published in literature and the results obtained from this work.

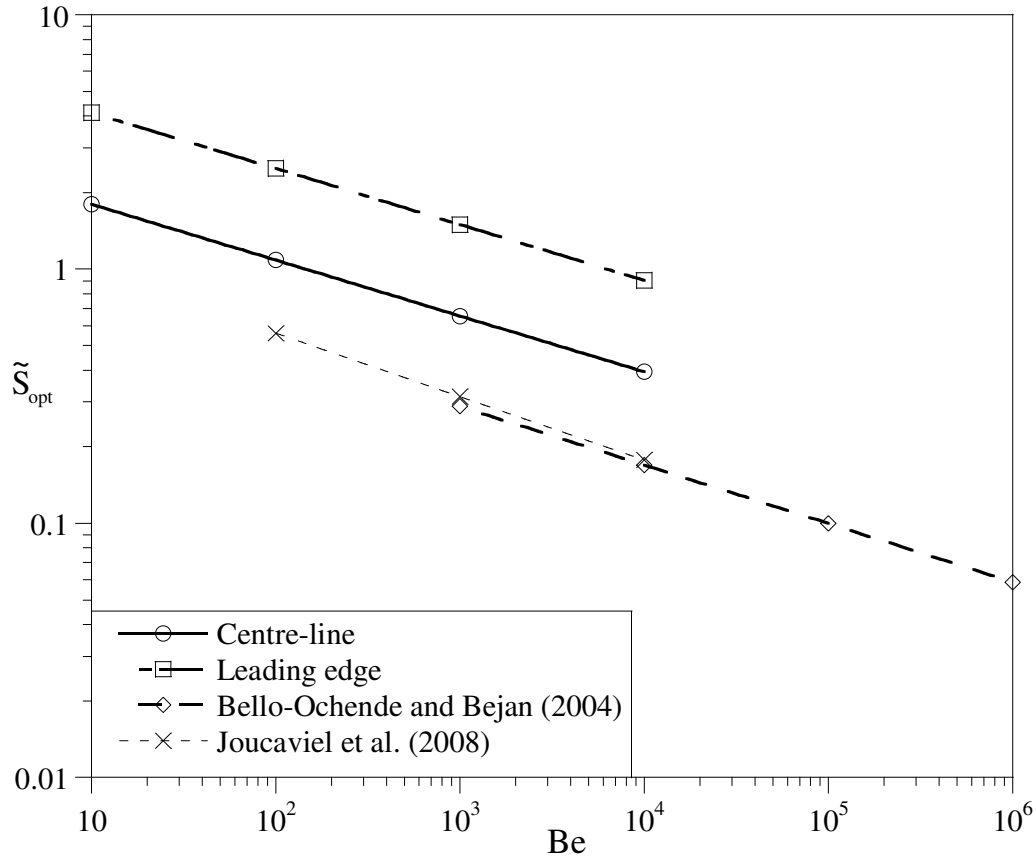

Figure 4.18 Optimal spacing between cylinders in stationary condition

In Figure 4.19, the maximum heat transfer rate density results of this study are compared with those of Bello-Ochende and Bejan (2004) and Joucaviel et al. (2008). It shows that the cylinders which are on the same leading edge displace more heat transfer at the highest Bejan number used.

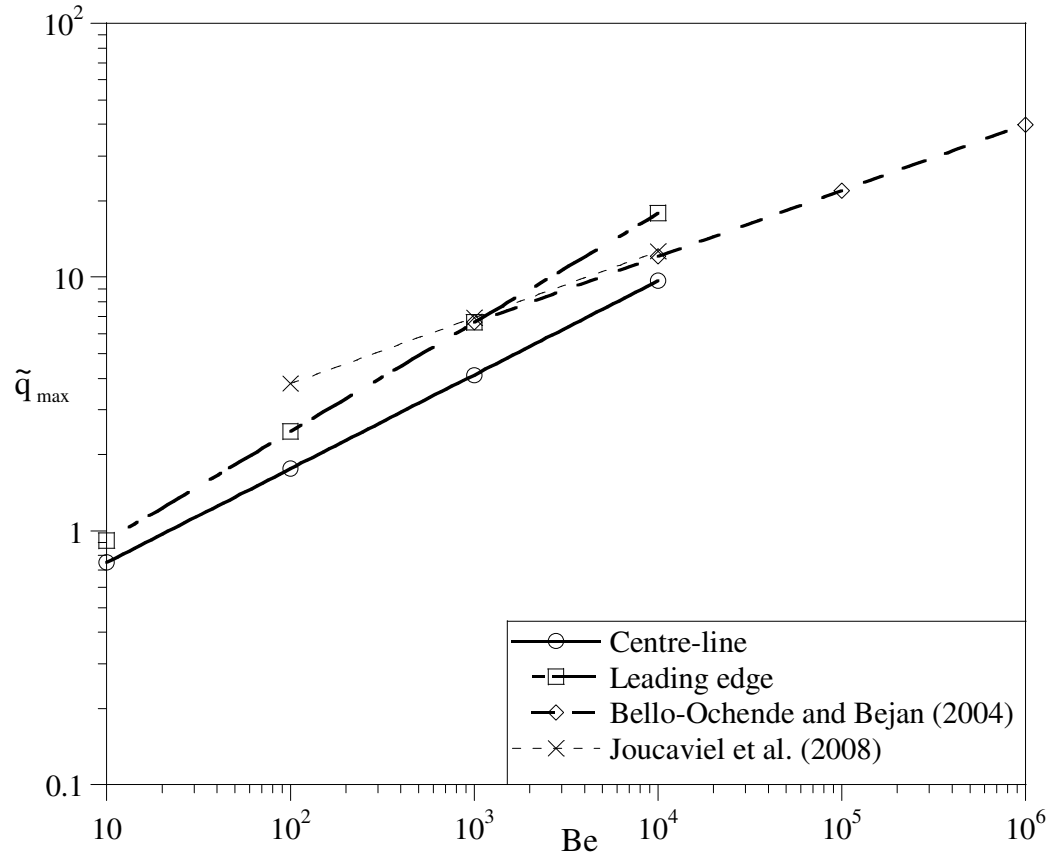

Figure 4.19 Comparison of the maximum heat transfer under the optimal rotational velocity

Furthermore, Figure 4.19 shows that in the range of $10^3 \leq Be \leq 10^4$ there is an overlap of the maximum heat dissipated from the cylindrical array aligned at the leading edge. The array dissipates equal or more heat than that obtained from the best-case scenario of Joucaviel et al. (2008). The drawback is in the positioning of the cylinders. To enable this, the multiscale array cannot be as compact as a single-scale array (Bello-Ochende and Bejan, 2004). At this juncture, an engineering decision has to be made as to what can be sacrificed to achieve the specified objective for more heat transfer, because as part of the solution, the multiscale array has to be larger.

4.6 Summary

In this chapter, the array of cylinders was arranged such that the leading edge of both cylinder scales was aligned on the same plane. The hypothesis behind this is that the cylinders experience the oncoming coolant simultaneously; this is believed to reduce the effect of the heated fluid from the bigger cylinder adversely affecting the smaller cylinder.

The results show that rotation is beneficial in the case of cylinders which are located on a plane across their centreline in the whole range considered, cf. Figure 4.17. However, there is no noted benefit from rotation for cylinders which are aligned along the leading edge. It is further seen that in the range of $10 \leq \mathrm{Be} \leq 10^2$, cylinders which are aligned on the centreline have a smaller optimal spacing than cylinders aligned on the leading edge, but in the range of $10^2 \leq \mathrm{Be} \leq 10^4$, the trend is reversed with cylinders aligned on the leading edge having a smaller optimal spacing between successive cylinders.

Comparisons done with literature show similar trends, and it is seen (cf. Figure 4.19) that at the range in which this study overlaps the works of Bello-Ochende and Bejan (2004) and Joucaviel et al. (2008), there is a better heat transfer from rotation of multiscale cylinders which are aligned along the leading edge.

Chapter 5 CONCLUSION

5.1 Summary

This work investigated a novel method in search of maximum heat transfer rate density from a laminar two-dimensional multiscale array of cylinders in cross-flow. Rotation was introduced into a multiscale array of cylinders and the effect was then simulated numerically to ascertain the advantages or disadvantages thereof. The diameter of one of the cylinders was optimised with respect to another cylinder, which was chosen as the characteristic length. This was followed by optimising the heat transfer from the assembly by numerically searching for the optimum distance between the cylinders, which allowed the array to dissipate the highest possible amount of heat.

The results obtained from this study show that only at certain fixed rotational velocities and directions can better heat transfer be achieved above and beyond that of a stationary array. This effect is somewhat supported in the literature, whereby it is noted that at certain rotational speeds there exists a thermal boundary layer, which acts as an insulation for the cylinders and thus limits the heat transfer from such a cylinder. An added explanation is the presence of a more uniform local heat transfer from the surface of the cylinder therefore causing a “levelling-off” of the dimensionless parameter which represents the heat transfer.

Another point seen in the course of this work is that the better heat transfer of certain rotational velocities comes at the price of less "compactness" of the array. This means, to achieve better heat transfer under the simulated conditions, the spacing between the rotating cylinder should be larger than between stationary cylinders.

5.2 Conclusions

At the beginning of this research it was thought that with rotation the heat transfer rate density from the array of rotating cylinders would be better than the heat transfer rate density obtained from the same array which is held stationary.

However, it has been indicated that such a proposition only holds true in a very limited case and this happens under co-rotating and counter-rotating conditions of flow for an array which is aligned on the centreline. Rotation dissipates more heat than the stationary configuration only in the case where the dimensionless angular velocity, $\tilde{\omega}$, is equal to 0.01. In all other cases tested, the stationary configuration provided more heat transfer and compact spacing than the configuration where rotation is taken into consideration. This leads to the proposition that in certain cases, rotation enables the suppression of heat transfer, which is beneficial in some applications. Some of these applications include devices for drying colloidal solutions, viscous fluids and textile materials.

5.3 Recommendations and Future work

Some recommendations which should be taken into consideration for future work include:

(i.) The scope of this work should be extended to a three-dimensional model.

(ii.) The boundary layer effect on the cylinders needs to be taken into consideration.

(iii.) In this work, the numerical solutions were obtained by brute force, i.e. generating the mesh, obtaining the solution and working through a chosen set of constraints manually. This method is not the most efficient possible and a more efficient method can be utilised via the implementation of numerical optimisation algorithms into the finite volume solver.

(iv.) It is also suggested that the degrees of freedom be increased, such that the use of the optimal smaller cylinder diameter under conditions of rotation should be relaxed.

(v.) The work done in pumping the coolant across the domain should be calculated to give the study an economic perspective.

(vi.) The simultaneous analysis of increased heat transfer and pumping work should be investigated through calculation of the assembly's entropy generation rate.

This would enable exhaustive investigation into the effects of rotation on the heat transfer rate density.

REFERENCES

Badr, H.M., Dennis, S.C.R. (1985) Laminar forced convection from a rotating cylinder. *International Journal of Heat and Mass Transfer,* Vol. 28, No. 1, pp. 253-264

Bello-Ochende, T., Bejan, A. (2004) Constructal multi-scale cylinders in cross-flow. *International Journal of Heat and Mass Transfer,* Vol. 48, pp. 1373-1383

Bello-Ochende, T., Bejan, A. (2005) Constructal multi-scale cylinders with natural convection. *International Journal of Heat and Mass transfer,* Vol. 48, pp. 4300-4306

Bejan, A., Morega, A.M. (1993) Optimal arrays of pin fins and plate fins in laminar forced convection. *Journal of Heat Transfer*, Vol. 115, pp. 75-81

Cheng, Y.J., Liao, Y.H., Huang, C.K. (2008) Heat transfer on a radially heated cylinder. *International Communications in Heat and Mass Transfer,* Vol. 35, pp. 1355-1359

Chiou, C.C., Lee, S.L. (1993) Forced convection on a rotating cylinder with an incident air jet. *International Journal of Heat and Mass Transfer,* Vol. 36, pp. 3841-3850

Fluent User's Guide, 1998 (www.fluent.com)

Gabe, D.R. (1974) The rotating cylinder electrode. *Journal of Applied Electrochemistry* Vol. 4, No. 2, pp. 91-108

Gabe, D.R., Wilcox, G.D., Gonzalex-Garcia, J., Walsh, F.C. (1998) The rotating cylinder electrode: its continued development and application. *Journal of Applied Electrochemistry* Vol. 28, No. 8, pp. 759-780

Gschwendtner, M.A. (2004) Optical investigation of the heat transfer from a rotating cylinder in a cross-flow. *Heat and Mass Transfer,* Vol. 40, pp. 561-572

Ingham, D.B. (1983) Steady flow past a rotating cylinder. *Computers and Fluids,* Vol. 11, No. 4, pp. 351-366

Jones, J., Poulikakos, D., Orozco, J. (1988) Mixed convection from a rotating horizontal heated cylinder placed in a low-velocity wind tunnel. *International Journal of Heat and Fluid Flow,* Vol. 9, No. 2, pp. 165-173

Joucaviel, M., Gosselin, L., Bello-Ochende, T. (2008) Maximum heat transfer density with rotating cylinders aligned in cross-flow. *International Communications in Heat and Mass Transfer,* Vol. 35, pp. 557-564

Kays, W.M., Bjorklund, J.S. (1958) Heat transfer from a rotating cylinder with and without cross-flow, *Transactions of the American Society of Mechanical Engineers*, Vol. 80, pp. 70-78

Khan, W.A, Culham, J.R., Yovanovich, M.M. (2005) Fluid flow around and heat transfer from an infinite circular cylinder. *Journal of Heat Transfer,* Vol. 127, pp. 785-790

Levich, V.G. (1962) Physicochemical Hydrodynamics. Prentice-Hall Inc., New Jersey.

Mandhani, V.K., Chhabra, R.P., Eswaran, V. (2002) Forced convection heat transfer in tube banks in cross flow, *Chemical Engineering Science,* Vol. 57, pp. 379-391

Misirlioglu, A. (2006) The effect of rotating cylinder on the heat transfer in a square cavity filled with porous medium. *International Journal of Engineering Science,* Vol. 44, pp. 1173-1187

Mohanty, A.K., Tawfek, A.A., Prasad, B.V.S.S.S. (1995) Heat transfer from a rotating horizontal heated cylinder placed in a low-velocity wind tunnel. *Experimental Thermal and Fluid Science,* Vol. 10, pp. 54-61

Paramane, S.B., Sharma, A. (2009) Numerical investigation of heat and fluid flow across a rotating circular cylinder maintained at constant temperature in 2-D laminar flow regime. *International Journal of Heat and Mass Transfer,* Vol. 52, pp. 3205-3216

Patankar, S.V. (1980) Numerical Heat Transfer and Fluid Flow. Hemisphere Publishing Corp., New York.

Sanitjai, S., Goldstein, R.J. (2004) Forced convection heat transfer from a circular cylinder in cross-flow to air and liquids. *International Journal of Heat and Mass Transfer,* Vol. 47, pp. 4795-4805

Silverman, D.C., (1988) Rotating cylinder electrode-geometry relationships for prediction of velocity-sensitive corrosion. *Corrosion–NACE* Vol. 44, No. 1, pp. 42–49.

Silverman, D.C., (2003) Simplified equation for simulating velocity-sensitive corrosion in the rotating cylinder electrode at higher Reynolds numbers. *Corrosion* Vol. 59, No. 3, pp. 207–211.

Stanescu, G., Fowler, A.J., Bejan, A. (1996) The optimal spacing of cylinders in free-stream cross-flow forced convection. *International Journal of Heat and Mass Transfer,* Vol. 39, No. 2, pp. 311-317

Versteeg, H.K., Malalasekera, W. (2007) An Introduction to Computational Fluid Dynamics: The finite volume method. 2nd Edition, Prentice-Hall Inc., New Jersey.

APPENDIX A: Temperature and Velocity contours of various configurations simulated

Centreline Aligned Cylinders simulated at Be = 100

Temperature contours of stationary cylinders at $\tilde{S}$ = 0.2

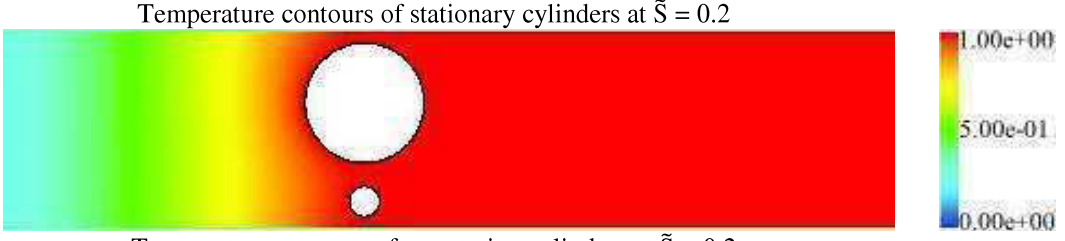

Temperature contours of co-rotating cylinders at $\tilde{S}$ = 0.2

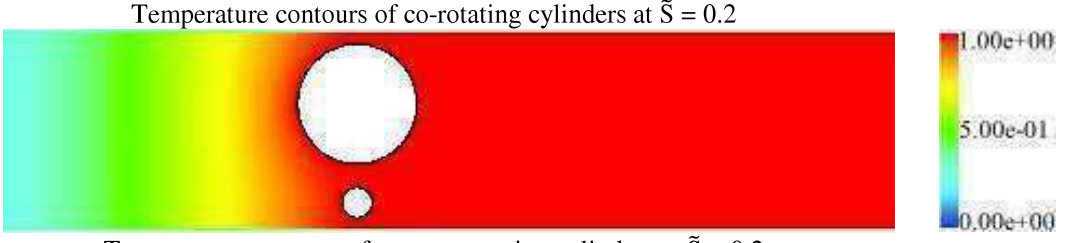

Temperature contours of counter-rotating cylinders at $\tilde{S}$ = 0.2

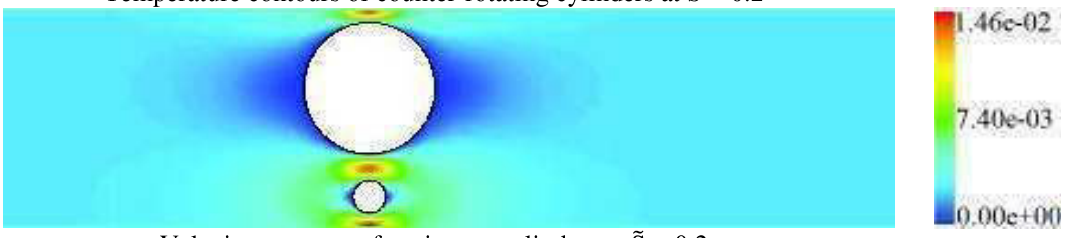

Velocity contours of stationary cylinders at $\tilde{S}$ = 0.2

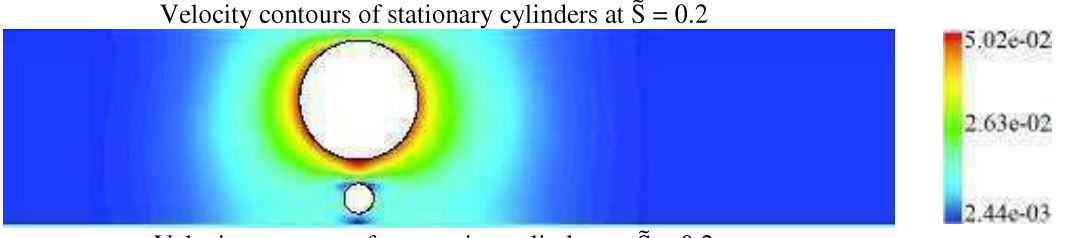

Velocity contours of co-rotating cylinders at $\tilde{S}$ = 0.2

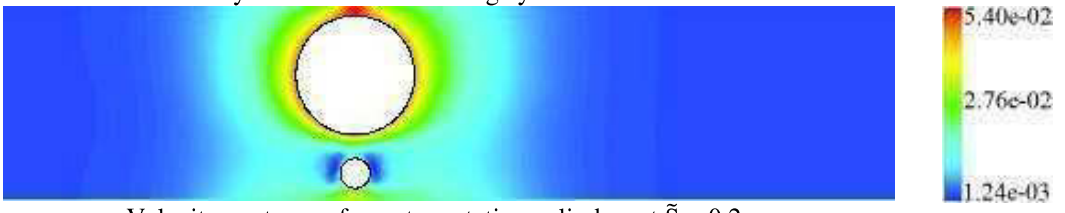

Velocity contours of counter-rotating cylinders at $\tilde{S}$ = 0.2

Temperature contours of stationary cylinders at $\tilde{S} = 0.5$

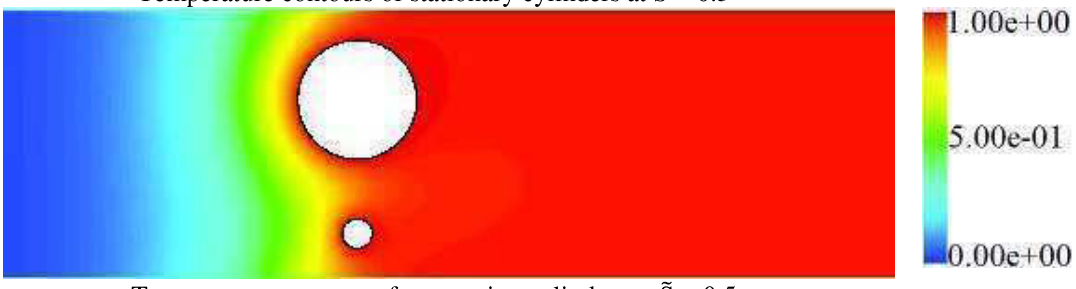

Temperature contours of co-rotating cylinders at $\tilde{S} = 0.5$

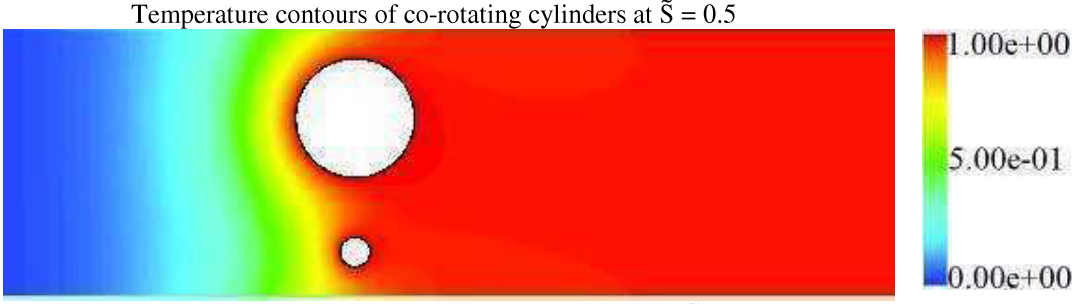

Temperature contours of counter-rotating cylinders at $\tilde{S} = 0.5$

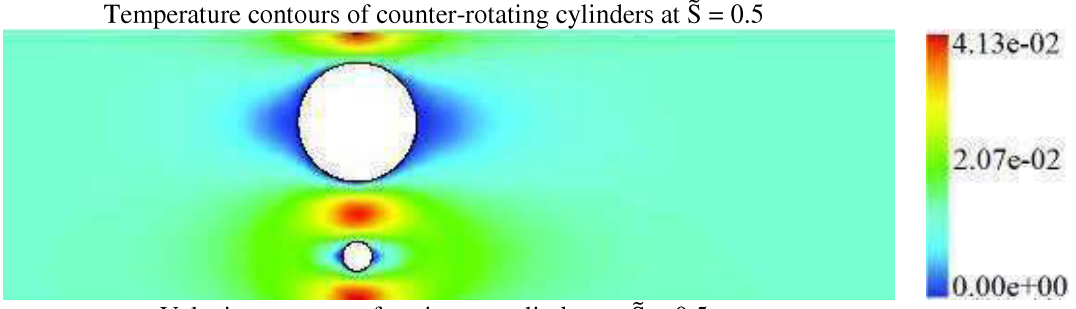

Velocity contours of stationary cylinders at $\tilde{S} = 0.5$

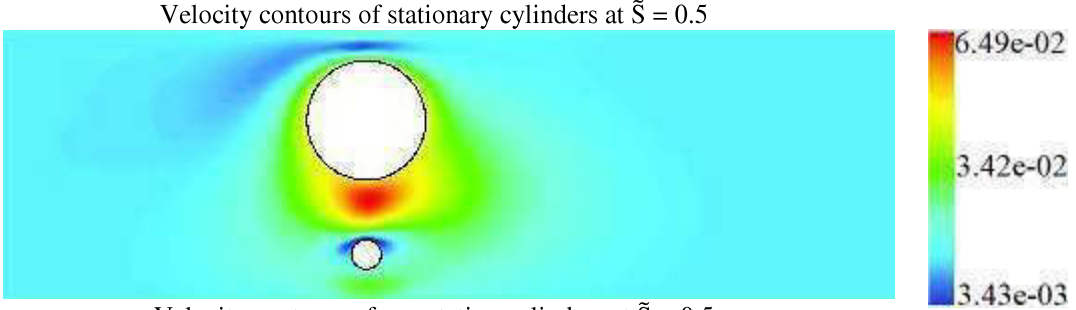

Velocity contours of co-rotating cylinders at $\tilde{S} = 0.5$

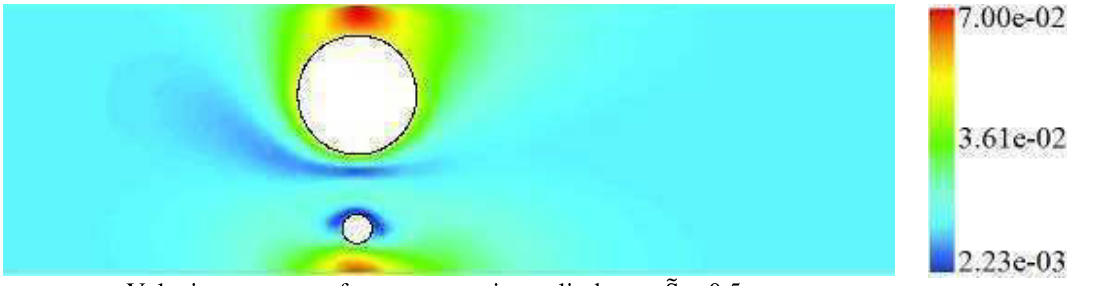

Velocity contours of counter-rotating cylinders at $\tilde{S} = 0.5$

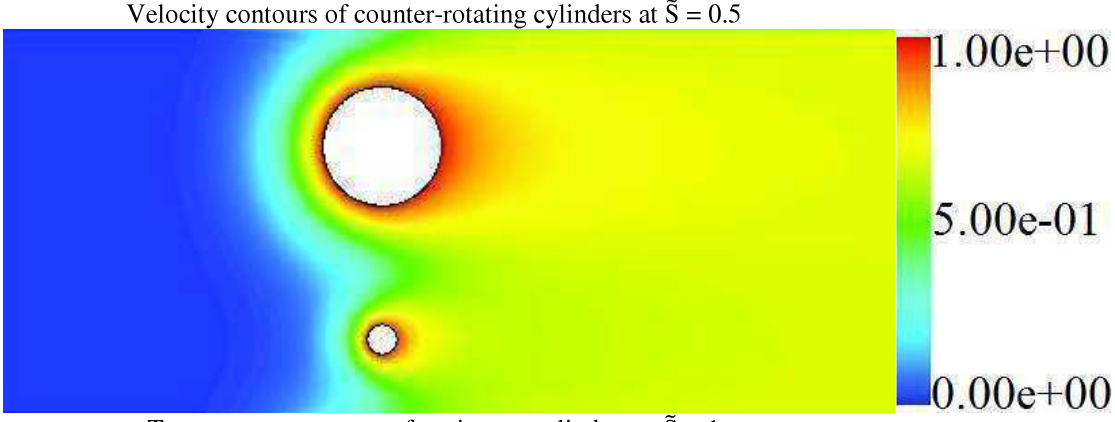

Temperature contours of stationary cylinders at $\tilde{S} = 1$

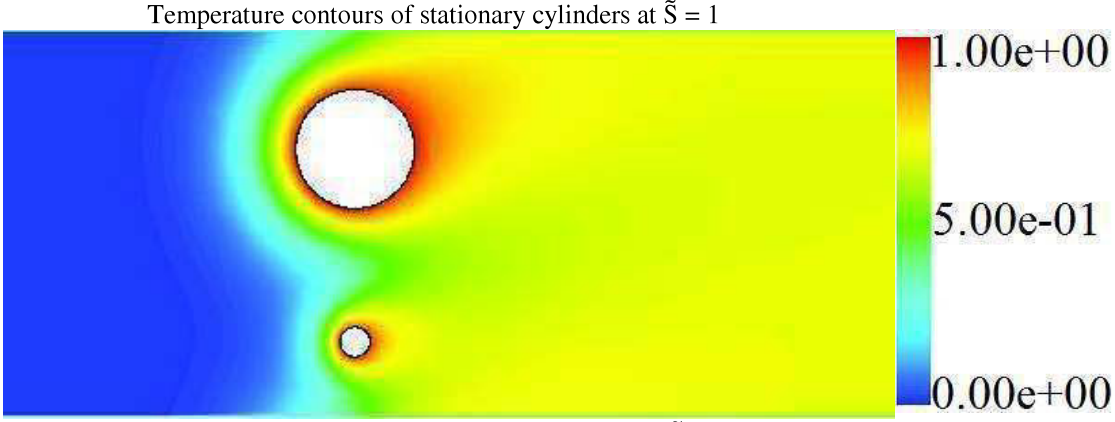

Temperature contours of co-rotating cylinders at $\tilde{S} = 1$

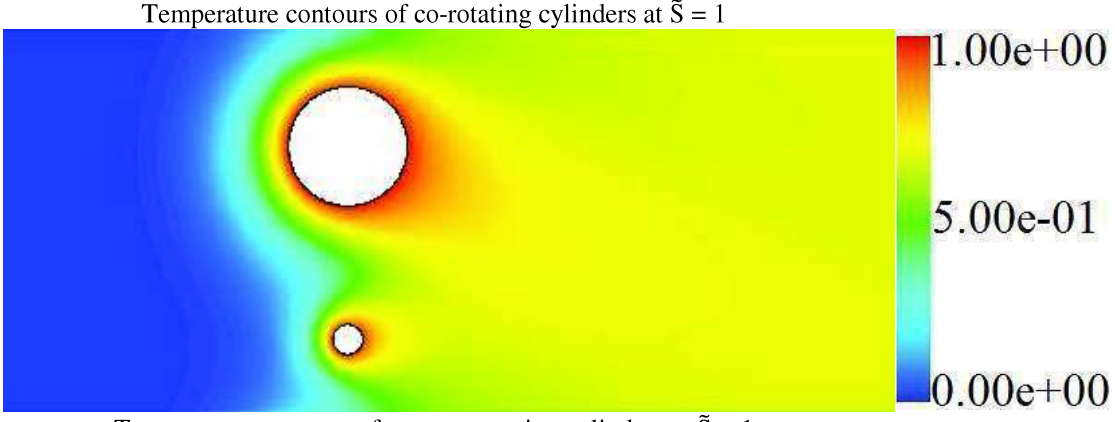

Temperature contours of counter-rotating cylinders at $\tilde{S} = 1$

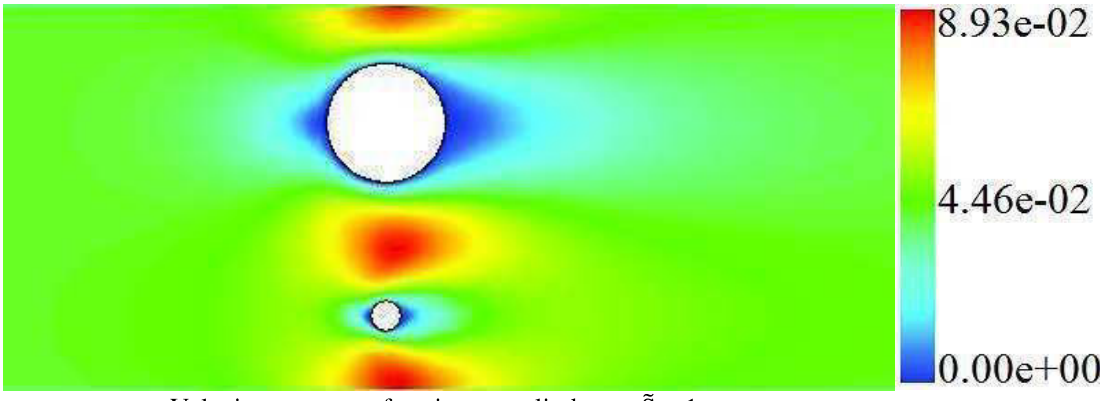

Velocity contours of stationary cylinders at $\tilde{S} = 1$

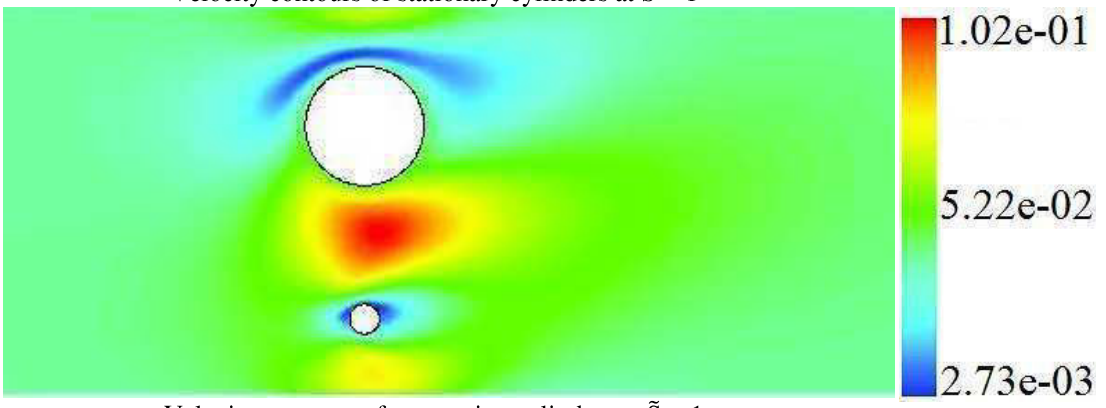

Velocity contours of co-rotating cylinders at $\tilde{S} = 1$

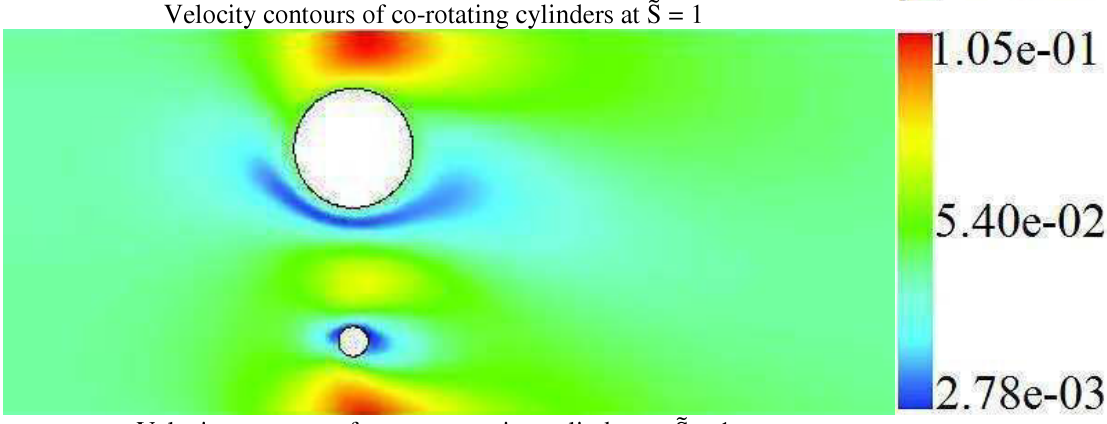

Velocity contours of counter-rotating cylinders at $\tilde{S} = 1$

Leading Edge Aligned Cylinders simulated at Be = 100

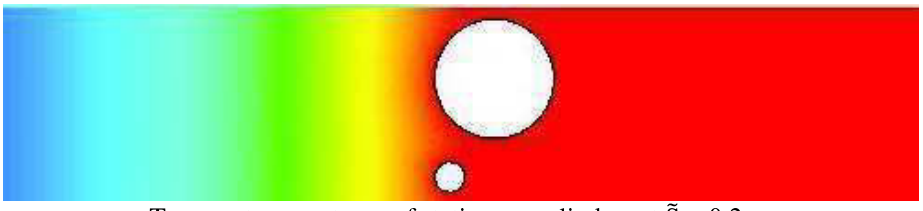

Temperature contours of stationary cylinders at $\tilde{S}$ = 0.2

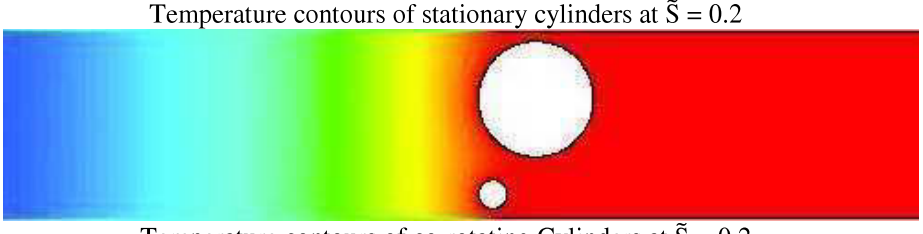

Temperature contours of co-rotating Cylinders at $\tilde{S}$ = 0.2

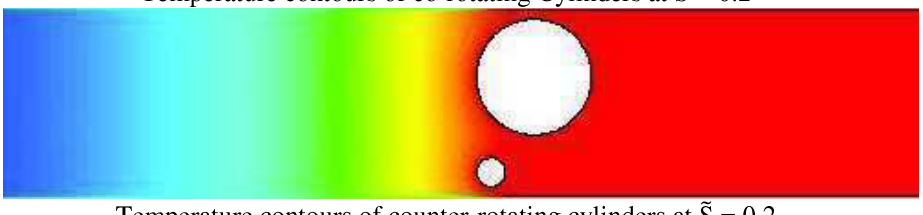

Temperature contours of counter-rotating cylinders at $\tilde{S}$ = 0.2

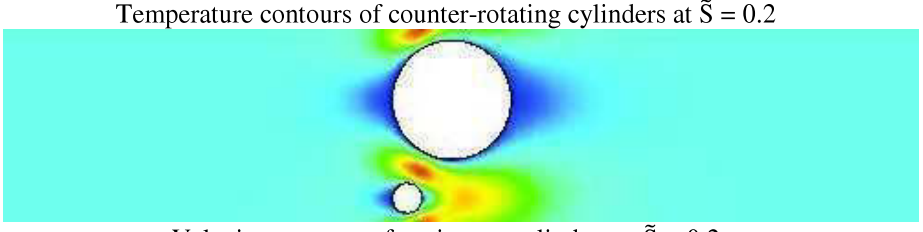

Velocity contours of stationary cylinders at $\tilde{S}$ = 0.2

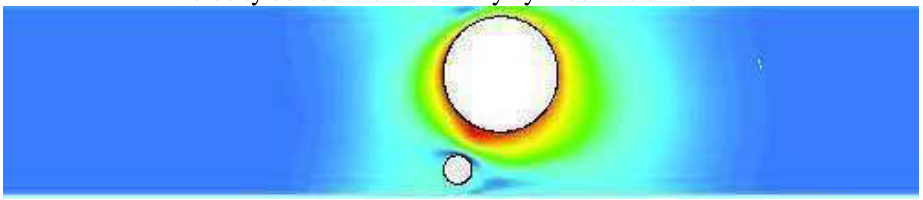

Velocity contours of co-rotating Cylinders at $\tilde{S}$ = 0.2

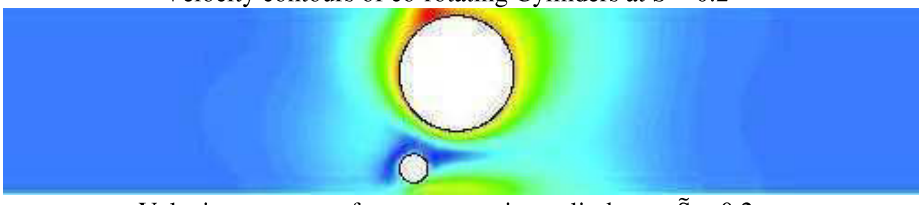

Velocity contours of counter-rotating cylinders at $\tilde{S}$ = 0.2

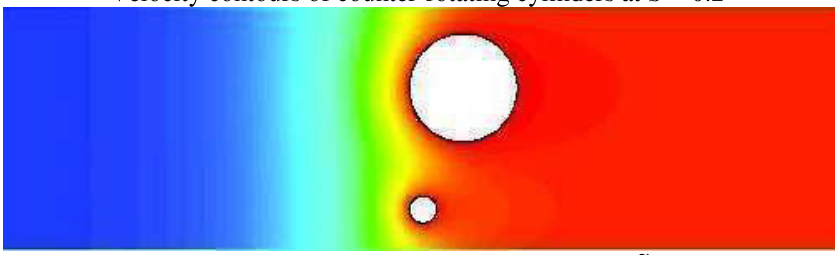

Temperature contours of stationary cylinders at $\tilde{S}$ = 0.5

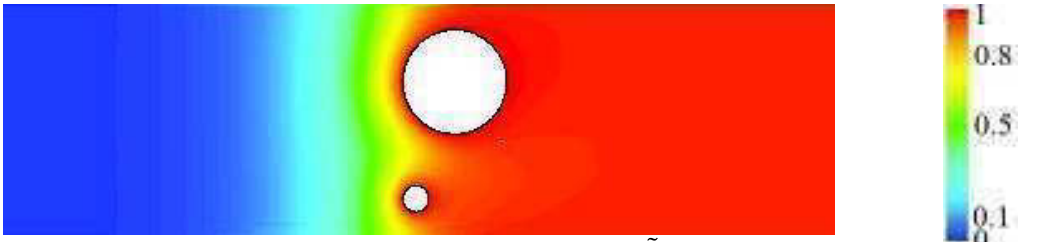

Temperature contours of co-rotating Cylinders at $\tilde{S} = 0.5$

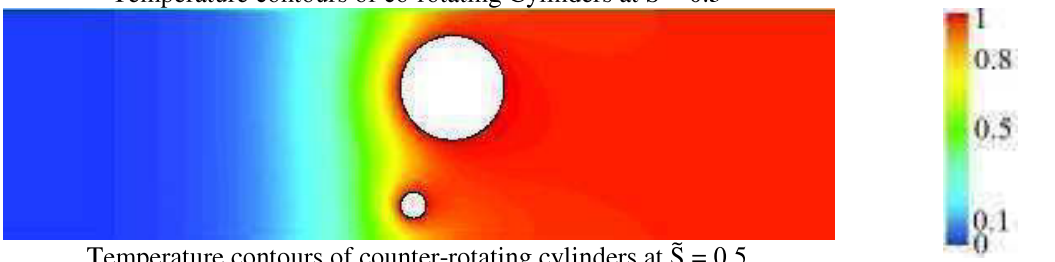

Temperature contours of counter-rotating cylinders at $\tilde{S} = 0.5$

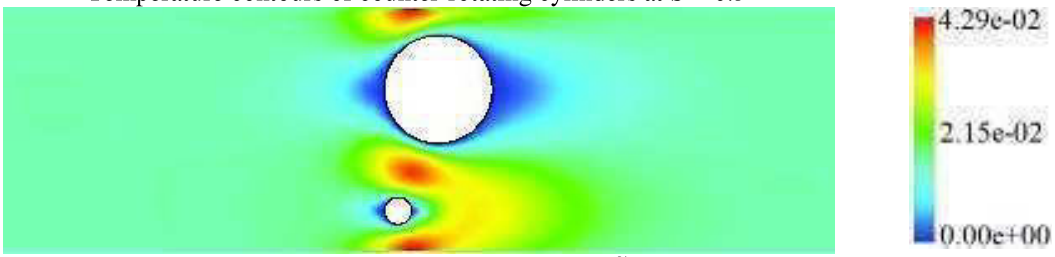

Velocity contours of stationary cylinders at $\tilde{S} = 0.5$

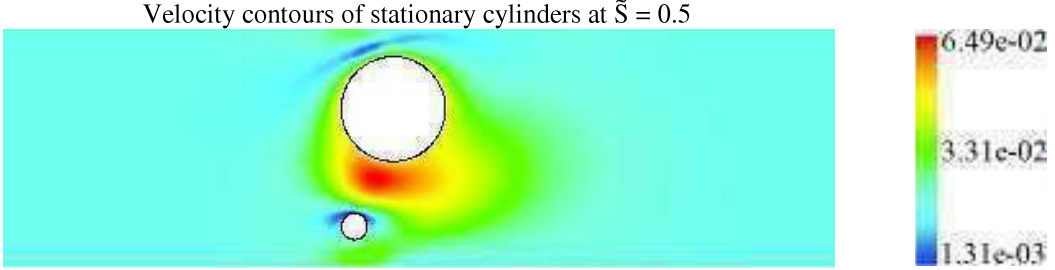

Velocity contours of co-rotating Cylinders at $\tilde{S} = 0.5$

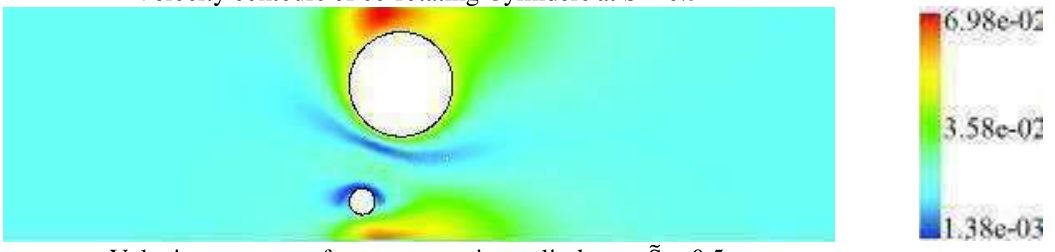

Velocity contours of counter-rotating cylinders at $\tilde{S} = 0.5$

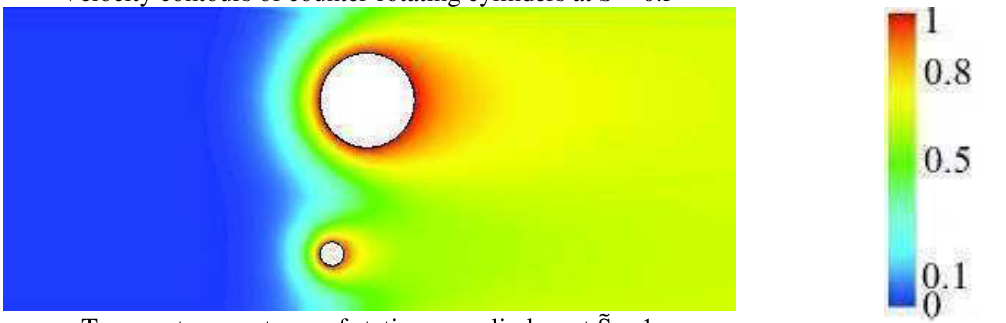

Temperature contours of stationary cylinders at $\tilde{S} = 1$

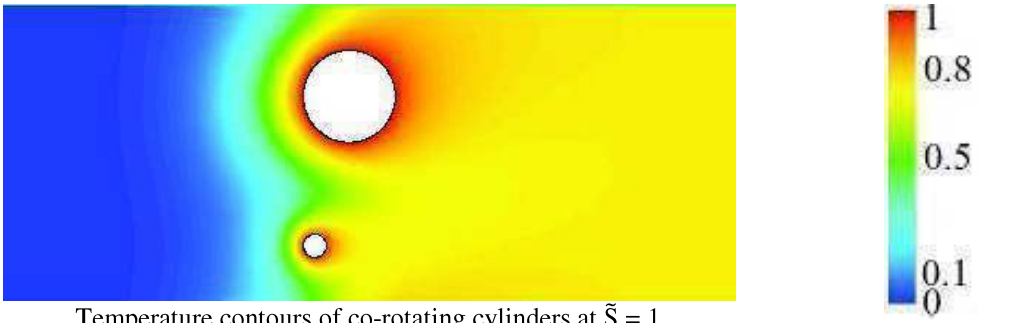

Temperature contours of co-rotating cylinders at $\tilde{S} = 1$

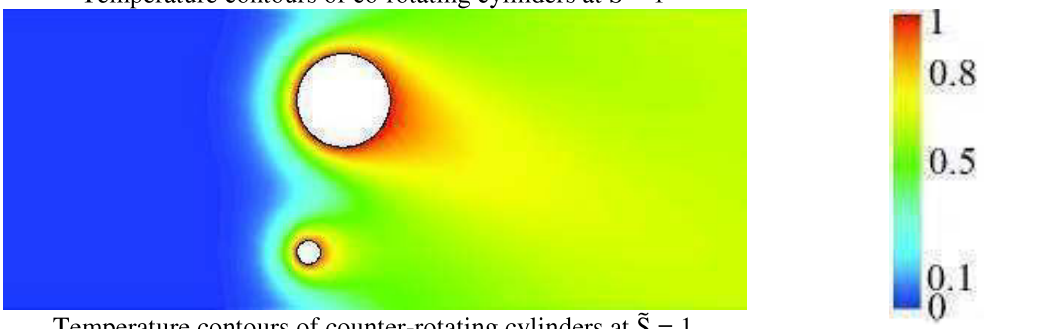

Temperature contours of counter-rotating cylinders at $\tilde{S} = 1$

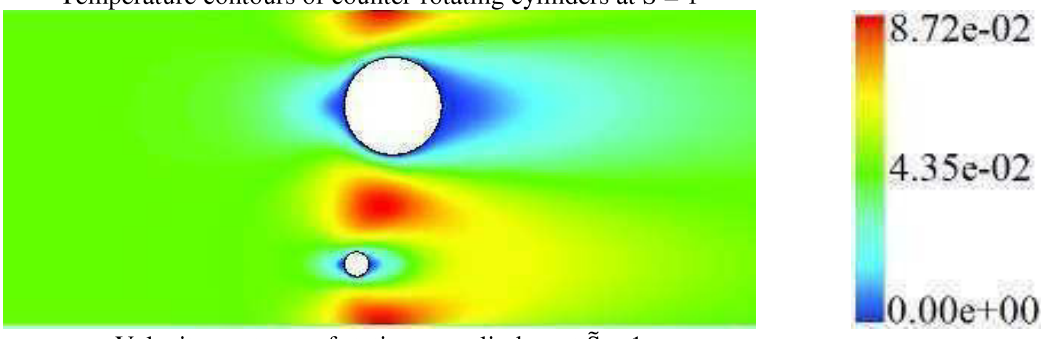

Velocity contours of stationary cylinders at $\tilde{S} = 1$

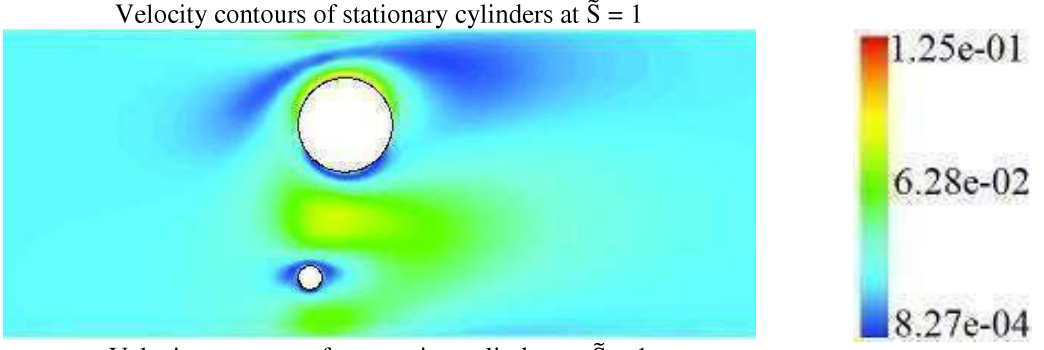

Velocity contours of co-rotating cylinders at $\tilde{S} = 1$

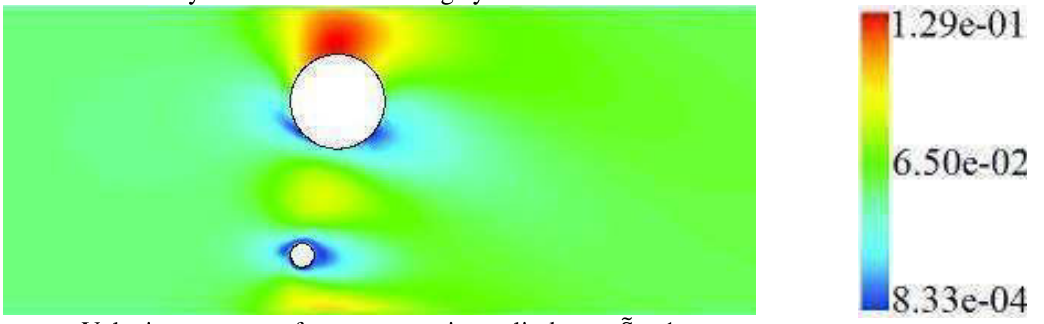

Velocity contours of counter-rotating cylinders at $\tilde{S} = 1$

APPENDIX B: EXAMPLE OF A FLUENT REPORT FILE

FLUENT
Version: 2d, dp, pbns, lam (2d, double precision, pressure-based, laminar)
Release: 6.3.26
Title:

Models

Model	Settings
Space	2D
Time	Steady
Viscous	Laminar
Heat Transfer	Enabled
Solidification and Melting	Disabled
Radiation	None
Species Transport	Disabled
Coupled Dispersed Phase	Disabled
Pollutants	Disabled
Pollutants	Disabled
Soot	Disabled

Boundary Conditions

Zones

Name	id	type
fluid	2	fluid
periodic	4	periodic
outlet	5	pressure-outlet
inlet	6	pressure-inlet
small_cyl	7	wall
big_cyl	8	wall
default-interior	10	interior

Boundary Conditions

fluid

Condition	Value
Material Name	air
Specify source terms?	no
Source Terms	()
Specify fixed values?	no
Fixed Values	()
Motion Type	0

X-Velocity Of Zone (m/s)	0
Y-Velocity Of Zone (m/s)	0
Rotation speed (rad/s)	0
X-Origin of Rotation-Axis (m)	0
Y-Origin of Rotation-Axis (m)	0
Deactivated Thread	no
Porous zone?	no
X-Component of Direction-1 Vector	1
Y-Component of Direction-1 Vector	0
Relative Velocity Resistance Formulation?	yes
Direction-1 Viscous Resistance (1/m2)	0
Direction-2 Viscous Resistance (1/m2)	0
Choose alternative formulation for inertial resistance?	no
Direction-1 Inertial Resistance (1/m)	0
Direction-2 Inertial Resistance (1/m)	0
C0 Coefficient for Power-Law	0
C1 Coefficient for Power-Law	0
Porosity	1
Solid Material Name	aluminum

periodic

Condition	Value
Rotationally Periodic?	no

outlet

Condition	Value
Gauge Pressure (pascal)	0
Backflow Total Temperature (c)	274.14999
Backflow Direction Specification Method	1
X-Component of Flow Direction	1
Y-Component of Flow Direction	0
X-Component of Axis Direction	1
Y-Component of Axis Direction	0
Z-Component of Axis Direction	0
X-Coordinate of Axis Origin (m)	0
Y-Coordinate of Axis Origin (m)	0
Z-Coordinate of Axis Origin (m)	0
is zone used in mixing-plane model?	no
Specify targeted mass flow rate	no
Targeted mass flow (kg/s)	1

inlet

Condition	Value
Gauge Total Pressure (pascal)	1
Supersonic/Initial Gauge Pressure (pascal)	0

Total Temperature (c)	273.14999
Direction Specification Method	1
X-Component of Flow Direction	1
Y-Component of Flow Direction	0
X-Component of Axis Direction	1
Y-Component of Axis Direction	0
Z-Component of Axis Direction	0
X-Coordinate of Axis Origin (m)	0
Y-Coordinate of Axis Origin (m)	0
Z-Coordinate of Axis Origin (m)	0
is zone used in mixing-plane model?	no

small_cyl

Condition	Value
Wall Thickness (m)	0
Heat Generation Rate (w/m3)	0
Material Name	aluminum
Thermal BC Type	0
Temperature (c)	274.14999
Heat Flux (w/m2)	0
Convective Heat Transfer Coefficient (w/m2-k)	0
Free Stream Temperature (c)	300
Wall Motion	0
Shear Boundary Condition	0
Define wall motion relative to adjacent cell zone?	yes
Apply a rotational velocity to this wall?	no
Velocity Magnitude (m/s)	0
X-Component of Wall Translation	1
Y-Component of Wall Translation	0
Define wall velocity components?	no
X-Component of Wall Translation (m/s)	0
Y-Component of Wall Translation (m/s)	0
External Emissivity	1
External Radiation Temperature (c)	300
Rotation Speed (rad/s)	0
X-Position of Rotation-Axis Origin (m)	0
Y-Position of Rotation-Axis Origin (m)	0
X-component of shear stress (pascal)	0
Y-component of shear stress (pascal)	0
Surface tension gradient (n/m-k)	0
Specularity Coefficient	0

big_cyl

Condition	Value
Wall Thickness (m)	0

Heat Generation Rate (w/m3)	0
Material Name	aluminum
Thermal BC Type	0
Temperature (c)	274.14999
Heat Flux (w/m2)	0
Convective Heat Transfer Coefficient (w/m2-k)	0
Free Stream Temperature (c)	300
Wall Motion	0
Shear Boundary Condition	0
Define wall motion relative to adjacent cell zone?	yes
Apply a rotational velocity to this wall?	no
Velocity Magnitude (m/s)	0
X-Component of Wall Translation	1
Y-Component of Wall Translation	0
Define wall velocity components?	no
X-Component of Wall Translation (m/s)	0
Y-Component of Wall Translation (m/s)	0
External Emissivity	1
External Radiation Temperature (c)	300
Rotation Speed (rad/s)	0
X-Position of Rotation-Axis Origin (m)	0
Y-Position of Rotation-Axis Origin (m)	0
X-component of shear stress (pascal)	0
Y-component of shear stress (pascal)	0
Surface tension gradient (n/m-k)	0
Specularity Coefficient	0

default-interior

Condition	Value

Solver Controls

Equations

Equation	Solved
Flow	yes
Energy	yes

Numerics

Numeric	Enabled
Absolute Velocity Formulation	yes

Relaxation

Variable	Relaxation Factor

Pressure	0.30000001
Density	1
Body Forces	1
Momentum	0.69999999
Energy	1

Linear Solver

Variable	Solver Type	Termination Criterion	Residual Reduction Tolerance
Pressure	V-Cycle	0.1	
X-Momentum	Flexible	0.1	0.7
Y-Momentum	Flexible	0.1	0.7
Energy	Flexible	0.1	0.7

Pressure-Velocity Coupling

Parameter	Value
Type	SIMPLE

Discretization Scheme

Variable	Scheme
Pressure	Standard
Momentum	Second Order Upwind
Energy	Second Order Upwind

Solution Limits

Quantity	Limit
Minimum Absolute Pressure	1
Maximum Absolute Pressure	5e+10
Minimum Temperature	1
Maximum Temperature	5000

Material Properties

Material: air (fluid)

Property	Units	Method	Value(s)
Density	kg/m3	constant	1388.9
Cp (Specific Heat)	j/kg-k	constant	0.72000003
Thermal Conductivity	w/m-k	constant	1
Viscosity	kg/m-s	constant	1

Molecular Weight	kg/kgmol	constant	28.966
L-J Characteristic Length	angstrom	constant	3.711
L-J Energy Parameter	c	constant	-194.55
Thermal Expansion Coefficient	1/k	constant	0
Degrees of Freedom		constant	0
Speed of Sound	m/s	none	#f

Material: aluminum (solid)

Property	Units	Method	Value(s)
Density	kg/m3	constant	2719
Cp (Specific Heat)	j/kg-k	constant	871
Thermal Conductivity	w/m-k	constant	202.4

APPENDIX C: EXAMPLE OF A GAMBIT JOURNAL FILE

Journal file for cylinders on the same centreline

```
$D = 1
$d = 0.25
$S = 0.5
$Lu = 4
$Ld = 7
$x1 = 0
$x2 = $Lu + $D + $Ld
$x3 = $x2
$x4 = $x1
$x8 = $Lu + ($D/2)
$x9 = $Lu + $D
$x10 = $x8
$x5 = $x8
$x6 = $x5 + ($d/2)
$x7 = $x5
$y1 = 0
$y2 = 0
$y3 = ($S/2) + $d + $S + $D + ($S/2)
$y4 = $y3
$y5 = ($S/2)
$y6 = $y5 + ($d/2)
$y7 = $y5 + $d
$y8 = $y7 + $S
$y9 = $y8 + ($D/2)
$y10 = $y8 + $D
/start size for size function
$ss = 0.01
/size limit for size function
$sl = 0.1
vertex create coordinates $x1 $y1 0
vertex create coordinates $x2 $y2 0
vertex create coordinates $x3 $y3 0
vertex create coordinates $x4 $y4 0
vertex create coordinates $x5 $y5 0
vertex create coordinates $x6 $y6 0
vertex create coordinates $x7 $y7 0
vertex create coordinates $x8 $y8 0
vertex create coordinates $x9 $y9 0
vertex create coordinates $x10 $y10 0
edge create straight "vertex.1" "vertex.2" "vertex.3" "vertex.4"
edge create straight "vertex.1" "vertex.4"
edge create threepoints "vertex.10" "vertex.9" "vertex.8" circle
edge create threepoints "vertex.7" "vertex.6" "vertex.5" circle
face create wireframe "edge.3" "edge.2" "edge.1" "edge.4" real
face create wireframe "edge.5" real
face create wireframe "edge.6" real
face subtract "face.1" faces "face.2"
face subtract "face.1" faces "face.3"
blayer create first 0.001 growth 1.2 total 0.00992992 rows 6 transition 1 \
```

```
  trows 0 uniform
blayer attach "b_layer.1" face "face.1" edge "edge.7" add
blayer create first 0.001 growth 1.2 total 0.00992992 rows 6 transition 1 \
  trows 0 uniform
blayer attach "b_layer.2" face "face.1" edge "edge.8" add
physics create "big cyl" btype "WALL" edge "edge.7"
physics create "small cyl" btype "WALL" edge "edge.8"
physics create "inlet" btype "PRESSURE_INLET" edge "edge.4"
physics create "outlet" btype "PRESSURE_OUTLET" edge "edge.2"
physics create "periodic" btype "PERIODIC" edge "edge.1" "edge.3"
face delete "face.1" lowertopology onlymesh
edge link "edge.1" "edge.3" directions 0 1 periodic
sfunction create sourceedges "edge.7" "edge.8" startsize $ss growthrate 1.2 \
  sizelimit $sl attachfaces "face.1" fixed
sfunction bgrid attachfaces "face.1"
face mesh "face.1" pave
export fluent5 "seuncyl.msh" nozval
```

Proceedings of COBEM 2009
20th International Congress of Mechanical Engineering
November 15-20, 2009, Gramado, RS, Brazil

MAXIMUM HEAT TRANSFER RATE DENSITY FROM A ROTATING MULTISCALE ARRAY OF CYLINDERS

O.I Ogunronbi, seun@tuks.co.za
T. Bello-Ochende, tbochende@up.ac.za
Department of Mechanical and Aeronautical Engineering, University of Pretoria, 0002, South Africa

J.P Meyer, josua.meyer@up.ac.za
Department of Mechanical and Aeronautical Engineering, University of Pretoria, 0002, South Africa.

Abstract. *This paper studies the effect of laminar flow on multiscale heated rotating cylinders in cross-flow. The objective is to maximize the heat transfer rate density of the assembly, under a given pressure drop and subject to the constraint of materials and volume. This problem is solved numerically, with two main configurations: i) Both cylinders share a common centre-line, and ii) Both cylinders share a leading edge to the advancing coolant. Results are reported for two types of configurations; firstly, counter-rotating cylinders in cross-flow and then co-rotating cylinders in cross flow. The spacing between these two types of configuration is optimized. Results shows that the counter-rotating cylinders is more effective than the co-rotating cylinders at a higher pressure drop, while the difference is less noticeable at lower pressure drop.*

Keywords*: multiscale rotating cylinders, heat-transfer-rate density, co-rotating, counter-rotating*

1. INTRODUCTION

Due to the need for more efficient removal of heat from heat transfer generating equipment, research is currently being conducted in this area with the aim of accommodating more and more heat generating devices within a given volume. This will help in the design, manufacture and operation of such equipment. Modern electronic systems do produce high amounts of heat due to the power to volume or weight ratio employed in such systems. The heat produced, if not removed could lead to failure of parts of the system and in some cases failure of the whole system.

Effects of heat transfer from cylinders as well as the optimisation of design of such material have been conducted by a long list of researchers such as Badr and Dennis (1985), Mahfouz and Badr (1999), Gschwendtner (2004), Misirlioglu (2006), Paramane and Sharma (2009) amongst others. Optimisation of the spacing between cylinders have been conducted by Stanescu et al (1996) who found that with an increase in the Reynolds number the spacing between the cylinders consequently decreases. Mohanty et al (1995) compared the effect of rotation against pure cross flow with the same set of Reynolds numbers; they reported that at equal rotational and free stream Reynolds numbers, the localised heat transfer at the stagnation point of the rotational cylinder is lower than that of the pure cross flow. This view is somewhat supported by Tzeng et al (2007) where they found that at higher Reynolds' number the cooling efficiency is increased on high-velocity rotating machines.

According to Jones et al (1988), the heat transfer from a cylinder is governed by three mechanisms viz.: forced convection due to the bounding volume within which the cylinder is located forced convection due to rotation and natural convection. Part of the assumptions made in this work disregards the third mechanism mentioned above. It was further stated by Jones et al (1988) and confirmed by Joucaviel et al (2008) that rotation does enhance heat transfer, "viscous forces acting in the fluid due to rotation cause mixing of the fluid and augment heat transport in a way similar to turbulence"

In the words of Bello-Ochende and Bejan (2004), "Strategy and systematic search mean that architectural features that have been found beneficial in the past can be incorporated and compounded into more complex flow structures of the present". This work involves the addition of more length scales to those of Joucaviel et al (2008). The length scales are the number of cylinders, the difference in diameters of subsequent cylinders and the spacing between the cylinders.

This paper builds on prior research conducted by Bello-Ochende and Bejan (2004) and more recently added to by Joucaviel et al (2008), in which it is proved that rotational effects increase the heat-transfer-rate density for single scale cylinders. This paper focuses on the optimisation of the heat-transfer-rate density of multiscale cylinders cooled by cross flow fluid in the laminar regime. The flow is driven by a fixed pressure difference across the domain in consideration. Applications of heat transfer from rotating cylinders are found in rotating machineries, heat exchangers, viscous pumps, rotating electrodes, spinning projectiles as well as contact cylinder dryers in the paper industry.

2. MODEL

2.1. Cylinders aligned along the same centre-line

We start by considering a case when the cylinders are aligned along the same centre-line. Figure 1 depicts the model which represents a multi-scale array of cylinders set along the same centre-line, and due to the repetitive nature of the stack a domain containing two different size cylinders is chosen to represent the numerical region of interest. The figure further shows the flow across the domain is driven by a fixed pressure drop ΔP, the tip to tip distance between the cylinder is S and are assumed equal for a case with no eccentricity. The cylinders rotate with an angular velocity ω. The fluid inlet temperature T_∞ is fixed and lower than the temperature of the wall of the cylinders, T_w which are assumed constant.

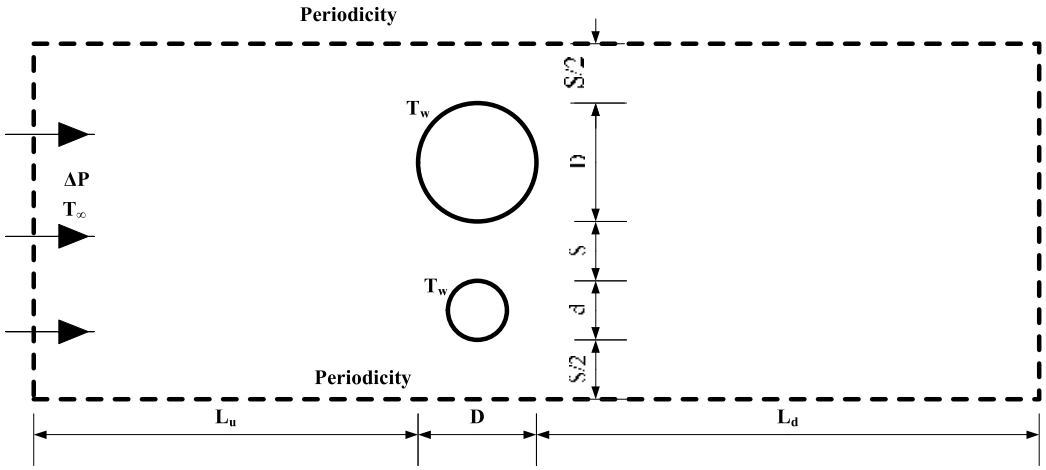

Figure 1 Both cylinders have a common centre-line.

Additional assumptions include steady, laminar, incompressible and two dimensional flow. All the thermo-physical properties are assumed constant. In this setup two configurations are investigated, that is, the cylinders rotating in the same direction (case I) and secondly both cylinders rotating in counter directions (case II) to each other. The domain upper and lower walls are chosen as periodic with the rotational direction reversed for cases of counter-rotation. The heat flux q′ removed from the assembly per unit length perpendicular to the above figure can be written in the following form,

$$q' = D\int_0^{2\pi} q_w d\theta + d\int_0^{2\pi} q_w d\theta \tag{1}$$

The volume per unit height of interest occupied by the modeled assembly is D(D + d + 2S) , where D is the diameter of the bigger cylinder, d is the diameter of the small cylinder, and q_w is the heat transfer from the cylinder. The heat transfer rate density is given as

$$q''' = \frac{q'}{D(D+d+2S)} \tag{2}$$

And this represents the total heat per unit volume.

2.2.Mathematical Formulation

The governing equations of the fluid flow through the multi-scale rotating cylinders are the conservation of mass, momentum and energy equations. The computational domain is in two dimensions as shown in figure 2 and the assumptions made with respect to its solution have been given in the previous section.

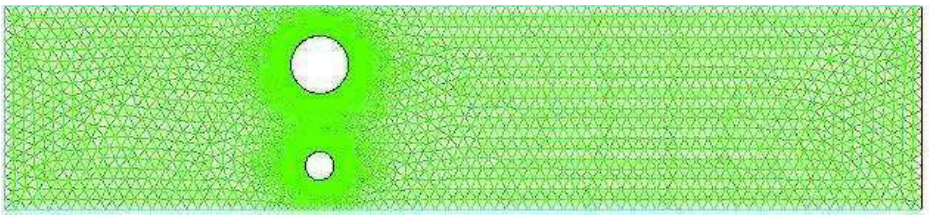

Figure 2 Discretized domain of cylinders with the same centre-line.

The equations, which represent the conservation of mass, momentum and energy equation in the primitive forms are

$$\frac{\partial u}{\partial x}+\frac{\partial v}{\partial y}=0 \tag{3}$$

$$\rho\left(u\frac{\partial u}{\partial x}+v\frac{\partial u}{\partial y}\right)=-\frac{\partial P}{\partial x}+\mu\nabla^2 u \tag{4}$$

$$\rho\left(u\frac{\partial v}{\partial x}+v\frac{\partial v}{\partial y}\right)=-\frac{\partial P}{\partial y}+\mu\nabla^2 v \tag{5}$$

$$\rho c_p\left(u\frac{\partial T}{\partial x}+v\frac{\partial T}{\partial y}\right)=k\nabla^2 T \tag{6}$$

Where u and v represent the velocity components in the Cartesian coordinate directions, x and y. ρ is the density, μ is the viscosity, k is the thermal conductivity, c_P is the heat capacity, P is the pressure, and T is the temperature . Additional assumptions include constant solid and fluid properties and the heat transfer due to radiation is negligible. Equations (3) – (6) in dimensionless forms are,

$$\frac{\partial \tilde{u}}{\partial \tilde{x}}+\frac{\partial \tilde{v}}{\partial \tilde{y}}=0 \tag{7}$$

$$\frac{Be}{\Pr}\left(\tilde{u}\frac{\partial \tilde{u}}{\partial \tilde{x}}+\tilde{v}\frac{\partial \tilde{u}}{\partial \tilde{y}}\right)=-\frac{\partial \tilde{P}}{\partial \tilde{x}}+\nabla^2\tilde{u} \tag{8}$$

$$\frac{Be}{\Pr}\left(\tilde{u}\frac{\partial \tilde{v}}{\partial \tilde{x}}+\tilde{v}\frac{\partial \tilde{v}}{\partial \tilde{y}}\right)=-\frac{\partial \tilde{P}}{\partial \tilde{y}}+\nabla^2\tilde{v} \tag{9}$$

$$Be\left(\tilde{u}\frac{\partial \tilde{T}}{\partial \tilde{x}}+\tilde{v}\frac{\partial \tilde{T}}{\partial \tilde{y}}\right)=\nabla^2\tilde{T} \tag{10}$$

The non-dimensionalized variables used are:

$$\tilde{\mathrm{d}}=\frac{\mathrm{d}}{\mathrm{D}}\quad \tilde{x},\tilde{y},\tilde{S}=\frac{x,y,S}{D},\ \tilde{u},\tilde{v}=\frac{u,v}{\Delta PD/\mu}\quad \tilde{P}=\frac{P}{\Delta P}\qquad \tilde{T}=\frac{T-T_\infty}{T_W-T_\infty} \tag{11}$$

Where the Bejan and Prandtl numbers are $\mathrm{Be} = \mathrm{D}^2\Delta\mathrm{P}/\mu\alpha$ and $\Pr = \nu/\alpha$.

The flow boundary conditions are: $\tilde{\mathrm{P}} = 1$ at the inlet plane and zero normal stress at the outlet plane. The thermal boundary conditions are $\tilde{\mathrm{T}} = 0$ at the inlet plane and $\tilde{\mathrm{T}} = 1$ on the cylinders surfaces. The horizontal surfaces of the domain correspond to periodic conditions due to the rotations of the multi-scale cylinders. The cylinders are rotating at ω and therefore an angular velocity is imposed as a boundary condition on the cylinder surfaces,

$$\tilde{\omega} = \frac{\omega\mu}{2\Delta P} \tag{12}$$

The objective function (i. e. heat transfer rate density), Eq. 2, can be written in dimensionless form as

$$\tilde{q} = \frac{q'''D^2}{k\left(T_w - T_\infty\right)} = \frac{1}{(1+\tilde{d}+2\tilde{S})}\int_0^{2\pi}\left[-\nabla\tilde{T} + \tilde{d}(-\nabla\tilde{T})\right]_n d\theta \tag{13}$$

2.3. Numerical solution

The finite volume code software FLUENT™ was employed to solve Eqs. (7) - (10). The domain was discretized using a second order discretization scheme. The pressure-velocity coupling was done with the SIMPLE algorithm. Numerical convergence was obtained in two ways, firstly convergence was obtained when the scaled residuals for mass and momentum equations were smaller than 10^{-4} and the energy residual was less than 10^{-7}. In the second option numerical convergence was obtained when there was no further change in the value of residuals for consecutive iterations in terms of the specified criteria such as conservation of mass flow rate in the domain.

An additional method used to ensure accuracy of the results was to perform grid refinement tests. The key quantity monitored in this regard was the overall heat transfer rate density. Figure 2 shows that the grid was refined by placing or concentrating the mesh in the region closest to the cylinders, where the thermal gradient was high. Virtual extensions, $\tilde{L}_u$ and $\tilde{L}_d$ had been added to the numerical domain downstream and upstream of the physical domain to adequately handle the pressure boundary conditions. The length of the virtual extension was chosen long enough so that with any further increase in length, the change in the heat transfer rate density between two iterations, i and i+1 is smaller than 1%.

Table 1a and 1b shows how the virtual extension was chosen. For Be = 10^3 and $\tilde{S}$ = 1, and $\tilde{\omega}$ = 0, the virtual extensions is $\tilde{L}_u = 5$, $\tilde{L}_d = 10$.

Table 1a. Keeping $\tilde{L}_d$ constant, $\tilde{\omega} = 0$, $\tilde{S} = 1$ and Be = 1000

$\tilde{L}_u$	$\tilde{q}$	$\left\lvert\frac{\tilde{q}_i - \tilde{q}_{i-1}}{\tilde{q}_i}\right\rvert$
3	17.5492	-
5	17.5788	0.0017
10	17.4778	0.0057
15	17.4218	0.0032

Table 1b. Keeping $\tilde{L}_u$ constant, $\tilde{\omega} = 0$, $\tilde{S} = 1$ and Be = 1000

$\tilde{L}_d$	$\tilde{q}$	$\left\lvert\frac{\tilde{q}_i - \tilde{q}_{i-1}}{\tilde{q}_i}\right\rvert$
5	17.4174	-
10	17.4778	0.0035
15	17.4587	0.0011
20	17.3673	0.0052

2.4.Optimal cylinder spacing

In order to obtain the optimized heat transfer rate density, the cylinder to cylinder distance is varied for a specified Bejan number, Prandtl number and dimensionless angular velocity. We proceeded with the optimisation by using the following criteria, the diameter of the bigger cylinder D was set at 1, while that of the smaller was fixed at $\tilde{d} = 0.25$, these values were obtained from previous work of Bello-Ochende and Bejan (2004) where it was found that for a multi-scale cylinder in cross-flow the optimal diameter of the second cylinder is robust and equal to 0.25. The range of parameter consider for this study is $10^3 \leq$ Be $\leq 10^5$, $0 \leq \tilde{\omega} \leq 0.1$ and Pr = 0.71. The Reynolds number equivalence is in the laminar region of $10 - 10^3$. Figures 3, 4 and 5 illustrate the heat transfer rate density obtained as a function of various rotational velocities and cylinder to cylinder spacing, $\tilde{S}$.

In the first case of cylinders on the same centre line with Be = 10^3 as seen in figure 3, it is observed that co-rotating cylinders provide better heat transfer rates with respect to the optimisation of the distance between the cylinders and the optimum distances between cylinders are smaller when compared to the optimal distance of the stationary cylinders.

The effect of counter rotating cylinders on the heat transfer rate densities is less when compared to stationary cylinders. For the co-rotating cylinders, an increase in the angular velocity translates to an increase in the heat transfer rate density.

Figure 4, shows the effect of rotation and cylinder to cylinder spacing on the maximum heat transfer rate density for Be = 10^4. The best configuration is that of the stationary flow, for both velocities used the co-rotating cylinders dissipate more heat than the counter rotating cylinders with a wide margin seen between 0.01 and 0.1, a possible explanation for

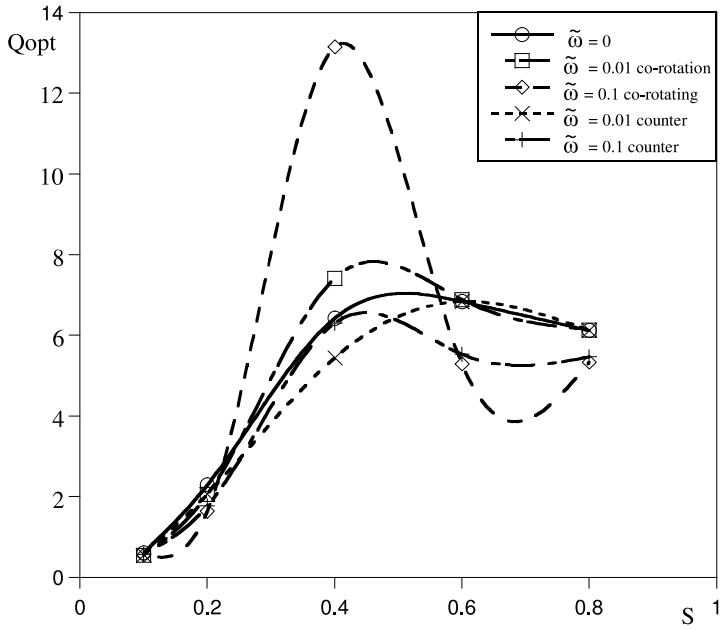

Figure 3 Optimal heat transfer rate density at Be = 10^3 for cylinders located inline.

this phenomenon is the entrainment of heated fluid due to the rotational direction of the cylinders.

Figure 5 shows the effect of rotation and the tip to tip spacing between the cylinders on the heat transfer rate density for Be = 10^5. At a lower dimensionless rotational velocity of 0.01 as shown in Figure 5, the effect of co-rotating cylinders on the heat transfer rate density is more noticeable when compare to the other two cases, that is there is heat transfer enhancement when the cylinders are co-rotating at that velocity. For other dimensionless rotational velocity their effect on the heat transfer rate density is insignificant when compared to that of a stationary cylinder.

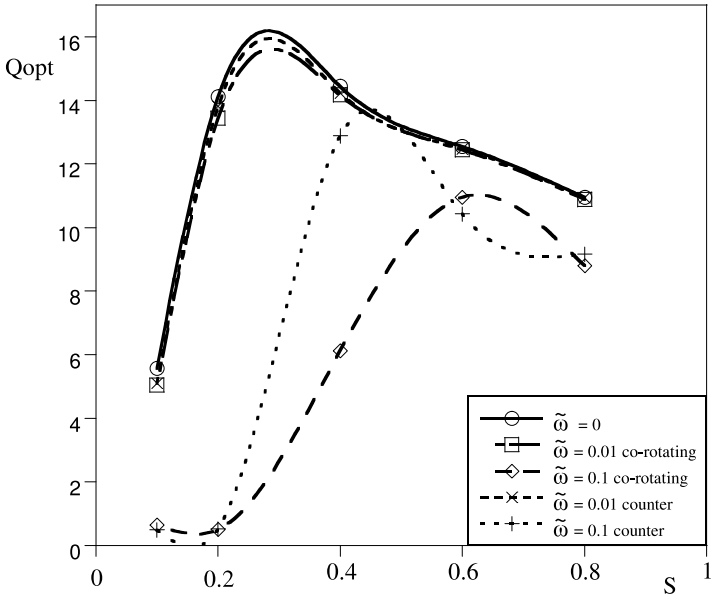

Figure 4 Heat Transfer Rate Density at Be = 10^4 for cylinders located inline.

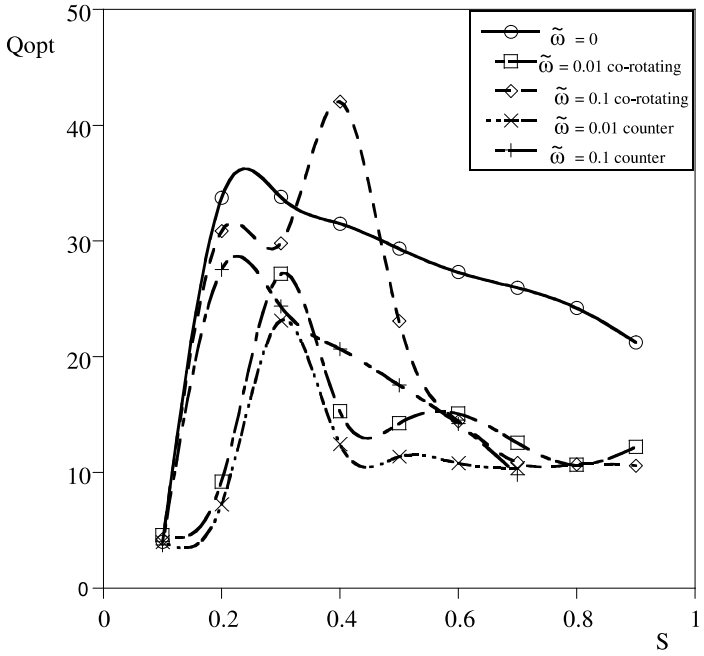

Figure 5 Heat transfer rate density for Be = 10^5 for cylinders located inline.

3. CYLINDERS ALIGNED ALONG THE LEADING EDGE

In the second type of configuration, we considered the case in which the cylinders share the same leading edge as is shown in figure 6 that is, both cylinders experience effect of the incoming coolant at the same time. The numerical procedure is the same as those of the case considered in Section 2 (when the cylinders are aligned along the same centre line) and described in Section 2.3. Figure 6 shows the computational domain while figure 7 shows the discretized domain for the second configuration.

We start the optimization procedure by setting the Bejan number to 10^2 and diameter of the smaller cylinder to 0.25 as obtained from Bello-Ochende and Bejan (2005) and shown in Figure 8. The result shows that there is no major improvement in heat transfer rate density by adding rotation to the array of cylinder, furthermore, the optimal distance is approximately equal to 1 for all the cases considered. The results also show for all the cases considered the heat transfer rate densities are identical and therefore all the curves in Figure 8 coalesce to a single curve at the optimal point.

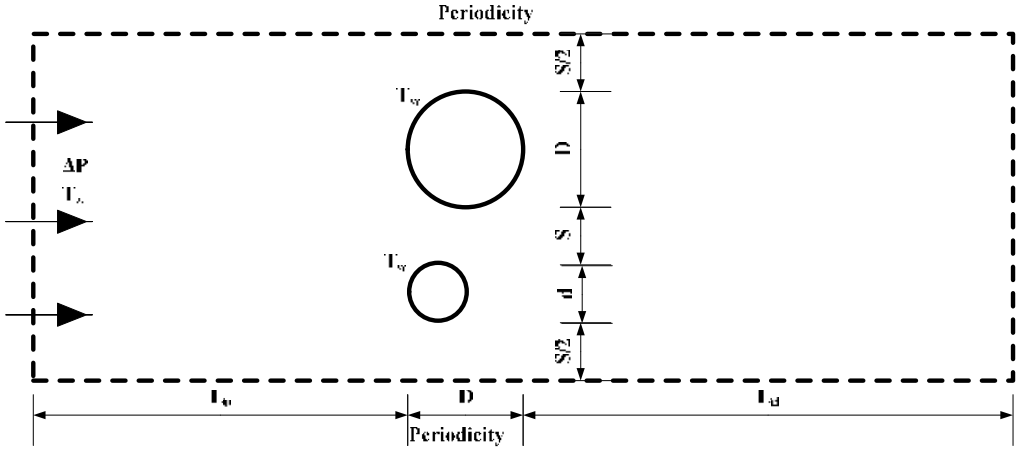

Figure 6 The cylinders with a common leading edge

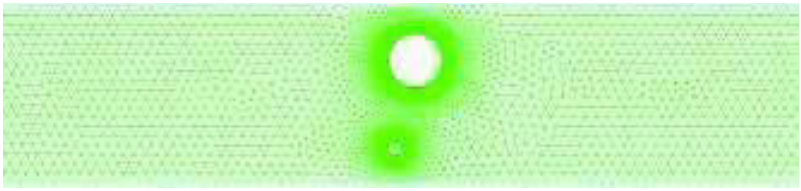

Figure 7 Discretized Domain of cylinders aligned along the leading edge

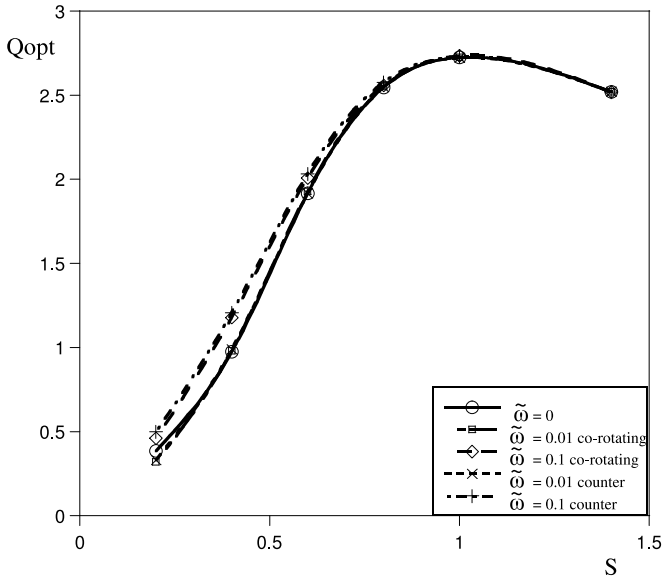

Figure 8 Heat transfer rate density at Be = 100 for cylinders sharing the same leading edge.

From Figure 9 we notice that the heat transfer rate density increases for both cases of co-rotating and counter-rotating cylinders when compared to the stationary cylinder for $\tilde{\omega} = 0.01$. Whereas, there is a significant difference in heat transfer rate density when compared to a stationary cylinder at a higher $\tilde{\omega}$ of 0.1. This might be due to the entrainment of heated fluids around the cylinder due to increase of rotation and the imposed pressure drop.

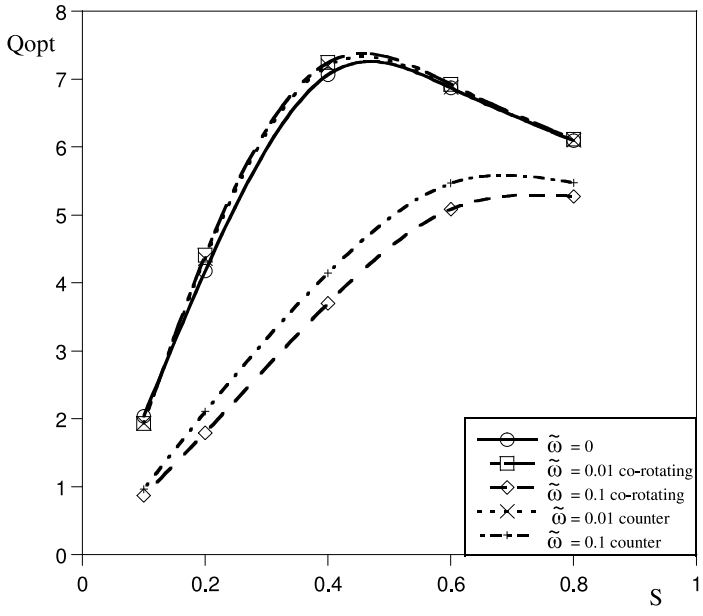

Figure 9 Heat transfer rate density at Be = 1000 for cylinders having the same leading edge.

Figure 10 shows that with rotation at a higher rotational speed there is a beneficial increase in the heat transfer and the optimal lower spacing is smaller as the Bejan number increases. From figure 10 it is seen that the heat transfer rate density at a higher angular velocity is higher than that of the lower angular velocity for both cases of co-rotating cylinders and counter-rotating cylinders. A further explanation for this is that the velocity of the incoming coolant fluid is more than that of the rotating cylinder hence a faster transfer of heat from the cylindrical surfaces.

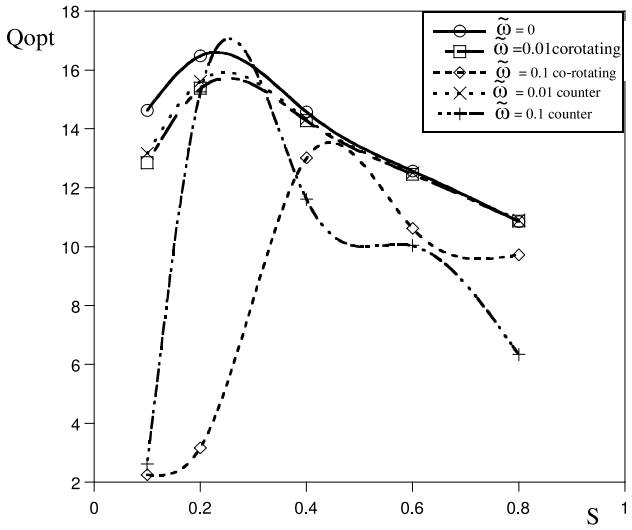

Figure 10 Heat transfer rate density at Be = 10^4 for cylinders having the same leading edge.

Figures 11 shows the velocity contours when the cylinders are aligned at the leading edge with the red region indicating the region of high velocity and blue indicates the region of low velocity and the colours between indicating the transition from the high velocity to the low velocity. In figure 12, the temperature contours of both stationary cylinders and co-rotating cylinders with the red region marking the points of high temperature, that is at the cylinder surface, $T_w = 1$ and the blue region marking places of low temperature, $T_\infty = 0$ corresponding to the freestream coolant.

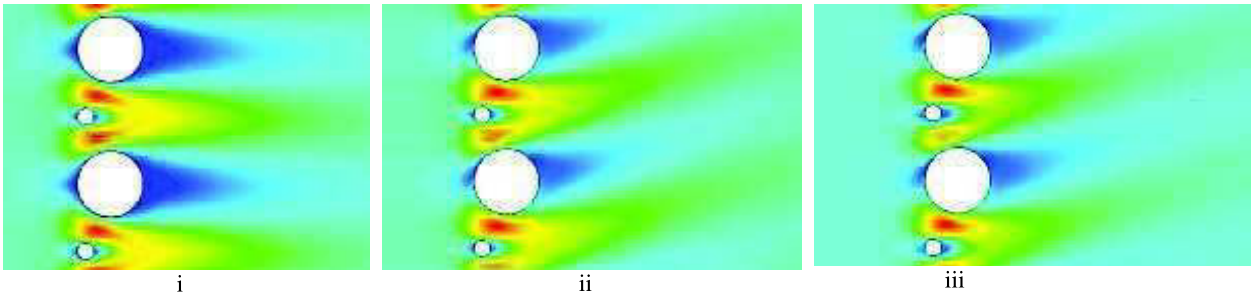

i ii iii

Figure 11 Velocity contour of i) stationary cylinders, ii) co-rotating cylinders with the same leading edge and iii) counter-rotating cylinders with the same leading edge

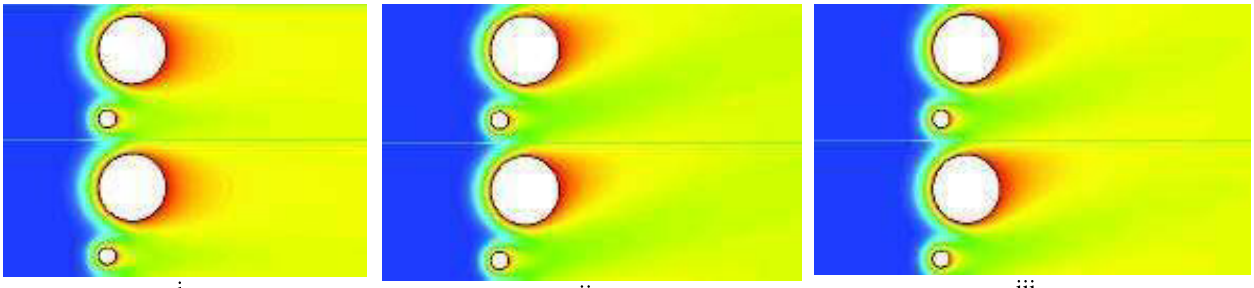

i ii iii

Figure 12 Temperature contours of i) stationary cylinders, ii) co-rotating cylinders with the same leading edge and iii) counter-rotating cylinders with the same leading edge

4. CONCLUSION

Rotation is beneficial to the heat transfer at certain velocities for an imposed Bejan number and at lower velocities the heat transfer is not significant when compared to that of a stationary cylinder. What is more salient in this work is that at higher pressure drop numbers the optimal spacing between the cylinders decreases, the heat transfer rate density also increases with increase in pressure drop number, that is the Bejan number.

5. ACKNOWLEDGEMENTS

This work was supported by the advanced engineering centre of excellence, NRF, TESP, EEDSM Hub and the CSIR.

6. REFERENCES

Badr, H.M., Dennis, S.C.R., 1985, “Laminar foced convection from a rotating cylinder” International Journal of Heat Mass Transfer, Vol. 28, No.1, pp. 253-264

Bello-Ochende, T., Bejan, A., 2004, “Constructal multiscale cylinders in cross-flow. Intl. J Heat and Mass transfer” International Journal of Heat and Mass Transfer, Vol. 48, pp. 1373-1383

Fluent User’s Guide, 1998 (www.fluent.com)

Gschwendtner, M.A, 2004, ”Optical investigation of the heat transfer from a rotating cylinder in a cross-flow” Heat and Mass Transfer, Vol. 40, pp. 561-572

Jones, J., Poulikakos, D., Orozco, J., 1988, “Mixed convection from a rotating horizontal heated cylinder placed in a low-velocity wind tunnel.” International Journal of Heat and Fluid Flow, Vol. 9, No.2

Joucaviel, M., Gosselin, L., Bello-Ochende, T., 2007, “Maximum heat transfer density with rotating cylinders aligned in cross-flow.” International Communications in Heat and Mass Transfer, Vol. 35, pp. 557-564

Mahfouz, F.M., Badr, H.M., 1999, “Heat convection from a cylinder performing steady rotation or rotary oscillation – Part I: Steady rotation” International Journal of Heat and Mass Transfer, Vol. 34, pp. 365-373

Misirlioglu, A., 2006 “The effect of rotating cylinder on the heat transfer in a square cavity filled with porous medium” International Journal of Engineering Science, Vol. 44, pp. 1173-1187

Mohanty, A.K., Tawfek, A.A., Prasad, B.V.S.S.S., 1995 “Heat transfer from a rotating horizontal heated cylinder placed in a low-velocity wind tunnel” Experimental Thermal and Fluid Science, Vol. 10, pp. 54-61

Paramane, S.B., Sharma, A., 2009 “Numerical investigation of heat and fluid flow across a rotating circular cylinder maintained at constant temperature in 2-D laminar flow regime” International Journal of heat and Mass Transfer, Vol. 52, pp. 3205-3216

Stanescu, G., Fowler, A.J., Bejan, A., 1996 “The optimal spacing of cylinders in free-stream cross-flow forced convection” International Journal of heat and Mass Transfer, Vol. 39, No. 2, pp. 311-317

Tzeng, S.C., Ma, W.P., Lin, C.W., Jywe, W.Y, Liu, C.H., Wang, Y.C.,2007, “Experimental investigation of lubrication and cooling effect of high-velocity rotating machines”